Aus dem Institut für Physiologie und Pathophysiologie
Geschäftsführender Direktor: Prof. Dr. Dominik Oliver

des Fachbereichs Medizin der Philipps-Universität Marburg

Control of cellular trafficking of mammalian voltage sensitive phosphatase (VSP) through protein-protein interactions

Inaugural-Dissertation zur Erlangung des Doktorgrades der Naturwissenschaften
dem Fachbereich Medizin der Philipps-Universität Marburg

vorgelegt von
Imran Gousebasha Shaikh
aus Pamur, Indien

Marburg, 2024

Angenommen vom Fachbereich Medizin
der Philipps-Universität Marburg
am: 21.05.2024

Gedruckt mit Genehmigung des Fachbereichs

Dekanin: Frau Prof. Dr. D. Hilfiker-Kleiner

Referent: Herr Prof. Dr. D. Oliver

1. Korreferent: Herr Prof. Dr. M. Rust

Table of Contents

ABBREVATIONS

Aa	Amino acid
AT	annealing temperature
BSG	Basigin
CAM	Cell adhesion molecule
CBR3	calcium binding region 3
CD	cluster of differentiation
cDNA	complementary deoxyribonucleic acid
CHO	Chinese Hamster Ovary
Co-IP	co-immunoprecipitation
CTD	C-terminal domain
DAG	Diacylglycerol
DMEM	Dulbecco's modified Eagles medium
DMSO	dimethyl sulfoxide
DNA	deoxyribonucleic acid
dNTPs	deoxynucleotide triphosphate
DPBS	Dulbecco's phosphate buffered saline
DTT	dithiothreitol
e.g.	exempli gratia
EDTA	ethylenediaminetetraacetic acid
EGFP	enhanced green fluorescent protein
EMB	embigin
EMMPRIN	extracellular matrix metalloproteinase inducer
ENTH	epsin N-terminal homology
ER	endoplasmic reticulum
FBS	fetal bovine serum
GAPDH	glyceraldehyde 3-phosphate dehydrogenase
GFP	green fluorescent protein
GPCR	G protein-coupled receptors
HG	high-glycosylated
ICC	immunocytochemistry
Ig	immunoglobulin-like
IgSf	Immunoglobulin Superfamily

IP3	inositol-1,4,5-triphosphate
LG	low-glycosylated
MCT	Monocarboxylate transporter
MHC	major histocompatibility complex
MMP	matrix metalloproteinase
mRNA	messenger ribonucleic acid
NPTN	neuroplastin
PAGE	Polyacrylamide Gel Electrophoresis
PBM	PIP2 binding motif
PBS	Phosphate-buffered saline
PBST	Phosphate-buffered saline with Tween®
PCR	polymerase chain reaction
PD	phosphatase domain
PH	Pleckstrin Homology
PI	phosphatidylinositol
$PI(3)P_2$	phosphatidylinositol-3-phosphate
$PI(3,4)P_2$	phosphatidylinositol-3,4-bisphosphate
$PI(3,4,5)P_3$	phosphatidylinositol-3,4,5-triphosphate
$PI(3,5)P_2$	phosphatidylinositol-3,5-bisphosphate
$PI(4)P_2$	phosphatidylinositol-4-phosphate
$PI(4,5)P_2$	phosphatidylinositol-4,5-bisphosphate
$PI(5)P_2$	phosphatidylinositol-5-phosphate
PI3K	phosphatidylinositol 3-kinase
PI3P	phosphatidylinositol-3-phosphate
PI4K	phosphatidylinositol 4-kinase
PI4P	phosphatdylinositol-4-phosphate
PIP	phosphorylated PI
PLC	phospholipase C
PM	PM
PMCA	Plasma Membrane Ca^{2+}-ATPases
PTEN	tumor suppressor Phosphatase and Tensin homolog
PTM	post-translational modification
PX	Phox homology
RFP	red fluorescent protein

RT-PCR	Reverse transcription polymerase chain reaction
SDS	Sodium dodecyl sulfate
SEM	standard error of the mean
TIRF	Total Internal Reflection Fluorescence
TM	transmembrane
TMEM	transmembrane protein
TPIP	TPTE and PTEN homologous inositol lipid phosphatase
TPTE	transmembrane phosphatase with
TubbyCT	C-terminal domain of tubby
VGIC	voltage gated ion channel
VSD	voltage-sensitive domain
VSP	voltage-sensitive phosphatase
VSP	voltage-sensitive phosphatase
Y2H	yeast-two-hybrid

ABSTRACT

Voltage-sensitive phosphatases (VSPs) possess a unique combination of a voltage sensor domain (VSD), akin to those found in voltage-gated ion channels (VGICs), and a catalytic domain similar to the tumor suppressor protein PTEN. This fusion of voltage sensing ability and lipid phosphatase activity makes them exceptional signaling enzymes that convert phosphoinositide's (PIs) in response to depolarization of the membrane potential. Thus, VSPs are known to directly link cellular electrical signaling to intracellular pathways. VSPs exist in several species. However, the physiological role of VSPs remains largely unknown, except for a role in regulating sperm motility in mammals. The remarkable voltage dependent phosphatase activity against PIs has been characterized functionally for VSPs from few non-mammalian species e.*g.*, *Ciona intestinalis* (Ci-VSP), facilitated by robust expression and plasma membrane (PM) targeting in heterologous expression systems. In contrast, mammalian VSPs are poorly understood due to their inability to reach the PM upon over-expression. This has led to speculation about their ability to dephosphorylate PIs upon membrane depolarization. The lack of reliable antibodies complicates the understanding of the physiological role of VSPs in the native environment.

In my PhD thesis, we aimed to perform an unbiased screening approach to uncover mechanisms of PM targeting of the VSP from mouse (mVSP) which in turn enabled examination of its electrochemical function in an over-expression system.

Using a membrane-based yeast two-hybrid screening, we identified the single-transmembrane-domain protein Basigin (BSG) as a putative protein-protein interaction partner of mVSP. Through co-expression experiments in a heterologous system, we found that BSG acts as an ancillary protein subunit for mVSP, which mediates trafficking from the endoplasmic reticulum (ER) to the PM. PM targeting of mVSP was also observed with other BSG family members, namely Neuroplastin (NPTN) and Embigin (EMB).

In order to gain a deeper understanding of the precise regions or domains of BSG that are involved in the PM targeting of mVSP, we took a mutational approach. Our investigations revealed that the single transmembrane region of BSG alone is sufficient to facilitate the trafficking of mVSP to the PM. Vice versa, we explored the regions of mVSP that determine intracellular localization in the absence of BSG. By employing a chimeric approach, we successfully identified that both the N and C-terminal sequence stretches of mVSP are responsible for its retention within the intracellular compartment.

Through the facilitation of BSG-mediated membrane trafficking, we were able to uncover the function of mVSP, which demonstrated its function as a voltage-activated lipid phosphatase. Specifically, mVSP is a 5'-phosphatase of $PI(4,5)P_2$ and $PI(3,4,5)P_3$ activated by depolarization of the membrane potential. Notably, mVSP and BSG were previously shown to be localized in the sperm tail and have been implicated in the regulation of sperm motility. These findings strongly suggest that BSG plays a critical role in targeting mVSPs within the sperm tail, thereby influencing sperm motility by modulating PI metabolism.

ZUSAMENFASSUNG

Spannungsemfindliche Phosphatasen (VSPs) weisen eine einzigartige Kombination aus einer Spannungssensordomäne (VSD), ähnlich der VSP spannungsabhängiger Ionenkanäle (VGICs), und einer katalytischen Domäne, homolog zum Tumorsuppressorprotein PTEN auf. Ihre Fähigkeit auf Membranspannung zu reagieren, in Verbindung mit ihrer Lipidphosphatase-Aktivität macht VSPs zu außergewöhnlichen Signalproteinen, die infolge einer Depolarisation der Zellmembran, Phoshoinositid-Lipide (PIs) konvertieren. Es ist bekannt, dass VSPs elektrische Signale auf diese Weise unmittelbar in intrazelluläre biochemische Signale umwandeln können. VSPs existieren in mehreren Spezies, allerdings ist ihre physiologische Rolle, von einer Beteiligung an der Regulation der Spermienmotilität in Säugetieren abgesehen, bisher weitestgehend ungeklärt. Die spannungsabhängige Phosphatase-Aktivität einiger Nicht-Säugetier-VSPs (z.B. aus *Ciona intestinalis*, CiVSP) gegenüber PIs konnte dank robuster Expression und Lokalisation in der Plasmamembran (PM) in heterologen Expressionssystemen bereits charakterisiert werden. Im Gegensatz dazu sind Säugetier-VSPs wenig erforscht, da sie die PM bei heterologer Expression nicht erreichen. Daher blieb bisher unklar, ob sie überhaupt spannungsabhängige Phosphatase-Aktivität aufweisen. Zusätzlich erschwerte das Fehlen eines verlässlichen Antikörpers die Aufklärung der physiologischen Rolle von VSPs in ihrem natürlichen Kontext.

Ziel meiner Dissertation war, ein Screeningverfahren zur Identifizierung von Protein-Interaktionspartnern der VSP der Maus durchzuführen, um die Mechanismen des zellulären Proteins-Transports und der subzellulären Lokalisation aufzuklären. Dies sollte es dann ermöglichen, die elektrochemische Funktion der mVSP in Überexpressionssystemen zu untersuchen.

Unter Verwendung eines Membran-basierten Yeast-Two-Hybrid-Screens konnten wir das Single-Transmembrane-Domain-Protein Basigin (BSG) als einen potentiellen Protein-Protein-Interaktionspartner von mVSP identifizieren. In Co-Expressionsexperimenten in Zellkultur konnten wir zeigen, dass BSG eine assoziierte Protein-Untereinheit von mVSP ist, die den Transport vom endoplasmatischen Retikulum (ER) zur PM vermittelt. Der Transport zur PM konnte ebenfalls durch Assoziation mit den homologen Proteine der BSG-Familie vermittelt werden, namentlich Neuroplastin (NPTN) und Embigin (EMB).

Um ein tieferes Verständnis der molekularen Domänen von BSG zu erlangen, die am

PM-Targeting von mVSP beteiligt sind, bedienten wir uns eines Mutationsansatzes. Unsere Untersuchungen zeigten, dass die Transmembranregion von BSG ausreichend ist, um den Transport von mVSP zur PM zu ermöglichen. Komplementär dazu untersuchten wir die Regionen von mVSP, die die ER-Lokalisation in Abwesenheit von BSG determinieren. Wir konnten sowohl N- als auch C-terminale Sequenzabschnitte von mVSP identifizieren, die kooperativ für die ER- verantwortlich sind.

Der BSG-vermittelte Transport an die PM, ermöglichte es schließlich, die Aktivität der mVSP als spannungsaktivierte Lipidphosphatase nachzuweisen. Wir konnten feststellen, dass mVSP eine durch Depolarisation des Membranpotentials aktivierte 5'-Phosphatase der Substrate PI(4,5)P2 und PI(3,4,5)P3 darstellt.

Bemerkenswerterweise wurde zuvor bereits die Lokalisation von mVSP wie auch BSG im Flagellum der Spermien gezeigt und mit der Regulierung der Spermienmotilität in Verbindung gebracht. Unsere Ergebnisse legen dementsprechend eine essentielle Rolle von BSG für den Transport von mVSP in die PM des Spermiums nahe. Dies wiederum ist die Versaussetzung für eine Kontrolle der Spermienmotilität über die Modulation des PI-Metabolismus.

1. Introduction.

1.1. Biological membranes

All cells have membranes that allow them to define their own boundaries by separating intracellular components from the extracellular space (Simons *et al*., 2022). In eukaryotic cells, the membrane system organizes the cell by creating physically and functionally distinct cellular organelles within the cell. This in turn allows the cells to compartmentalize and carry out both metabolic tasks and signaling pathways efficiently (Poser *et al*., 2022,).

Biological membranes are composed of fluid lipid bilayers harbouring membrane proteins and extrinsic proteins. The majority of the membrane consists of phospholipids; however, it also contains cholesterol and glycolipids, especially eukaryotic membranes contain significant amounts of cholesterol. These lipid bilayers are packed with phospholipids, molecules consisting of a hydrophilic head group, and hydrophobic fatty acid chains. This unique property of lipid amphipathicity allows the cell to segregate its internal components from the external stimuli. Membranes are known to be asymmetric having different compositions at the inner and outer leaflet (Alberts *et al*., 2002). The composition of phospholipids in a membrane can vary based on factors such as size, shape, and charge of the head group of the phospholipid. This variability in phospholipid types contributes to the structural diversity of biological membranes, influencing their properties and functions. The outer leaflet of the PM consists of phosphatidylcholine, sphingomyelin and glycolipids, while the inner leaflet contains phosphatidylethanolamine and phosphatidylserine. The positions of these phospholipids are crucial for the function of several membrane proteins (Casares *et al*., 2019). In addition, many cytosolic enzymes bind specifically to phospholipid head groups which are exposed on the cytosolic side of the membrane resulting in their recruitment to perform their enzymatic activity. One such group of phospholipids known as phosphoinositide is present in smaller amounts in the inner cell leaflet of the PM, which is functionally very important in cell signaling and regulation of membrane homeostasis (Ernst *et al*., 2018; Alberts *et al*., 2002).

1.2. Phosphoinositides and their cellular roles

The eukaryotic cell membrane contains a family of phospholipids known as phosphoinositide’s (PIs), which are essential for many biological processes. Each

compartment of the cellular membrane consists of specific PIs that recruit peripheral proteins to the membrane in order to carry out their functional activity. Despite being present only in minute amounts, PIs are essential for cellular processes such as signaling, membrane trafficking and ion channel regulation (Nakada-Tsukui, *et al*., 2019; Balla *et al*., 2013).

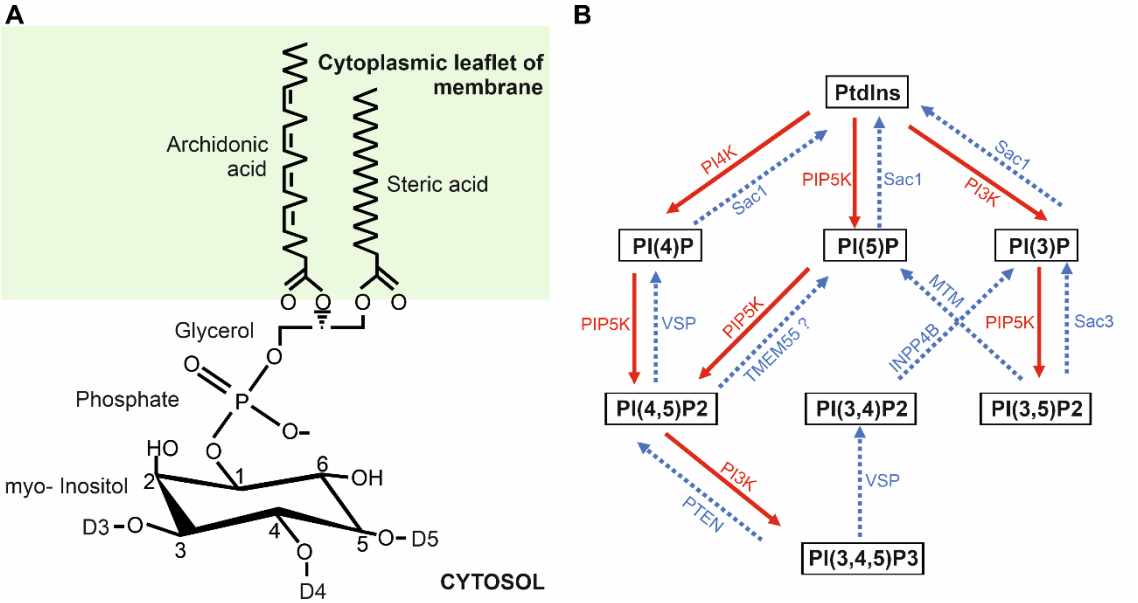

Figure 1.1: Structure of Phosphoinositide and generation of its derivatives. (A) Schematic diagram representing Phosphoinositide which is composed of long chain fatty acid group inserted into a lipid bilayer, with the hydrophilic glycerol moiety and the inositol head group exposed on the cytosolic surface of the cell membrane. D3, D4 and D5 are the hydroxyl positions of the inositol ring, which can be interconverted by lipid kinases and Phosphatases. **(B)** Schematic representation of reversible metabolic reactions by specific lipid kinases (red) and phosphatases (blue) that generate seven derivatives of phosphoinositide (Modified from Falkenburger *et al*., 2010 and Balla *et al*., 2013).

Phosphatidylinositol, the precursor of phosphoinositide, is present on the inner cytosolic leaflet of the cell membrane. Like other phospholipids, it consists of a d-myo-inositol head group, glycerol backbone extending into the cytoplasm with two acyl chains that are partially diffused into the lipid bilayer of the membrane (Figure 1.1A). The inositol head group consists of free hydroxyl groups at position D2 and D6, whereas the hydroxyl groups at positions D3, D4 and D5 are differentially phosphorylated and dephosphorylated by cytoplasmic kinases and phosphatases respectively. This phosphatidylinositol interconversion by phosphatases and kinases leads to the generation of seven distinct PI derivatives which are present in different concentrations at the membrane, which are formally named as phosphatidylinositol phosphates (PIPs) (Figure 1.1B). Each of these PIPs show a distinct subcellular distribution with abundant

localization in membrane compartments (Table 1) (Dickson *et al*., 2019). This unique distribution of PIPs in intracellular compartments and their ability to be phosphorylated and dephosphorylated enables them to act as agonists in major signaling events. As mentioned above, regulatory enzymes are involved in maintaining a homeostatic equilibrium of PIP concentrations so that cellular processes such as growth, survival, metabolism, and proliferation can function in a controlled and measured manner (Di Paolo *et al*., 2006; Falkenburger *et al*., 2010; Balla *et al*., 2013)

Table 1: Distribution of PI and PI derivatives in cellular compartments. ER, Endoplasmic reticulum; Plasma membrane, PM. Modified from Dickson *et al*., 2019.

Lipid	**Distribution**
PI	Abundant in ER but potentially all membranes
PI(3)P	PM, endosomes, trans-Golgi
PI(4)P	Early endosomes
PI(5)P	PM, endosomes, nuclear envelope
$PI(4,5)P_2$	PM, recycling endosomes, lysosomes
$PI(3,5)P_2$	PM, early endosomes
$PI(3,4)P_2$	Late endosomes and Lysosomes
$PI(3,4,5)P_3$	PM, some endocytic compartments

1.2.1. Phosphoinositide binding Biosensors

PIPs bind to the conserved Lipid binding site of proteins, allowing them to recruit essential cytoplasmic proteins to the membrane and exert their activity. This lipid binding site consists of PIP binding domains such as Pleckstrin Homology (PH), Epsin NH2-terminal homology (ENTH), Phox homology (PX), FYVE domains etc. (Table 2). These domains are isolated as recombinant proteins and fused to fluorescent proteins in order to track PIPs in the cytosolic membrane of a living cell using microscopy (Wills *et al*.,2018). In order to use these biosensors, certain criteria should always be considered: Firstly, sensor binding should be target specific. Secondly, the affinity of these biosensors should be strong enough to ensure that the localization of the biosensor is highly dependent on the specific PIP. The most commonly used biosensors to study $PI(4,5)P_2$ population at the membrane are the PH domain of PLCδ1 (PLCδ1-PH) (Wills *et al*., 2018; Balla *et al*., 2013) and the C-terminal domain of tubby (TubbyCT) (Santagata *et al*., 2001).

One popular method involves the manipulation and monitoring of PI levels in living cells using voltage-sensitive phosphatases (VSPs). To accomplish this, a biosensor such as PLCδ1-PH is utilized which binds to $PI(4,5)P_2$ at the membrane when the cell is at resting membrane potential. However, after depolarization, VSPs become activated and

hydrolyze $PI(4,5)P_2$, causing the dissociation of PLCδ1-PH from the membrane and its translocation to the cytoplasm (Halaszovich *et al*., 2012).

Table 2: Inositide binding protein domains and commonly used lipid biosensors. FYVE, named after the four proteins in which they were first identified: Fab1, YOTB/ZK632, Vac1p, and EEA1; PX, phox homology; PH, pleckstrin homology; ENTH, epsin NH2-terminal homology; ANTH, AP180 NH2-terminal homology; FERM, named after the first proteins in which they were found:4.1-ezrin-radexin-moiesin; PTB, phosphotyrosine binding; BAR, Bin-Amphiphysin-Rvs; PDZ, postsynaptic density protein, disks large, zonula occludens; GLUE, GRAM-like ubiquitin-binding in Eap45. Modified from Balla *et al*., 2013 and Wills *et al*., 2018

Lipid	**Name of domain**	**Biosensors**
PI(3)P	FYVE domain PX domain	FYVE-Hrsx2
PI(4)P	Eps 15 homology (EHD) domain PH domain	PH-OSBP
PI(5)P	?	3xPHD (ING2)
$PI(4,5)P_2$	PH domain ENTH domain ANTH domain FERM domain Eps 15 homology (EHD) domain PTB domain BAR domain PDZ domain	PLCδ1-PH TubbyCT PLCδ4-PH TubbyCT R332H ENTH/ANTH
$PI(3,5)P_2$	PH domain	ML1-Nx2
$PI(3,4)P_2$	PH domain	PH-TAPP1-CT
$PI(3,4,5)P_3$	GLUE domain PH domain	PH-Akt PH-Btk PH-ARNO

1.2.2. Role of kinases and phosphatases involved in PIP signaling

1.2.2.1. Kinases

Prior to the discovery of PI kinases in the early 1960s, the phosphorylation of phosphatidylinositol (PtdIns) to phosphatidylinositol 4-phosphate (PI(4)P) and the subsequent phosphorylation of PI(4)P to phosphatidylinositol 4,5-bisphosphate (PI(4,5)P2) were believed to be two separate enzymatic processes. PI kinases were discovered to be the enzymes responsible for catalyzing these phosphorylation reactions,

and their discovery helped clarify the mechanisms involved in the synthesis of PI(4)P and PI(4,5)P_2 in cellular processes (Balla *et al*., 2013).

The phosphoinositide 3-kinase (PI3K) family of lipid kinases are known to regulate multiple cellular functions including cell survival, proliferation, metabolism and migration. PI3Ks are a group of enzymes which play a significant role in phosphorylating the 3-position hydroxyl group on the inositol lipid. They are classified into three different classes based on their substrate specificity (Sasaki *et al*., 2009). The main substrate for class I PI3Ks is phosphatidylinositol 4,5-biphosphate (PI(4,5)P_2), which is converted into phosphatidylinositol 3,4,5-triphosphate (PI(3,4,5)P_3) through phosphorylation. On the other hand, class II PI3Ks phosphorylate PI(4)P to produce PI(3,4)P2, and also generate PI(3)P by phosphorylating PtdIns. Finally, class III PI3Ks specifically target PtdIns to generate PI(3)P (Nakada-Tsukui *et al*., 2019).

PI4-kinases play a crucial role in phosphorylating Ptdlns to generate PI(4)P, a vital precursor for the synthesis of other essential phosphoinositides, such as PI(4,5)P_2 and PI(3,4,5)P_3. Among these, PI(4,5)P_2 acts as the primary substrate for phospholipase C enzymes, leading to the production of key messengers, inositol 1,4,5-trisphosphate [Ins(1,4,5)P3] and diacylglycerol, integral to Ca^{2+} signal transduction (Li *et al.*, 2017). The synthesis of these signaling phosphoinositides relies on the activity of their synthetase and the availability of precursors. Consequently, PI4K serves as a critical regulator capable of modulating various phosphoinositide-dependent signaling pathways and cellular regulatory functions (Li *et al*., 2021).

Another major category of kinases includes the phosphatidylinositol phosphate kinase (PIPK) family of enzymes, which convert singly-phosphorylated phosphatidylinositol derivatives into phosphatidylinositol bisphosphates. PIPKs are further categorized into three types: Type I and Type II, responsible for phosphorylating PI(4)P and PI(5)P, respectively, to generate PI(4,5)P2, while Type III PIPKs produce PI(3,5)P2 from PI(3)P. All PIPKs possess a conserved core domain (PIPKc), a distinctive catalytic domain absent in other kinases (Sasaki *et al*., 2009; Balla *et al*., 2013).

1.2.2.2. Phosphatases

Phosphoinositide (PI) phosphatases, together with PI kinases, play a crucial role in the conversion of through different phosphorylation states. These phosphatases are categorized into two main classes based on their catalytic mechanisms.

The first class includes inositol polyphosphate 5-phosphatases, which function by hydrolyzing the D5 phosphate of the inositol ring in both soluble inositol polyphosphates and membrane-bound PIs (Astle *et al.,* 2006). Within this 5-phosphatase family, members like INPP5A and INPP5B exhibit distinct substrate preferences. For example, INPP5A selectively hydrolyzes the soluble inositol polyphosphates Ins(1,4,5)P_3 and Ins(1,3,4,5)P_4, whereas INPP5B targets PI(4,5)P_2 and PI(3,4,5)P_3 in addition to Ins(1,4,5)P_3 and Ins(1,3,4,5)P_4 (Mitchell *et al.,* 1989; Matzaris *et al*, 1994). Another member, Synaptojanin1 (SYNJ1), is responsible for the hydrolysis of PI(4,5)P_2 on synaptic vesicles at the nerve terminal (Mcpherson *et al.,* 1996; Hsu *et al.,* 2015). Additionally, SHIP1 and SHIP2, were identified to exhibit distinct activities, with SHIP1 acting on PI(3,4,5)P_3 and Ins(1,3,4,5)P_4 in vitro (Damen *et al.,* 1996; Ware *et al*., 1996; Rohrschneider Chi *et al.,*2000; Hsu *et al.,* 2015*),* while SHIP2 hydrolyzes Ins(1,3,4,5)P_4, PI(3,5)P_2, and PI(3,4,5)P_3, but not PI(4,5)P_2 (Chi *et al.,*2004; Pesesse *et al.,* 1998; Hsu *et al.,* 2015).

The second class of PI phosphatase possess a highly conserved CX5R motif within their active site. In this category, the cysteine residue acts as a nucleophile and the arginine residue positions the scissile phosphate group (Hsu *et al.,* 2015). Sub-families within this class include 4-phosphatase, Sac1 domain-containing phosphatase, myotubularin and PTEN.

The first discovered member of the CX5R motif-based phosphatase family exhibited specific hydrolysis of the D4 phosphate of PI(3,4)P_2 using proteins purified from rat brain (Norris *et al.,* 1994). Subsequently, two mammalian genes encoding PI(3,4)P_2 4-phosphatases, INPP4A and INPP4B, were identified (Norris *et al.,* 1995, 1997).

Another member of CX5R motif-based phosphatase family is the Sac1 family, which is known to play a crucial role in various processes. In vitro studies have demonstrated that Sac1 dephosphorylates a number of PIs, including PI(3)P, PI(4)P, and PI(3,5)P_2 (Guo *et al.,* 1999). Sac2 (INPP5F) exhibits 5-phosphatase activity specific for PI(4,5)P_2 and PI(3,4,5)P_3, influencing Akt signaling and heart hypertrophy (Minagawa *et al.,* 2001). Sac3 is a PI-5-phosphatase that hydrolyzes PI(3,5)P2 to generate PI(3)P in-vitro and in-vivo studies (Hsu *et al.,* 2015).

The myotubularin family, consisting of 15 members (MTM1 and MTMRs 1–14), is exclusively found in eukaryotes with a high degree of conservation. The first member of this family, MTM1, is a PI-3-phosphatase, hydrolyzing PI(3)P and PI(3,5)P_2 (Blondeau

et al., 2000). Complete genome sequencing revealed 14 myotubularin-related (MTMR) genes, which together form the largest family of CX5R-dependent PI phosphatases.

The phosphatase and tensin homolog (PTEN) has been studied for its dual specificity in hydrolyzing PI(3,4,5)P_3 to PI(4,5)P_2 and PI(3,4)P_2 to PI(4)P by removing the 3-position phosphate group. Dysfunction of PTEN leads to PIP3 accumulation and uncontrolled activation of downstream signaling, making it a recognized tumor suppressor that inhibits cell growth, survival and motility.

VSPs are PI phosphatases homologous to PTEN, sharing a similar catalytic domain but with different substrate specificities Unlike PTEN, which acts as a 3-phosphatase on PI(3,4)P_2 and PI(3,4,5)P_3, VSPs function primarily as 5-phosphatases on these molecules. This distinction is partially attributed to a residue substitution within the catalytic CX5R motif, where VSP incorporates G365 as opposed to A126 within the PTEN amino acid sequence. Consequently, G365A mutation in VSP abolishes its activity against PI(4,5)P_2 (Iwasaki *et al*., 2008).

1.2.3. PIPs are key regulators in cellular signaling

PIPs regulate diverse cellular activities such as cell growth, proliferation, apoptosis, cytoskeletal changes and vesicle trafficking (Mayinger *et al*., 2012; Falkenburger *et al*., 2010). Their aberrant regulation leads to multiple human diseases. They are known to modulate activity of many integral membrane proteins leading to a multitude of downstream effects.

PI(4,5)P_2 is a major signaling PIP derivative abundantly found at the PM and serves as an important second messenger in intracellular signaling. When Gq proteins are activated, via G protein-coupled receptors (GPCRs) like acetylcholine receptors, they stimulate the activity of phospholipase C (PLC) enzymes, which break down PI(4,5)P_2 into inositol 1,4,5-trisphosphate (IP3) and diacylglycerol (DAG). IP3 acts at the ER, where it activates IP3 receptor/ Ca^{2+} channels that release calcium ions from the ER into the cytosol, while DAG activates protein kinase C (PKC), which in turn can phosphorylate different downstream signaling proteins (Kadamur *et al*., 2013).

PI(4,5)P_2 is also known to regulate many ion channels such as Kir1.1 (ROMK1), Kv7.1 (KCNQ1), Kv7.2/Kv7.3 (KCNQ2/3), HCN, voltage-gated Ca^{2+} channels etc. (Okamura *et al*., 2018). Among these channels, KCNQ2/3 channels are extensively studied due to their important role in regulating neuronal excitability, and reduced activity of these channels has been linked to various disorders such as epilepsy and tinnitus (Kalappa *et*

al., 2015). The regulation of $PI(4,5)P_2$ has garnered substantial research attention due to its indirect modulation of ion channels, which can have significant implications for physiological function in a biological system. Any modulation of ion channels through PIPs may have a notable impact on cellular function. Additionally, disturbances in the distribution of PIs resulting from compromised activity of enzymes involved in PIP metabolism are linked to various cellular pathways associated with diseases (Majerus *et al*., 2009). Non-mammalian voltage-sensitive phosphatases (Ci-VSP) have been demonstrated to possess 5-phosphatase activity against PIPs. Specifically, they dephosphorylate $PI(4,5)P_2$ to PI(4)P in response to membrane depolarization, as demonstrated by Murata *et al*. in 2005. Their ability to modulate the phosphorylation status of $PI(4,5)P_2$ showcases their crucial function in regulating cellular responses to changes in membrane potential

1.3. Voltage sensitive Phosphatases

Mammalian VSPs were first identified in the early 2000s and were named as transmembrane phosphatases with tensin homology (TPTE), due to their homology to the tumor suppressor protein (PTEN) (Guipponi *et al.,* 2001; Walker, *et al.,* 2001; Wu Y *et al.,* 2001). Initially, researchers were predominantly interested in characterizing the PTEN-homologous C-terminal part of the protein, whereas the functional relevance of N-terminal transmembrane domain was not recognized, even though by 2002, a bioinformatic study revealed that the transmembrane region had sequence similarity to the voltage-sensing domain (VSD) of an ion channel (Kumánovics *et al.,* 2002). Only years later, another bioinformatic analysis identified a VSP in the marine invertebrate *Ciona intestinalis* (Ci-VSP) and particularly recognized the homology of the transmembrane N-terminal domain to the VSD of voltage gated ion channels (VGICs), in addition to the C-terminal phosphatase domain similar to PTEN (Figure 3). For the first time, this non-mammalian VSP from *Ciona intestinalis* (Ci-VSP) showed a voltage-dependent phosphatase activity when heterologously expressed in *Xenopus laevis* oocytes (Murata *et al.,* 2005). This discovery was intriguing because the enzymatic activity of the protein was controlled by the VSD unlike the VSD in VGICS, where it was known to work only with the pore-gated domain (Lu Z *et al.,* 2002; Jiang Y *et al.,* 2003). The phosphatase activity of Ci-VSP was probed using fluorescent biomarkers which showed that the enzyme was activated by membrane depolarization, resulting in dephosphorylation of $PI(3,4,5)P_3$ and $PI(4,5)P_2$ (Halaszovich *et al*.,2009). Furthermore,

the 3-phosphatase activity of Ci-VSP was also seen against PIP_2 when heterologously expressed in *Xenopus* oocytes (Matsuda *et al*., 2011).

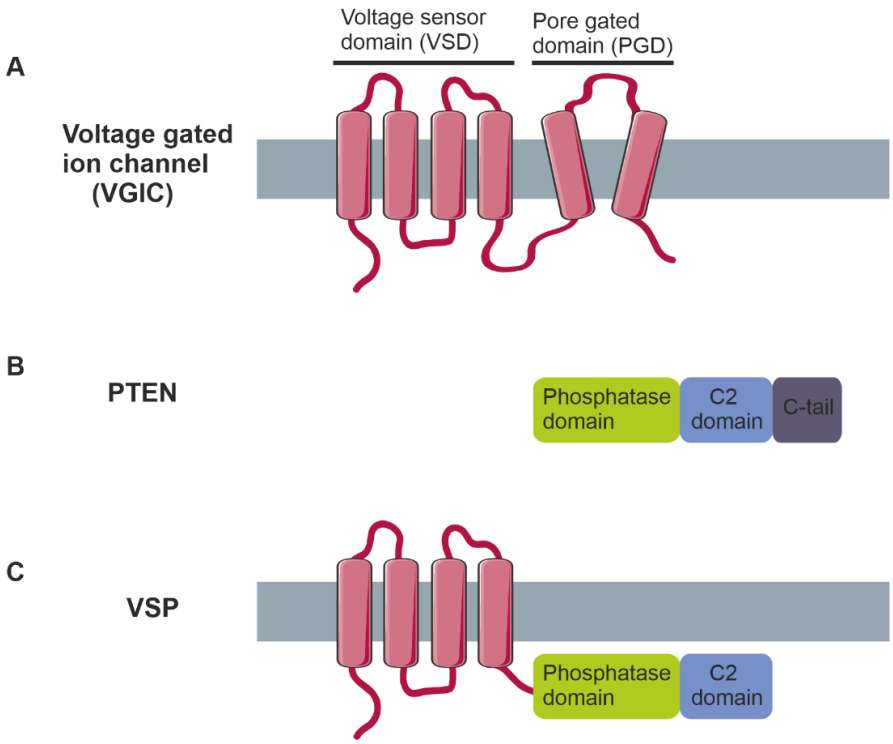

Figure 1.2: Schematic diagram of Voltage gated Ion channel, PTEN and VSP. (A) VGIC containing a VSD (first four transmembrane segments) and a pore gated domain (last two transmembrane segments) **(B).** PTEN consists of a Phosphatase domain (green) attached to a C2 domain(blue) and a C-tail (purple). **(C)** VSP consists of a VSD similar to VGICS attached to a phosphatase domain (green) and C2 domain(blue) similar to PTEN.

Soon after the discovery of Ci-VSP other VSPs were isolated from vertebrates, such as zebrafish (Dr-VSP) (Hossain *et al.*, 2008), *Xenopus* (Ratzan *et al*., 2011), chick (Gg-VSP) (Yamaguchi *et al.*, 2014) and their respective voltage dependent activity was characterized. Most of the non-mammalian VSPs were targeted to PM and showed their voltage dependent enzymatic activity against PIPs when heterologously expressed in mammalian cells. In contrast, the voltage-dependent activity of mammalian VSPs (TPTE, TPIP, mVSP) in heterologous systems is still unclear due to their insufficient targeting to the PM. Therefore, Ci-VSP is the best characterized among other orthologs of VSP due to its robust PM reaching capability in heterologous system and efficient enzymatic activity against PIPs.

1.3.1. Structure of VSP

The voltage-sensing domain of VSP consists of four transmembrane helical segments (S1-S4) (Murata, *et al*., 2005). The positively charged residues in the S4 segment of the VSD are responsible for the voltage-sensing ability of the protein, also observed among other VGICs. The number of charged residues differs between the orthologs of VSPs. An X-ray crystallographic study of Ci-VSP showed that positively charged residues in the S4

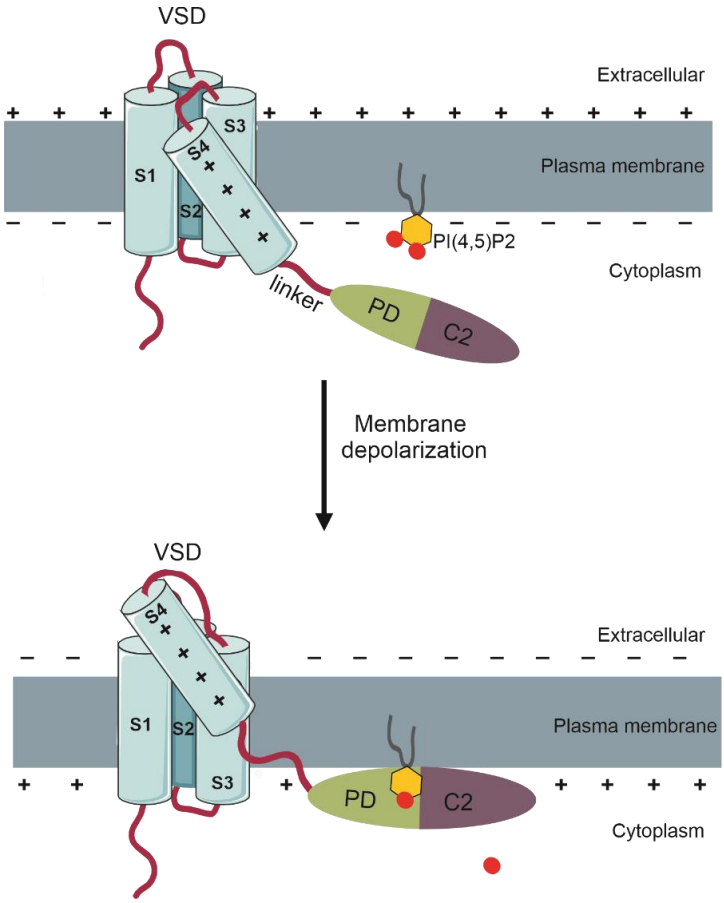

Figure 1.3: Schematic representation of VSP structure and its catalytic activity. VSPs consists of VSD with four transmembrane domains S1-S4 which are fused to the cytoplasmic catalytic domain via a short linker. Upon membrane depolarization, VSD domain is activated and the positively charged arginine residues at the S4 segment act as sensing charges allowing the S4 segment to move upwards. Activation signals are then transmitted from VSD to the phosphatase domain via the linker, which has positively charged residues that allow it to bind to negatively charged head groups at the PM. Upon activation, the phosphatase domain then removes the phosphate group at the fifth position on PI(4,5)P_2.

segment interact with negatively charged residues in the S1 and S3 segments forming a salt bridge that leads to conformational changes in the S4 segment allowing it to undergo upward displacement upon membrane depolarization (Figure 1.3) (Li *et al*., 2014).

X-ray crystallography studies have also successfully determined the structural configuration of the C-terminal portion of Ci-VSP (Matsuda *et al*., 2011 and Liu *et al*., 2012). The enzymatic domain of VSP, located in the cytoplasmic region, consists of a phosphatase domain (PD) and a C-terminal domain, C2. The PD contains an HcX5R motif which is responsible for the catalysis of PIPs and is conserved in all other protein tyrosine phosphatases (PTPs). The cysteine residue within this motif is the most critical residue for the enzymatic activity of the protein and substitution of cysteine with serine abolishes the catalytic activity of VSP. The motif is located within a loop called the phosphatase-binding loop (P loop), which together with the TI-loop (threonine/isoleucine) and the WPD-loop (tryptophane/proline/aspartic acid) forms an active PIP-binding pocket. The C2 domain containing the CBR3 (Calcium-Binding Region3) loop at the extreme C-terminus, is responsible for mediating the interaction between the PD and C2 domains (Figure 1.4).

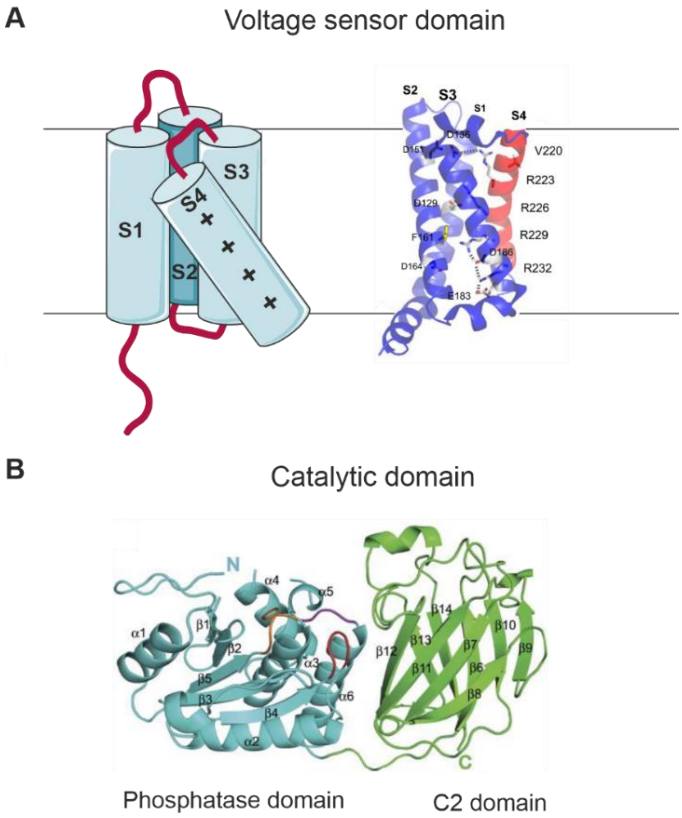

Figure 1.4: Structure of VSD and catalytic domain of Ci-VSP. (A) structure of the VSD of Ci-VSP with four transmembrane domains S1-S4. S4 segment (red) consists of positively charged arginine residues (R223, R226, R229, R232). Modified from (Okamura et al., 2018). **(B)** schematic diagram of catalytic domain of Ci-VSP. The Phosphatase domain (cyan) consist of four β strands and six α helices. The PD also houses the PI-binding pocket, which consists of the P-loop containing the HCKGGK motif (orange), the T1-loop (magenta) and the WPD-loop (red). The PD domain interacts with C2 domain (green) via the CBR3 loop. The C2 domain consists of nine β strands. Image obtained from (Matsuda et al., 2011).

The VSD and the cytoplasmic domain of VSP are connected by an approximately 20 amino acid sequence stretch. This 'linker' region plays a crucial role in modulating the electrochemical coupling between the VSD and the catalytic domain (Liu *et al.,* 2012; Hobiger *et al.,* 2013). The linker serves a dual function in VSP activity. Positively charged amino acids within the linker bind to the negatively charged lipids at the PM, enabling the catalytic domain to come into close proximity with the PM. Additionally, it binds to the PD, thereby facilitating the active substrate-binding pocket (Hobiger *et al*., 2013).

1.3.2. Gene diversity and cellular localization of mammalian and non-mammalian VSPs

VSP genes are present across a variety of animal phyla, including Choanozoa (monosiga), Cnidaria (hydra, sea anemones, nematostella, and coral), Platyhelminthes, Mollusca (octopus, shell, snail, and Aplysia), Annelida, Arthropoda (mites, spiders, and water fleas), Echinodermata (sea urchin and starfish), and Chordata, but not found in bacteria, archaea and plants. There is a single VSP gene in most non-vertebrates, with the exception of *Xenopus laevis,* which has two VSP genes (Xl-VSP1 and Xl-VSP2) (Ratzan *et al.,* 2011). However, in primates, including humans eight VSP like genes have been identified of which only two are known to be functional in in-vitro assays: TPIP (hVSP1) and TPTE (hVSP2) (Chen *et al.,* 1999; Giuponni *et al.,* 2001; Tapparel *et al.,* 2003; Wu *et al.,* 2001). Both hVSP1 and hVSP2 undergo differential exon splicing resulting in multiple isoforms. For hVSP1, four splice variants exist in human testis cDNA, of which only one incorporates the complete VSD and the catalytic domain (Tapparel *et al.,* 2003; Walker *et al.,* 2001; Mishra *et al.,* 2011). Similarly, four variant transcripts of hVSP2 were identified, three of which share a conserved VSD but differ in the size of their N-terminal cytoplasmic region (Chen *et al.,* 1999; Tapparel *et al.,* 2003). The longest forms of hVSP1 (hVSP1 gamma) and hVSP2 (hVSP2 alpha) each have a complete VSD and catalytic domain but demonstrate different cellular localization when heterologously expressed in mammalian cell lines. hVSP2 gamma localizes to the PM, whereas hVSP1 gamma localizes intracellularly. hVSP1 gamma is known to exert phosphatase activity against PIPs in vitro, but the phosphatase activity is absent in hVSP2 (Chen *et al.,* 1999; Tapparel *et al.,* 2003; Walker *et al.,* 2001).

Although the VSD is highly conserved between mammalian and non-mammalian VSPs, the voltage-dependent enzymatic activity has only been experimentally verified in non-mammalian VSPs, possibly due to their unique membrane translocation proficiency.

Therefore, the enzymatic activity and its potential voltage-dependence remains elusive for mammalian VSPs. It was only by using a chimeric approach in which the C-terminal region of hVSP was fused to Ci-VSP that it was shown that the catalytic domain of hVSP has the capability to be regulated by a voltage sensor of Ci-VSP (Halaszovich *et al.*, 2012). Furthermore, a similar chimeric study was done by fusing the catalytic domain of mVSP to Ci-VSP, which showed voltage regulated phosphatase activity towards PIPs (Rosasco *et al.,* 2015). However, the membrane targeting proficiency and voltage-dependent phosphatase activity of complete the protein have not yet been investigated.

1.3.3. Mouse VSP

In *Mus musculus*, the VSP gene has been mapped to chromosome 8 (Guipponi *et al.*, 2001). In the early 2000s, an RT-PCR analysis from cDNA of mouse testis showed the presence of VSP transcripts (Wu *et al.*, 2001). Due to the homology to PTEN, mVSP was initially termed PTEN2. Unlike in human, only one VSP gene is present in mouse. A study in 2015 showed the presence of a splice variant of mVSP lacking exon 9 which exhibited subcellular localization differing from the complete protein, when expressed in heterologous systems (Rosasco *et al*., 2015). It was initially thought that the expression of mVSP was restricted to the mouse testis prior to the discovery of the mVSP in the mouse brain, where it was found to be differentially regulated in young mice (Rosasco *et al.,* 2015).

Mammalian VSPs, including mVSP, have not been thoroughly studied due to their lack of membrane localization in any heterologous expression system studied so far (Walker *et al*., 2001; Tapparel *et al.,* 2003; Halaszovich *et al*., 2012; Rosasco *et al*., 2015). A study conducted in 2001 demonstrated the presence of mVSP in the Golgi apparatus, while subsequent studies indicated its localization in the ER when expressed heterologously in mammalian cell lines (Wu *et al*., 2001). Despite their structural similarity to Ci-VSP, which targets to the PM, the reason for the intracellular localization of mammalian VSPs is still unclear. To address this issue, we characterized mVSP in terms of its membrane targeting ability. In general, there are multiple factors for a protein to be restricted to intracellular compartments, such as improper folding or organelle-specific retention signals, which we aimed to investigate and address in our study.

1.3.4. Gene expression and Physiological role of VSPs

VSP gene expression studies have been performed across various animal species, revealing the highly conserved nature of VSPs. RT-PCR studies have indicated the

expression of VSP in early developmental stages of frog, *Xenopus laevis* (Ratzan *et al*., 2011); zebrafish, *Danio rerio* (DR-VSP) (Hossain *et al.*, 2008); chick, *Gallus gallus* (Gg-VSP) (Yamaguchi *et al.*, 2014); mouse, *mus musculus* (mVSP) (Wu *et al.*, 2001); and human, *Homo sapiens* (hVSP) (Chen *et al*., 1999). Despite these findings, the precise cellular localization and biological function of VSP in its native environment have remained elusive. A recent study conducted by the Okamura group suggest that the VSP plays a major role in regulating the sperm motility by controlling the polarized distribution of $PI(4,5)P_2$ by responding to changes in voltage. Mouse sperm express the PIP-sensitive potassium channel slo3, which is localized at the PM in the principal piece of sperm flagellum. This channel indirectly enhances calcium influx during capacitation, a process essential for fertilization. Interestingly, it was observed that VSP-deficient sperm exhibited increased calcium influx upon capacitation compared to sperm with heterozygous deficiency for VSP. Furthermore, the distribution of PIP_2 was found to be uneven in wild-type sperm tails, with a higher concentration in the midpiece rather than the principal piece, where mVSP and slo3 channels are located. However, VSP-deficient mice did not display this polarized PIP_2 distribution. These observations suggest that mVSP plays a crucial role in the regulation of PIP_2 distribution, which in turn influences ion channel activity and sperm motility.

1.4. Aim of the study

This study aims to accomplish the following objectives:

1. Investigate the PM targeting mechanism of mouse VSP in a heterologous expression system, addressing the current knowledge gap in this area.
2. Characterize BSG as a potential interaction partner of mVSP, employing the split-ubiquitin membrane yeast two-hybrid system, co-immunoprecipitation experiments, immunocytochemistry, and live-cell imaging in the heterologous expression systems.
3. Perform dissection studies on BSG to identify the region responsible for its effect on mVSP.
4. Conduct truncation studies on mVSP to elucidate the factors contributing to its intracellular localization by dissecting its C- and N-terminal regions.

5. Utilize a chimeric approach by fusing the N- and C-terminal regions of mVSP with Ci-VSP to identify the regions or domains responsible for its retention in the endoplasmic reticulum.
6. Investigate the voltage-dependent catalytic activity of mVSP in ROMK flip in HEK293 cells by enhancing the surface expression of mVSP through BSG.

2. Material and Methods

2.1. Materials

2.1.1. Chemicals and Reagents

Table 3: List of chemicals and reagents used in this study.

Name	**Manufacturer**
6x Loading Dye Solution	Fermentas
Acetic acid	Carl Roth
-Ade/-His/-Leu/-Trp DO Supplement	Takara Bio
Acrylamide/ Bisacrylamide Solution	Carl Roth
Adenine sulphate	Sigma
Agarose	Sigma
Ammonium persulfate (APS)	Carl Roth
BSA: albumin fraction V	Carl Roth
Calcium chloride dihydrate	Merck
Dimethyl sulfoxide (DMSO)	Sigma
dNTPs (100mM)	Thermo-scientific
GelRed Ethylenediaminetetraacetic Acid (EDTA)	Sigma
Ethanol	Carl Roth
GelRed (10,000x in water)	Biotium
Glycerol	Sigma
HEPES	Sigma
LB agar	Carl Roth
LB medium	Carl Roth

-Leu/-Trp/-His DO Supplement	Takara Bio
-Leu/-Trp DO Supplement	Takara Bio
-Leu DO Supplement	Takara Bio
Lithium acetate dihydrate	Sigma
Magnesium chloride hexahydrate	Sigma
Minimal SD Base	Takara Bio
Nitrocellulose Membrane	GE health care
Polyethylene Glycol (PEG)	Sigma
Protease inhibitor cocktail	Roche
Potassium chloride (KCl)	Merck
Sodium chloride (NaCl)	Carl Roth
Sodium Dodecyl Sulfate (SDS)	Roth
Sodium pyruvate	Sigma
N'N'N'N Tetramethylethylenediamine (TEMED)	Roth
Theophylline	Sigma
Tris-Base	Carl Roth
YPD Broth	Sigma
Tween 20	Roth
Triton X-100	Sigma Aldrich

2.1.2. Kits

Table 4: List of kits used in this study.

Name	**Manufacturer**
PfuUltra II Hotstart PCR Mastermix	Agilent
AmpliTaq Gold DNA-Polymerase Kit	Applied Biosystems

DNA Clean and Concentrator	Zymo Research
E.Z.N.A. Plasmid Mini Kit I	Omega Bioscience
QIAGEN Plasmid Plus Midi Kit	Qiagen
Zymoclean Gel DNA Recovery Kit	Zymo Research
2x Phusion High-Fidelity PCR Mastermix	Thermo Scientific
Pierce BCA Protein Assay Kit	Thermo Scientific
SuperScript II Reverse Transcriptase	Thermo Scientific
Quick-RNA Miniprep Kit	Zymo Research

2.1.3. Buffers and solutions

Table 5: 50X TAE (Tris/acetate/EDTA) electrophoresis buffer recipe.

Component	**Amount**
Tris	252 g
Acetic acid conc.	57 mL
0.5M EDTA (pH = 8.0)	100 mL
H_2O	ad 1 l

Table 6: Liquid Broth (LB) Medium recipe

Component	**Amount**
LB medium	25 g
H_2O	ad 1 l

Table 7: LB Agar recipe

Component	**Amount**
LB Agar	40 g
H_2O	ad 1 l

Table 8: Yeast Peptone Dextrose (YPAD) medium recipe

Component	**Amount**
YPD Broth	50 g /L
Adenine sulphate	40 mg/ L
H_2O	ad 1 l

Table 9:Synthetic Defined (SD) Medium recipe

Component	Volume / Concentration
SD medium	27 g/l
dropout mix	600-700 mg/l

Table 10: SCE (Sorbitol/Na citrate/EDTA) solution 100mL recipe

Component	Volume / Concentration
Sorbitol 1M	18.2 g
Na citrate pH 7.6 0.1M	2.94 g
EDTA 60 mM	2.23 g

Table 11: SCE / Zymolase / 2-mercaptoethanol solution recipe for x plasmid

Component	Volume / Concentration
SCE solution	x * 250 µl
Zymolase	x * 3 µl
2 ME	x * 0.5 µl

Table 12: Potassium acetate solution recipe

Component	Volume / Concentration
Potassium 5M	60 ml
Acetic acid conc.	11.5 ml
ddH2O	28.5 ml

Table 13: Western blotting buffer (Towbin) recipe

Component	Volume / Concentration
Tris	5.82 g
Glycine	2.93 g
10% SDS	3.75 ml
Methanol	200 ml
Filtered water to total volume	1 l

pH adjusted to 8.3

Table 14:10X SDS-PAGE electrophoresis buffer recipe

Component	Volume / Concentration
Tris	1.5 M
Glycine	52 mM
SDS	17 mM
Filtered water to total volume	1 l

Table 15: SDS gel loading buffer (2x) recipe

Component	Volume / Concentration
Tris-Cl (pH 6.8)	1.5 M
Bromophenol blue	0.01% (v/w)
SDS	4% (v/v)
Glycerol	20% (v/v)
DTT (dithiothreitol)	100mM

2.1.4. Equipment

Table 16: Equipment used in this study.

Name	Manufacturer
Agarose gel electrophoresis system	Pharmacia biotech
Large capacity centrifuge	Rotanta 460r, Hettich
Benchtop centrifuge	Biofuge Fresco 16, Heraeus
Electroporator	Micro Pulser, Bio-Rad
Confocal microscope	ZEISS 710 LSM
TIRF microscope	DMi8 upright microscope with TIRF module, Leica
Digital pH meter	766 Laboratory pH Meter, Knick
PCR Thermocycler	T 100 Thermal cycler, Bio-Rad
Power supply	PowerPac™ HC High-Current Power Supply, Bio-Rad
SDS gel system	Mini-PROTEAN Tetra Vertical Electrophoresis Cell, Bio-Rad
Semidry blotter	Transblot Turbo, Bio-Rad
Nanodrop	SmartSpec®3000, Biorad Nanodrop 2000c, Thermo Scientific
Chemidoc system	Chemidoc MP, Bio-Rad
Microplate reader	Sunrise Remote, Tecan

FACS sorter	FACS Aria III, BD Bioscience
Osmometer	Osmomat 030, Gonotec
CO2 incubator	Function Line BB 16, Heraeus
Bacterial incubator	Eltest T1, Noctua

2.1.5. Data analysis Software

Table 17: List of software used in this study

Product	**Source**
Zen 3.0	Carl Zeiss
Prism7	GraphPad
Image Lab	Biorad
Fiji	Open source
CorelDraw Graphic suite	CorelDraw
SnapGene Viewer	SnapGene
LAS X	Leica
Chromas	Technelysium

2.1.6. cDNA library

Mouse brain cDNA library (NubG-x) was obtained from MoBitec.

2.1.7. Cell lines

Henrietta Lacks (HeLa), Human embryonic kidney cells (HEK293), Chinese hamster ovarian cells (CHO), Stably integrated FRT site in Human embryonic kidney cells (HEK Flp-In 293)

2.1.8. Length Standard

DNA markers: Lambda DNA / Eco47I (AvaII) Marker, 13 (0,5µg / µl) – Fermentas.

Protein Markers: Prestained Peq gold V, 10-250 kDa (100-200ng / µl)- Avantor.

2.1.9. Standard Oligonucleotide sequencing Primers

Table 18: List of DNA oligos used for PCR amplification and sequencing.

Primer name	**Primer sequence**
pEGFP-N-for	CGTCGCCGTCCAGCTCGACCAG
pEGFP-C-for	CATGGTCCTGCTGGAGTTCGTG
T7	TAATACGACTCACTATAGGG
pCDNA3.1 rev	CTCTGGCTAACTAGAGAAC
pPR3N-for	GTCGAAAATTCAAGACAAGG

pPR3N-rev	AAGCGTGACATAACTAATTAC

2.1.10. Antibodies

Table 19: List of antibodies used in this study

Name	Company	Catalogue Number
Mouse anti GFP	Santa Cruz Biotechnology	sc-9996
Rabbit anti Myc	Cell Signaling	2278
Mouse anti flag	Sigma	F3165
Mouse anti HA	Sigma	H3663
anti- mouse IgG IR Dye CW800	LICOR	926-32210
anti- Rabbit IgG IR Dye CW800	LICOR	926-32211
anti- Rat IgG IR Dye CW800	LICOR	926-32219
Alexa Fluor 488 Goat anti Mouse	Thermo Scientific	A-11029
Alexa Fluor 594 Goat anti Mouse	Thermo Scientific	A-11032

2.1.11. Constructs and plasmids

Table 20: List of expression vectors used in this study.

	Gene	Accession nr.	Construct	Source
Live cell Imaging	mVSP	NM_199257.2	• mVSP-pEGFPC1 • mVSP K515 stop-pEGFPC1 • mVSP E451 stop-pEGFPC1 • mVSP D426 stop-pEGFPC1 • mVSP Y417 stop-pEGFPC1 • mVSP Y410 stop-pEGFPC1 • mVSP K352 stop-pEGFPC1 • mVSP Q331 stop-pEGFPC1 • mVSP Y417N-pEGFPC1 • mVSP R420S-pEGFPC1 • mVSP Y417N, R420S-pEGFPC1 • mVSP RRR418,420,421	generated in Oliver lab

			AAA-pEGFPC1 • mVSP(412-416 Ci-VSP)-pEGFPC1 • mVSP M60 start-pEGFPC1 • mVSP M110 start-pEGFPC1 • mVSP M160 start-pEGFPC1 • mVSP M188 start-pEGFPC1 • mVSP M204 start-pEGFPC1 • mVSP ΔExon9-pEGFPC1	
	Ci-VSP/ mVSP	Chimeras	• $_{mVSP}$-mVSP-$_{Ci\text{-}VSP}$-pEGFPC1 • $_{Ci\text{-}VSP}$-mVSP-$_{mVSP}$-pEGFPC1 • $_{Ci\text{-}VSP}$-mVSP-$_{Ci\text{-}VSP}$-pEGFPC1 • $_{Ci\text{-}VSP}$-CiVSP-$_{mVSP}$-pEGFPC1 • $_{mVSP}$-CiVSP-$_{mVSP}$-pEGFPC1 • $_{mVSP}$-CiVSP-$_{Ci\text{-}VSP}$-pEGFPC1	generated in Oliver lab
	mBSG	NM_001077184.1	• BSG-pRFPN1 • BSG ΔIg-pRFPN1 • BSG ΔCter -pRFPN1 • BSG E222D-pRFPN1 • BSG E222Q-pRFPN1 • BSG E222K-pRFPN1 • BSG-myc-pCDNA3.1	generated in Oliver lab
	hBSG	NM_001322243.2	• hBSG-pRFPN1	generated in Oliver lab
	mEMB	NM_010330.4	• mEMB-pRFPN1	generated in Oliver lab
	mNPTN	NM_009145.2	• mNPTN-pRFPN1	generated in Oliver lab
	βGlycosyl-transferase	NM_001497.3	• βGlycosyltransferase-pDsRed	generated in Oliver lab

	PLCδ1	NM_006225.3	• PLCδ1-PH-pRFP	Várnai and Balla, 1998; obtained from T. Balla
	Lyn11	a.a. 1–11 of Lyn; GCIKSKGKDSA	• Lyn11-pDsRed	generated in Oliver lab
Yeast-two-hybrid Analysis	mVSP	NM_199257.2	• mVSP-pBT3N	generated in Oliver lab
	mBSG	NM_001077184.1	• BSG-pPR3C	generated in Oliver lab
	ALG5	X77573.1	• pAI-Alg5 • pDL2-ALg5	Obtained from MoBiTec kit
Protein Biochemistry	mVSP	NM_199257.2	• mVSP-pEGFPC1 • 3xflag-mVSP-pCDNA3.1	generated in Oliver lab
	mBSG	NM_001077184.1	• Flag-BSG-pCDNA3.1 • BSG-pEGFPN1 • BSG-pRFPN1 • BSG ΔIg- myc-pCDNA3.1 • BSG ΔCter- myc-pCDNA3.1 • BSG E222D- myc-pCDNA3.1 • BSG E222Q- myc-pCDNA3.1 • BSG E222K- myc-pCDNA3.1 • BSG-myc-pCDNA3.1	generated in Oliver lab
High K^+ experiments in ROMK Flp-In HEK293 cells	mVSP	NM_199257.2	• flag-mVSP-pRFPC1 • flag-mVSP C458S-pRFPC1	generated in Oliver lab
	BSG	NM_001077184.1	• BSG-myc-pCDNA3.1	generated in Oliver lab
	PLCδ1	NM_006225.3	• PLCδ1-PH-pEGFPN1	Várnai and Balla, 1998; obtained from T. Balla
	TAPP1	NM_001001974.4	• TAPP1PH-pEGFPC1	Kimber *et al.*, 2002
Immunocyto chemistry	mVSP	NM_199257.2	• mVSP ExHa-pEGFPC1	generated in Oliver lab
	mBSG	NM_001077184.1	• BSG-myc-pCDNA3.1	generated in Oliver lab

2.2 Methods

2.2.1 Split-ubiquitin yeast two-hybrid system

The Split ubiquitin yeast two-hybrid (Y2H) membrane kit from MoBiTec was utilized for screening mVSP interaction partners. This assay enables the researchers to use full-length integral membrane proteins as baits, and allows for detection of interactions with membrane-associated proteins or other integral membrane proteins in their native environment.

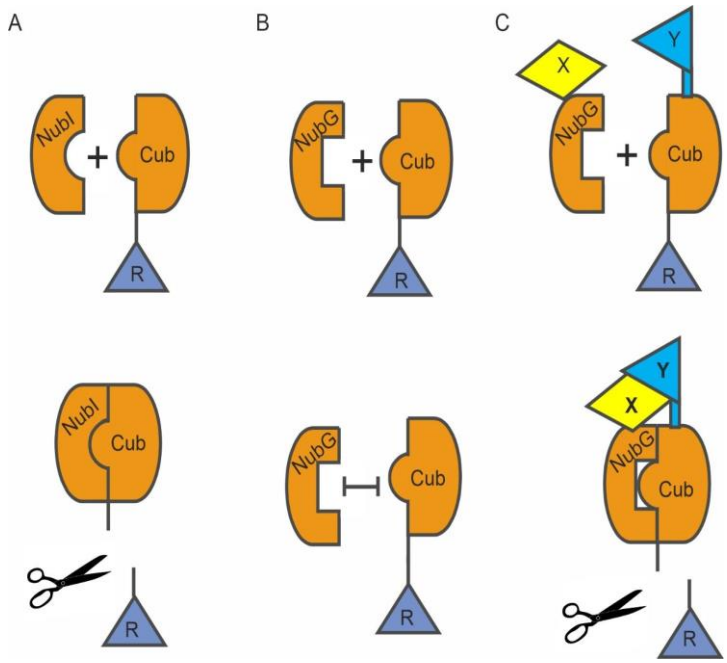

Figure 2.1: Split-ubiquitin system approach. (A) If wild type ubiquitin is split into an N-terminal fragment (Nub, light orange semi-circle) and a C-terminal fragment (Cub, red orange semi-circle), the two halves will spontaneously associate. If a reporter construct is attached to the N-terminal of Cub (triangle, R), ubiquitin specific proteases (UBPs, scissors) will cleave the reporter from Cub upon re-association of ubiquitin. **(B)** If a mutation is generated in the Nub portion of ubiquitin (NubG), the NubG and Cub portions no longer spontaneously associate and therefore the reporter remains associated with the Cub domain. **(C)** If interacting proteins X and Y are fused to the NubG and Cub domains, the interaction between X and Y brings the NubG and Cub domain into close proximity which causes partial re-association of ubiquitin, recognition by the UBPs and release of the reporter from the membrane (modified from Fetschko *et al*., 2004)

The Y2H membrane protein system is based solely on the reconstitution of a protein called ubiquitin (Hershko *et al*, 2005). In this case, ubiquitin is separated into two halves called Nub (N-terminal ubiquitin) and the Cub protein (C-terminal ubiquitin). In general, when the two halves are expressed in the yeast cell, they have a strong affinity for each other. The strong affinity between wild type Nub and Cub is due to the isoleucine at position 3 of the Nub protein (also termed Nub I). A point mutation at NubI introduced by exchanging an isoleucine for glycine (NubG) terminates the strong interaction of Nub (NubG) towards Cub. As a result, the mutant Nub has almost no affinity for Cub when

co-expressed in the same cell.

In order to detect a protein interaction, membrane protein of interest (the bait) is fused to one half (Cub) and the artificial transcription factor LexA-VP16. A second protein of interest (the prey) is fused to the mutant Nub (NubG). When the two proteins (bait and prey) interact with each other, Nub G and Cub come into close proximity and re-form a complete split ubiquitin complex again. This reconstituted ubiquitin is then recognized by Ubiquitin-specific Proteases (UBPs). UBPs cleave the polypeptide chain between Cub and LexA-VP16, resulting in the release of the artificial transcription factor from the Cub which then translocates into the nucleus, where it leads to the expression of the reporter genes HIS3, ADE2 and lacZ (figure 2.4). The lacZ gene encodes for β-galactosidase. The activation of HIS3 and ADE2 allows the yeast to grow on minimal medium lacking histidine and adenine. Thus, the interaction between bait and prey results in growth of yeast on selective medium.

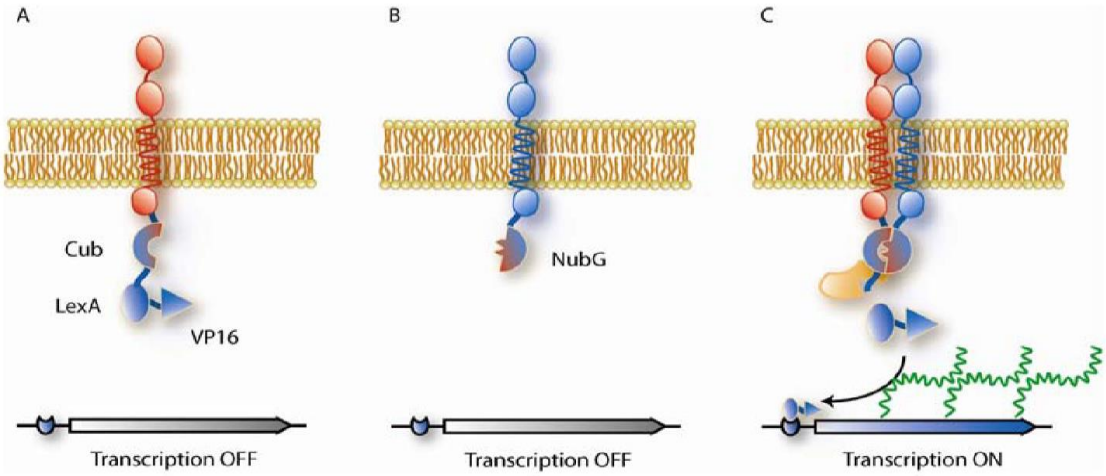

Figure 2.2: Principle of yeast two-hybrid system. The interaction between the bait protein and the prey protein brings the N-terminal and C-terminal of the cleaved ubiquitin into close proximity. UBPs reconstitute the ubiquitin and release the transcription factor LexA-VP16, which then translocates to the nucleus, resulting in the activation of reporter genes (modified from MoBiTec manual.

The fusion of the bait (mVSP) to the corresponding split-ubiquitin half (Cub) was achieved by cloning the gene segments between Sfi interfaces into a yeast expression vector called pBT3C. Whereas the prey (mouse brain CDNA library) obtained from MoBiTec was cloned into pPR3N (NubG) vector according to manufacturer's guidelines. Protein–protein interaction was determined by growth on plates lacking the amino acids leucine, tryptophan, histidine, (–LWH). Positive colonies were further verified using the

second marker galactosidase.

2.2.1.1 Transformation of Bait and Prey vectors into Yeast strain (NMY51)

Bait and prey vectors were transformed in to yeast, 50 ml YPAD medium was inoculated with several colonies of NMY51 yeast strain and allowed to grow overnight at 30 °C with shaking. The next morning, Optical density (OD) of the culture was measured at 600 nm. The culture grown overnight was diluted to OD 0.2 and re-grown at 30°C with shaking until the OD reached 0.6. The 50 ml of re-grown culture was pelleted by centrifugation at 2500 g for 5 minutes and resuspended in 2.5 ml of distilled water.

Table 21: PEG/LiOAc Master mix.

Component	Amount
50 % PEG	x 240 µl
1M LiOAc	x 36 µl
denatured salmon sperm	25 µl

300 µl of PEG/LiOAc master mix (prepared as mentioned above), 100 ul of yeast suspension and 0.5 µg of the bait and prey vectors were mixed in microcentrifuge tube, vortexed thoroughly for 20 seconds and incubated at 42 °C for 45 minutes. Thereafter, the reactions were pelleted by centrifugation at 1500 x g for 5 minutes. The supernatant was discarded and the pellet was resuspended in 100 µl of 0.9 % NaCl and plated on selective medium lacking tryptophan and leucine (SD-LW) plates. Plates were incubated at 30 °C for 3 days.

2.2.1.2 Plasmid isolation from yeast

Yeast colonies expressing the bait and prey plasmids on SD-LWH plates were identified and harvested in 3 ml of SD-LW medium by shaking overnight at 30°C in order to isolate the plasmids from the yeast cells. The yeast cells containing the desired plasmids were then pelleted at 5000 rpm for 5 minutes, incubated at 37°C for 1 hour, and the pellet was resuspended in 200 µl of solution containing SCE/zymolase/2ME mixture. The mixture was then mixed with 400ul of 0.2N NaOH/ 1% SDS and incubated on ice for 5 minutes. 300 µl of cold potassium acetate (3m K/5M LioAC) solution was added and again incubated on ice for 5 minutes. Reaction tubes were centrifuged for 2 minutes at 13000 x g; supernatant was collected in a fresh microcentrifuge tube and mixed with 300µl of isopropanol and 30 µl of sodium acetate, briefly vortexed and incubated at room temperature for 5 minutes. This was followed by a centrifugation step at 13000 x g for 5

minutes, then the pellet was washed with 70% ethanol, dried, and resuspended in 30 µl of sterile water.

2.2.1.3 X-gal assay

The X-gal assay was used to determine the strength of protein interactions in the yeast expression system. The transcription factor LexA-VP16 is released upon interaction between two proteins, leading to activation of the growth reporter genes HIS3, ADE2 and the color reporter gene lac Z. The lac Z gene encodes the enzyme β-galactosidase, which converts the colorless substrate x-gal into a blue compound called 5,5'-dibromo-4,4'-dichloro-indigo, indicating a strong protein interaction.

Overlay mix was prepared and incubated in 50 °C water bath for 30 minutes.

Table 22: X-gal overlay mix.

Component	Volume / Concentration
Agarose	5 g / L (0.5%, w / v)
X-Gal-Stock-Solution (10%)	1 mL (1 mg / mL)
1 x PBS pH 7.4	ad 1 l

Yeast colonies were transferred from SD-LW plates onto Whatman filter paper by placing the filter paper directly on the agar plate for 10 minutes. The filter paper was then frozen in liquid nitrogen for 5 minutes and thawed in a petri dish at room temperature. The filter paper was overlaid with an overlay mix containing X-Gal substrate. The strength of interaction between proteins was determined by the time it took for the colonies producing β-galactosidase to turn blue, which varied from 30 minutes to 8 hours during library screening, depending on the intensity of the blue color development.

2.2.1.4 Conformation of positive interactors

To reduce false positive clones in the Y2H membrane system, the bait and prey vectors were re-transformed into a yeast expression system. Each vector (500 ng) was retransformed into yeast cells and plated on SD-LW plates, which were incubated for 2 days at 30°C. A single colony was picked from the grown SD-LW-plates and resuspended in 20 µl of NaCl. A 2 µl resuspended pellet was then spotted on fresh SD-LW and SD-LWH plates and incubated at 30°C for 2 days. Interactors that grew on the SD-LWH plates were considered true positives.

2.2.2. Molecular biology

2.2.2.1. Polymerase chain reaction (PCR)

Polymerase chain reaction (PCR) was used to amplify a specific region of a DNA fragment. All PCR reactions were carried out using a T100 Thermal Cycler (Bio-Rad). The reaction mixture was pipetted into a PCR tube as described below:

Table 23: PCR Reaction Mixture

Component	Volume/ Concentration
DNA template (100ng)	1µl
Primer for (10mM)	2.5µl
Primer-rev (10mM)	2.5µl
Phusion DNA polymerase	0.25µl
5X PCR buffer	5µl
dNTP (2mM)	2.5µl
DMSO	0.75µl
H_2O	10.5µl
Total	25µl

The Polymerase Chain Reaction (PCR) employs thermal cycling to amplify DNA fragments, exposing the reaction mixture to different temperatures in repeated cycles. In the initial step, the double-stranded DNA template is denatured by heating at 95°C, yielding single-stranded DNA (ssDNA) that is amplifiable. Subsequently, the temperature is lowered to facilitate primer hybridization, during which oligonucleotide primers anneal to complementary sites on the single-stranded target DNA. Finally, the temperature is raised to 72°C, at which point Phusion DNA polymerase initiates DNA synthesis by adding deoxynucleotide triphosphates (dNTP's) from the 3'-OH group of the ssDNA. As this cycle is repeated, multiple copies of the desired DNA fragment are generated.

Table 24: Thermo Cycling Condition for PCR reaction

Cycling Condition	Cycles	Temperature	Duration
Activation of the polymerase	1	96 °C	30 s
Denaturation	25	96 °C	30 s
Primer annealing		55 °C	1 min
Elongation		72 °C	1kb / min
End elongation	1	72 °C	2 min
Cooling		4 °C	∞

Following completion of the PCR reaction, the parental methylated template DNA was digested by incubating it with 1 µl of Dpn1 enzyme to reduce background, at 37°C for 1 hour.

2.2.2.2. Reverse transcription polymerase chain reaction.

The total RNA of HeLa, HEK293 and COS7 cells was isolated by using the (Quick-RNA Miniprep Kit, Zymo Research, Freiburg, Germany). The RNA was reverse transcribed into cDNA by using Superscript II reverse transcriptase (Invitrogen). RT-PCR was performed with AmpliTaq Gold DNA polymerase (Applied Biosystems, Darmstadt, Germany) using the following intron-spanning primers:

Table 25: Gene specific primers for Reverse transcription polymerase chain reaction

Gene	**Primer sequence**	
BSG	sense	5′-TCACTACCGTAGAAGACCTTGG-3′
	antisense	5′-TCTCAATGTGTAGCTCTGACCG-3′
NPTN	sense	5′- GTGAGTGTGCTGAGAATAACCC-3′
	antisense	5′- TTGTTCTCACTCCGTTTATGGC-3′
EMB	sense	5′- GCCTTTTACAAGTCCACCTCTC-3′
	antisense	5′-ACAGGAACCTTTACACTCCCAT-3′
GAPDH	sense	5′-CATCACCATCTTCCAGGAGCGA-3′
	antisense	5′-GTCTTCTGGGTGGCAGTGATGG-3′

PCRs were performed with the following program: (95°C, 10 min) × 1 cycle, (95°C, 40 s; 55°C, 40 s; 72°C, 1 min) × 30 cycles, and (72°C, 5 min) × 1 cycle. The identity of all PCR products were confirmed by sequencing.

2.2.2.3 Purification of PCR products

All PCR products were purified using the DNA Clean & Concentrator kit (Zymo Research), following the manufacturer's protocol. An appropriate volume of DNA binding buffer was mixed with the PCR reaction and the resulting mixture was transferred to a DNA binding column. After centrifuging the PCR reaction mixture at 10,000 x g for 1 minute, the DNA was bound to the column. The column was then washed twice with 750 µL DNA wash buffer, and the bound DNA was finally eluted with 30-50 µl of elution buffer.

2.2.2.4 Agarose gel preparation and Gel electrophoresis

To separate DNA fragments according to size, gel electrophoresis was performed on 1-2% agarose gels. A desirable amount of agarose (1%, 1 g dissolved in 100 ml) was dissolved in an appropriate amount of TAE buffer and the mixture was microwaved for a few minutes. 10 µl of GelRed (a DNA staining dye, diluted 1:10,000) was added, and the entire mixture was poured into the casting tray with appropriate combs. The gels were allowed to solidify at room temperature and then stored at 4°C for later use.

For loading DNA samples onto the 1% gel, 6x loading buffer (Fermentas) was mixed with the DNA. To estimate the size of the DNA fragments, 5µl of DNA size marker was loaded into a neighboring well. Electrophoresis was performed at 80 V for 30 minutes. After the completion of electrophoresis, the gels were visualized under UV light and documented using documentation software.

2.2.2.5. Gel extraction and Purification

The DNA samples were mixed with gel loading buffer and loaded onto a 1% agarose gel for gel electrophoresis. To purify the DNA, the Gel DNA Recovery kit (Zymo Research) was used, following the manufacturer's instructions. The desired DNA band was excised from the gel under UV light, and the excised gel containing the desired DNA fragment was transferred to a fresh microfuge tube. It was then dissolved in an appropriate amount of ADB buffer at 55°C for 7 minutes with shaking. The melted agarose solution was applied onto a DNA binding column and centrifuged at 10,000 x g for 1 minute. The flow-through was collected and discarded. The DNA-bound column was further washed twice with 200 µl of Wash Buffer, followed by elution with 30-50 µl of elution buffer.

2.2.2.6. Restriction digestion and Ligation

To clone the desired DNA fragment into the vector, both the vector and the DNA fragments were digested with the appropriate restriction endonucleases. For most of the cloning procedures, FAST digest restriction enzymes (Fermentas) were used. The restriction digestion was performed by incubating 1-2 µg of DNA with 1 µl of enzyme at 37°C for 1 hour. For Sfi1, special conditions were used, following the manufacturer's instructions at 50°C (New England Biolabs).

Table 26: Restriction digestion reaction (10µl) with Fast Digest enzymes.

Component	Volume / Concentration
DNA (~ 1-2 µg)	x µl
10x Fast Digest restriction buffer	1 µl
Restriction enzyme	1 µl (10U /µl)
DNase free water to total volume	10 µl

Table 27: Restriction digestion reaction (10µl) with Sfi 1 enzyme.

Component	Volume / Concentration
DNA (~ 2-3 µg)	x µl
Smart cut buffer	1 µl
Restriction enzyme Sfi-1	1 µl 10(U /µl)
DNase free water to total volume	10 µl

Alkaline phosphatase (AP) treatment for plasmid vectors

To prevent re-ligation of plasmid vectors in ligation reactions the 5' phosphate group of the plasmid vector was removed using alkaline phosphatase. The restriction digested plasmid vectors were treated with alkaline phosphatase enzyme for 20 minutes at 37°C. The phosphatase treatment was terminated by incubating the reaction mixture at 75 °C for 5 minutes.

Ligation

For all ligation reactions, T4 DNA ligase from New England Biolabs was used. The ligation mixture was incubated at room temperature for 1 hour, after which it was transformed into the desired competent bacterial cells.

Table 28: Ligation reaction mixture.

Component	Volume / Concentration
DNA fragment (insert)	6 µl
Digested vector	2 µl
10x T4 ligase buffer	1 µl
T4 DNA Ligase 400000U/ µl	1 µl
Total	10 µl

2.2.2.7. Electrocompetent cells preparation

To prepare electrocompetent cells, 50 µl of E. coli strain XL-1 blue was inoculated into 4 ml of LB medium and incubated for 16-18 hours at 37°C using a shaker. The inoculated culture was then transferred to a pre-heated flask containing 400 ml of LB medium. Cells were allowed to grow at 37 °C with vigorous shaking at 200 rpm until an optical density OD 600 of 0.5-0.7 was reached. All steps were performed on ice in order to minimize the damage to the bacterial cells. The culture flask was divided into four 50 ml tubes and centrifuged at 3500 x g for 10 minutes at 4 °C. The pellet obtained after centrifugation was washed with double-distilled autoclaved water by gentle pipetting up and down, followed by centrifugation. Thoroughly washed bacterial pellets were gently resuspended in 25 ml of cold solution containing 10% glycerol. The centrifugation step was repeated one more time with 15 ml of cold solution containing 10 % glycerol. Finally, the pellet obtained was resuspended in the remaining glycerol by pipetting. The competent cells were then aliquoted in small volumes (100 µl) into microcentrifuge tubes and stored at -80 °C for later use.

2.2.2.8. Transformation of DNA into competent E. coli cells.

Chemical transformation

DH5α strain was used for chemical transformations. For a single transformation 4-5 µl of plasmid DNA sample was mixed with 50 µl of chemically competent cells (DH5 α) and incubated on ice for 30 minutes. The mixture was then subjected to heat shock at 37 °C for 30 sec and incubated on ice for a further 2 min. Finally, 900µl of LB medium was added and incubated at 37 °C on shaking at 250 rpm for 1 hr. Subsequently, the cells were centrifuged at 10,000 rpm for 1 min and plated on to LB agar plates containing suitable antibiotic. Plates were incubated overnight at 37 °C for selecting single colonies.

Electroporation

Electrocompetent bacterial cells (XL1 Blue) were thawed on ice for 5 min. Purified ligation mixture or plasmid DNA was added to the electroporation cuvettes containing 50 µl of electrocompetent cells. Current pulses were applied using an electroporator following the manufacturer's recommendations. Finally, 900 µl of LB medium was added to the electroporation mixture and transferred in to microcentrifuge tube. The cells were then incubated in a shaker at 37 °C for 1 hour. 100 µl of transformed cells were plated on agar plates containing appropriate selection antibiotics and allowed to grow overnight at 37 °C.

2.2.2.9. Extraction of plasmid DNA from bacteria

Mini Preparation

ENZA plasmid mini kit from OMEGA was used for the extraction of plasmid DNA on a small scale (mini prep). A single bacterial colony containing the desired plasmid was inoculated into 2.5 ml of LB medium containing appropriate antibiotics and incubated at 37 °C with shaking at 200 rpm overnight. The inoculated culture tube was centrifuged at 10,000 x g for 1 minute. The supernatant was discarded and the pellet was resuspended in 250 µl of solution 1 containing RNase. 250 µl of solution 2 and 350 µl of solution 3 were added and mixed by simple inversion of the tubes. The mixture was centrifuged at 13,000 x g for 10 minutes and the supernatant was transferred to the DNA binding column and centrifuged again for 1 minute. The flow-through was discarded and the column was washed with 500 µl HBC buffer, followed by a repeat wash step with 750 µl DNA wash buffer. The column was then centrifuged at 13000 x g for 2 minutes to completely dry the column. Finally, the plasmid DNA was eluted into 30-50 µl of elution buffer. All buffers and columns were provided in the kit.

Midi Preparation

Large-scale preparation of plasmid DNA was carried out using Plasmid Midiprep kit from QIAGEN. According to manufacturer's protocol, a single bacterial colony was inoculated in to a 50 ml LB medium flask with suitable antibiotics and allowed to grow overnight at 37 °C with shaking. The cells were centrifuged at 5300 x g for 15 minutes and resuspended in 8 ml of buffer P1 by vortexing. 8 ml of buffer P2 and 8 ml of buffer P3 was added to the mixture and mixed well by inversion of the tube several times. The complete mixture was transferred to a filter tube containing provided by the manufacturer and allowed to stand for 7 minutes at room temperature. The lock from the filter tube was released to collect flow through. Flow through containing desired plasmid DNA was mixed with 8 ml binding buffer and transferred to DNA binding column. The DNA binding column was centrifuged to bind the DNA to the column and the flow-through was discarded. The column was then washed twice with 800 µl wash buffer 1 and 800 µl wash buffer 2. Finally, DNA was eluted in 100-150 µl of elution buffer and the concentration was determined using Nano Drop. All the buffers and the columns were provided in the kit.

2.2.3 Protein Biochemistry

2.2.3.1 Protein extraction

Protein extraction was carried out 48 hours after the transfection. The entire extraction procedure was performed on ice to minimize protein degradation. At first, the cells were washed with 5 ml of Phosphate–buffered saline (PBS) to remove all the medium components. The cells were scraped out into 1 ml of PBS with a cell scraper and transferred to 1.5 ml tube. The tube containing the cells was centrifuged at 1500 x g for 5 minutes at 4 °C to obtain the cell pellet. The supernatant was discarded and the pellet fraction was lysed with 500 µl of Triton X- 100 lysis buffer together with 10 µl of protease-Inhibitor cocktail. The mixture was disrupted with fine tips until a clear solution was obtained. The mixture was further incubated on ice for 30 minutes and then centrifuged at 13000 x g for 30 minutes at 4 °C. Finally, the supernatant containing soluble proteins was transferred to a fresh sterile 1.5 ml tube for later use.

2.2.3.2. Protein Quantification using BCA assay

The Thermo Scientific™ Pierce™ BCA Protein Assay Kit, which is based on bicinchoninic acid (BCA), was used for the colorimetric detection and quantitation of total protein. This method involves the reduction of Cu^{+2} to Cu^{+1} by protein in an alkaline medium (the biuret reaction), combined with the highly sensitive and selective colorimetric detection of the cuprous cation (Cu^{+1}) using a unique reagent containing bicinchoninic acid. The chelation of two molecules of BCA with a cuprous ion result in the purple-colored reaction product. This water-soluble complex exhibits strong, nearly linear absorbance at 562nm with increasing protein concentration over a broad working range (20-2000 µg/ml). To prepare BSA standard solutions, stock solutions were diluted to concentrations ranging from 0.125 to 2.0 mg/mL in microcentrifuge tubes. Protein samples were diluted with distilled water to a concentration of 1-5 mg/mL. Then, 25 µL of each BSA standard solution and 25 µL of protein samples were added to separate wells of a 96-well microplate in duplicate, followed by the careful addition of 200 µL of BCA working reagent to each well to ensure uniform mixing. The microplate was incubated at 37°C for 30 minutes and then allowed to cool to room temperature. The absorbance of each well was measured at 562 nm using a microplate reader (Tecan). The standard curve was plotted using the absorbance values of the BSA standard solutions, and the protein concentrations of the unknown samples were determined by comparing their absorbance values to the standard curve. Protein concentrations were calculated using a regression

equation obtained from the standard curve, which was plotted with the absorbance values of the BSA standard solutions on the x-axis and their corresponding protein concentrations on the y-axis. The protein concentrations of the unknown samples were reported in mg/mL.

2.2.3.3. Separation of proteins by SDS- poly Acrylamide gel Electrophoresis (SDS-PAGE)

The protein samples were mixed with 2x Sodium dodecyl sulphate (SDS) sample buffer in 1:1 ratio and boiled at 72°C for 10 minutes. The protein mixture was loaded onto appropriate (6-12%) SDS gels along with prestained protein marker (peqlab) and electrophoresed at 200 V and 25 mA.

2.2.2.4. Western Blotting

Separated proteins on SDS PAGE were transferred from gel onto nitrocellulose membrane using the Transblot Turbo Transfer system (Bio-Rad) for 30 minutes at 45mA. Immunochemical detection of GFP, myc and flag-tagged fusion proteins was performed using mouse anti-GFP (Santacruz; 1:1000), rabbit anti-myc (Cell signaling; 1:1000) and mouse anti flag (Sigma;1:1000) antibodies, respectively. The membrane was washed with TBS-Tween and incubated with fluorescence conjugated IRDye LICOR-secondary antibodies (1:5000; LI-COR Biosciences). Immunoreactivity was detected using Bio-Rad ChemiDoc MP imaging system.

2.2.3.5. Co-immunoprecipitation

Immunoprecipitations were performed using anti-Flag M2 magnetic beads (Sigma) following the manufacturer's guidelines. For the assay, flag-tagged (EQKLISEEDL) BSG cloned in the mammalian pCDNA3.1 expression vector (Invitrogen) was co-transfected with GFP-tagged mVSP in HeLa cells. After 48 hours of transfection, cells were lysed using Triton X 100 lysis buffer containing of 10µl/mL of protease-Inhibitor cocktail. flag-tagged BSG co-transfected with GFP-tagged mVSP were co-immunoprecipitated along with Flag coated magnetic beads for 12 hours at 4° C in a rotating chamber. Immunoprecipitates were washed extensively (3x) with PBS and eluted in 2x sodium dodecyl sulphate (SDS) loading buffer by boiling at 72° C for 10 min. Eluted proteins were separated on (6-12%) SDS-polyacrylamide gels (PAGE), blotted and probed with Rabbit anti-flag antibody (Cell Signaling; 1:1000) and mouse anti-GFP antibody (Santacruz; 1:1000) for overnight at 4° C. The membrane was then washed and incubated

with fluorescence conjugated secondary antibody (1:5000; LI-COR Biosciences) for 1 hour. The bands were visualized using the Bio-Rad Chemidoc MP imaging system.

2.2.4 Cell culture

2.2.4.1 Cell culture and Transfections

HeLa cells were cultured in DMEM medium containing 10% fetal calf serum (FCS, Invitrogen), 1% penicillin/streptomycin (PAA). Cells were seeded on to 35 mm culture dishes and incubated at 37° C and 5 % CO_2. Transfection was carried out after 24h using DNA jetPRIME (polyplus) kit following the manufacturer's guidelines. Plasmid DNA was mixed with an appropriate volume of jetPRIME buffer and vortexed vigorously. Transfection reagent was mixed in a 1:2 DNA ratio and incubated at room temperature for 15 min by brief vortexing. The entire transfection mixture was pipetted onto the cells and the dishes were incubated for 24-48 hours at 37° C and 5 % CO_2 in an incubator.

2.2.4.2. Generation of BSG KO HEK293 or HeLa cell lines

The human BSG gene was targeted using a guide RNA scaffold sequence published by Satchwell and colleagues (Satchwell *et al*., 2019) that was cloned into pSpCas9(BB)-2A-GFP (Addgene) (Ran *et al*., 2013). HEK293 and HeLa cells were transfected according to the protocol described in 2.2.3.1 section. After 48 hours, cells were removed from the culture plates, washed with PBS, passed through a 70 μm cell strainer, and resuspended in PBS with 1% (v/v) FBS. Fluorescence-activated cell sorting (FACS) was performed using a FACS Aria III (BD Bioscience) under aseptic conditions with the assistance of Dr. Hartmann Reifer (BMFZ, Marburg). Single cells were sorted into 96-well plates with DMEM supplemented with 20% (v/v) FBS and 15 mM HEPES and cultivated further. After 21 days, fresh medium was supplied, and cells from individual wells were expanded in 6-well plates. Lysed cells were collected as described in section 2.2.3.1 and hBSG expression was assessed qualitatively through immunodetection on a western blot. Concurrently, genomic DNA was extracted and PCR was performed to confirm a homozygous BSG -/- genotype. The identity of clones was confirmed through sequencing.

2.2.5. Live cell imaging

HeLa cells were analyzed after 24-48 hours of transfection. Live cell images were captured using ZEISS 710 LSM upright confocal microscope. EGFP and RFP images were acquired by excitation of two lasers at 488 and 561 wavelengths and emission was

measured using 493-556 and 578-696 nm filters, respectively. Live images were acquired and later analyzed using ZEN Black SR 3.0 software.

2.2.5.1. Immunocytochemistry

In a 24 well plate filled with coverslips, $5x10^4$ HeLa cells were seeded per well and plasmid DNA was transfected using jetPRIME reagent. 48 hours after transfection, cells were washed with 1 x PBS at room temperature and then fixed for 10 min at 4°C in PBS containing 4% paraformaldehyde. Cells were permeabilized with 0.1% Triton X-100 for 5 min at room temperature. After blocking the cells with 1x PBS containing 5% FCS for 30 min at room temperature, cells were then incubated with primary antibody for 2 h at room temperature. The cells were then washed with 1x PBS and incubated with fluorescently conjugated secondary antibodies, Alexa Flour 488 or Alexa Flour 594 for 1 h at room temperature. The cells were extensively washed four times with 1x PBS buffer and mounted with Mowiol 4-88 (Carl Roth, Karlsruhe, Germany).

2.2.5.2. Quantitative Assessment of mVSP Localization in the PM through Membrane-to-Cytosol Ratio Calculation

In order to determine the surface localization of mVSP at the PM, HeLa cells were co-transfected with GFP-tagged mVSP and RFP-tagged BSG, and imaged 48 hours after transfection using a ZEISS 710 LSM upright confocal microscope. The resulting data was analyzed using FIJI/ImageJ software (Schindelin *et al*., 2012).

For each cell, a line profile was generated to show the fluorescence intensity (Y-axis) with respect to the distance along the line (X-axis). To determine the localization of the PM, BSG-RFP fluorescence was used, making use of the knowledge that BSG predominantly targets PM. Thus, localization of peak RFP was taken as the intersection of the line profile with the PM. The corresponding values of GFP-tagged mVSP were extracted along the same line (from Figure 2.1, panels A and B).

Next, the extracted data was analyzed further using Excel software (Microsoft/Redmond/USA). The position of the PM was determined by identifying the maximum fluorescence signal (marked as reference points R1 and R2 in figure 2.1 of BSG-RFP). Corresponding values from the mVSP fluorescence intensity profile were taken as PM (PM) and cytosolic points. The obtained PM peak values (G1 and G2) were divided by the cytosolic values (all values between G1 and G2). Values greater than 1 were classified as mVSP localized to the PM, while values less than 1 represented mVSP retained in the cytosol.

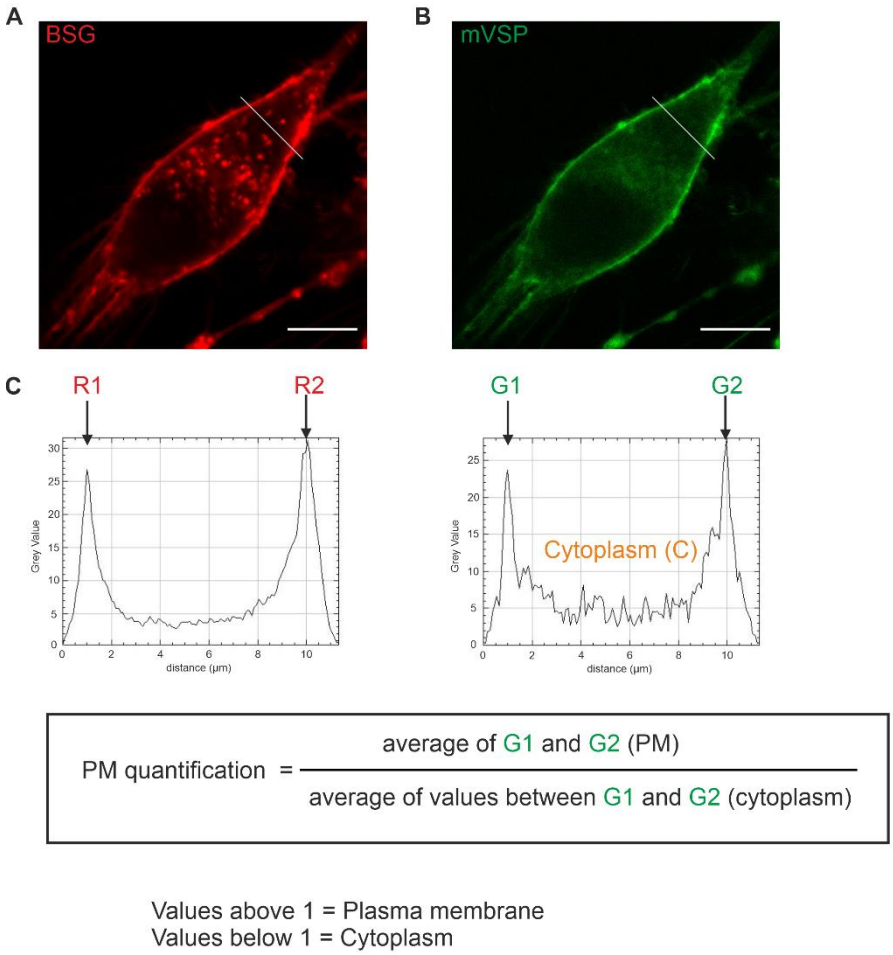

Figure 2.3: Determination of mVSP localization at PM using PM/cytosol ratio. Figure shows live cell imaging of HeLa cells co-transfected with RFP-tagged BSG and GFP-tagged mVSP, along with the corresponding fluorescence intensity profiles. The top panel of **(A)** shows the RFP fluorescence of BSG with its line profile, while the bottom panel shows the fluorescence intensity profile of selected regions. Membrane peaks for BSG (marked as R1 and R2) were identified as membrane values. The top panel of **(B)** shows the GFP fluorescence of mVSP with its line profile, while the bottom panel shows the fluorescence intensity profile of selected regions. Membrane peaks for mVSP (marked as G1 and G2) were identified, with the fluorescence intensity between the two peaks labeled as cytosol. **(C)** illustrates the calculation of the membrane-to-cytosol ratio. The scale bar is 10 µm

2.2.5.3. High K^+ stimulation Induces Depolarization in Flp-In-ROMK HEK293 Cells

To assess the catalytic activity of VSP without relying on electrophysiological methods, we utilized ROMK2 Flp-In-HEK293 cells (originally described by Renigunta *et al.*, 2011). ROMK2 stably expressed in this cell line is an inward rectifier potassium channel that enables depolarization of the cells through the addition of extracellular potassium (150 mM K^+). VSP was activated by depolarizing the cells, and its enzymatic activity against PI substrates was then measured using genetically encoded fluorescence-proteins-fused PI probes specifically recognizing individual PI species (Figure 2.2 A).

ROMK2 Flp-In-HEK293 cells were seeded on a glass bottom μ-slide VI $^{0.5}$ flow chambers (ibidi, Martinsried, Germany) and co-transfected with GFP-tagged PH probes (PLCδ1-PH, TAPP1PH) and RFP-tagged VSP (Myc-tagged BSG was co-transfected with mVSP). After 48hrs of transfection, the cells were analyzed under a TIRF microscope. A gravity-driven perfusion system containing alternatively delivering solutions with either 2mM K^+ or 150mM K^+ was used to perfuse the flow chamber. The transfected ROMK2 Flp-In-HEK293 cells were mounted on to TIRF setup and the perfusion system was connected to μ-slide VI $^{0.5}$ flow chamber. Using a 3-way stopcock, the 2mM K^+ solution in the syringe was allowed to pass through the flow chamber flowing from one side and leave the flow chamber from the other. The cells were illuminated with 488nm at critical angle to obtain TIRF illumination at approximately 90 nm penetration depth and images were acquired at 5 second frame rate. For the first 1 min cells were flushed with 2mM K^+ solution, then the cells were switched to 150 mM K^+ solution for 1 min, and then finally switched back to 2mM K^+ solution for the last 2 min.

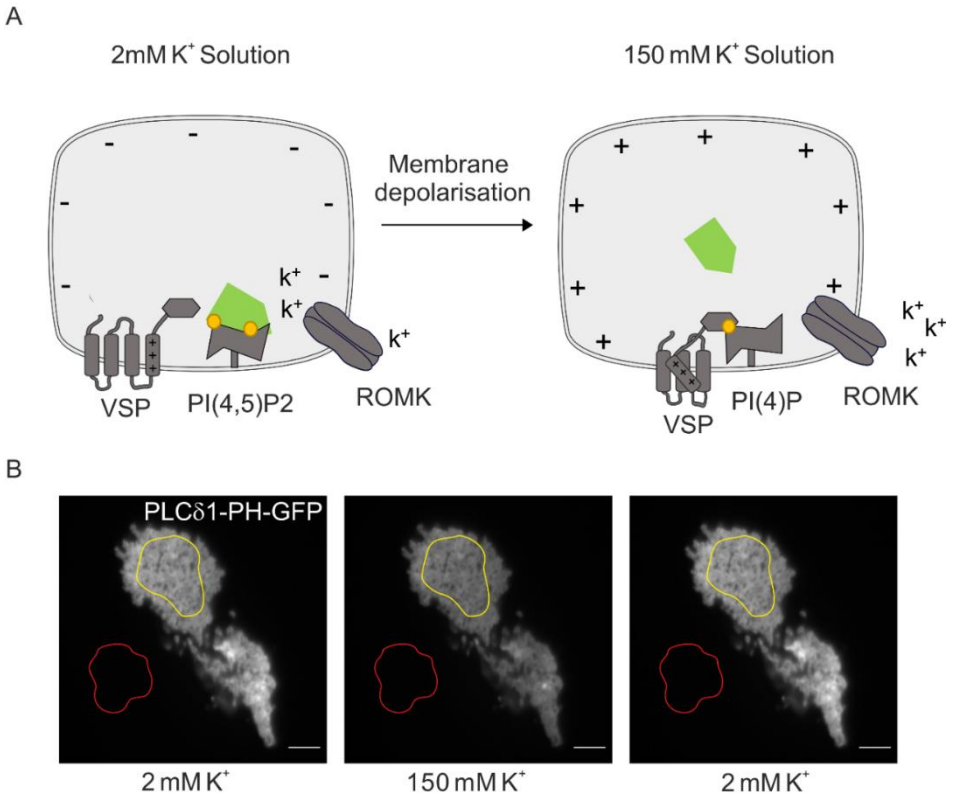

Figure 2.4: Method used to measure the catalytic activity of VSP by depolarizing ROMK2 Flp-In-HEK293 cells. (A) is a schematic diagram of the ROMK2 Flp-In-HEK293 cells co-transfected with Ci-VSP and PLCδ1-PH. Ci-VSP is a voltage-sensitive phosphatase that depletes $PI(4,5)P_2$ upon depolarization under a high K^+ solution. This results in the translocation of PLCδ1-PH from the membrane to the cytosol. **(B)** shows the TIRF images of ROMK2 Flp-In-HEK293 cells expressing Ci-VSP and $PI(4,5)P_2$ sensor PLCδ1-PH GFP. The selected region of interest (yellow) within the cell shows the depletion of TIRF signal upon the application of 150 mM K^+ solution. The scale bar represents 10 μm.

The TIRF microscopy data was analyzed using Fiji software by drawing a region of interest (ROI) within the cell and performing background subtraction using an ROI outside the cell (Figure 2.2 B). The fluorescence intensity of the ROI was calculated over time (i.e. for each frame) and normalized by dividing the obtained fluorescence intensity values (F) by the value of the time point 12 of the time series (F0) when 150 mM K^+ was applied. The normalized fluorescence intensity (F/F0) was then plotted as a function of time.

2.2.6. Statistical analysis

Graphs and statistical analyses were carried out using GraphPad Prism software (GraphPad Software, San Diego, CA, USA). Data are reported as means ± SEM. Statistical significance was determined using an unpaired t-test or one-way ANOVA for more than two groups. For multiple comparisons to a single control condition, Dunnett's test was performed following ANOVA. In the figures, statistically significant differences to control values are marked by an asterisk (*P < 0.05, **P < 0.01, ***P < 0.001, ****P < 0.0001); ns indicates not significant differences (P > 0.05). Tests used and P values are given in legends.

3. Results

3.1. BSG identified as putative interaction partner of mVSP

3.1.1. Screening and validation of mVSP interactions using Split Ubiquitin-based Yeast Two-Hybrid System

To identify novel protein interaction partners of mVSP, a split ubiquitin-based yeast two-hybrid screen was performed, which enables the use of full-length integral membrane proteins as baits for interactions with integral membrane proteins and membrane-associated proteins. Since mVSP is robustly expressed in mouse brain (Rosasco *et al*, 2015), a mouse brain cDNA library constructed in a prey vector was obtained from the manufacturer (MoBiTec) and was screened with the mVSP cloned into the bait vector. Briefly, the C-terminal half of ubiquitin, along with an artificial transcription factor, was fused to the N-terminus of mVSP (Figure 3.1A). Screening was performed by introducing the bait and prey vectors into the yeast strain NMY51 on SD-LWH-plates, which lack the amino acids leucine, tryptophan and histidine. Interaction of bait and prey proteins is reported by colony growth on SD-LWH-plates. Briefly, bait-prey interaction brings the two halves of ubiquitin, Nub and Cub into close proximity, resulting in assembly of the complete split ubiquitin complex, which is recognized and cleaved by UBPs subsequently releasing the artificial transcription factor LexA-VP16. LexA reporter moiety translocates into the nucleus and activates reporter gene His3, which enables the yeast to grow on minimal medium without histidine. In addition, it results in activation of the lacZ gene, a color reporter gene encoding enzyme β-galactosidase which produces a blue-colored compound when treated with X-Gal substrate.

To commence the screening process, it was crucial to verify the correct orientation of mVSP in the bait vector. To address this issue, mVSP was fused to the C-terminal (pBT3C) and N-terminal (pBT3N) parts of Cub. The expression of both bait proteins was confirmed by performing a control assay, wherein the bait vectors were tested with the control prey vectors pAIAlg5 and pDL2-Alg5 provided in the kit (Figure 3.1B and C, respectively). The co-expression of bait vectors was tested with Alg5-NubI (positive control), demonstrating a strong affinity between the wild type NubI and Cub, resulting in colonies appearing on SD-LW and SD-LWH plates. Conversely, the co-expression of both bait vectors along with pDL2-Alg5 (negative control) should not activate the reporter genes, as the mutated NubG moiety lacks affinity for Cub.

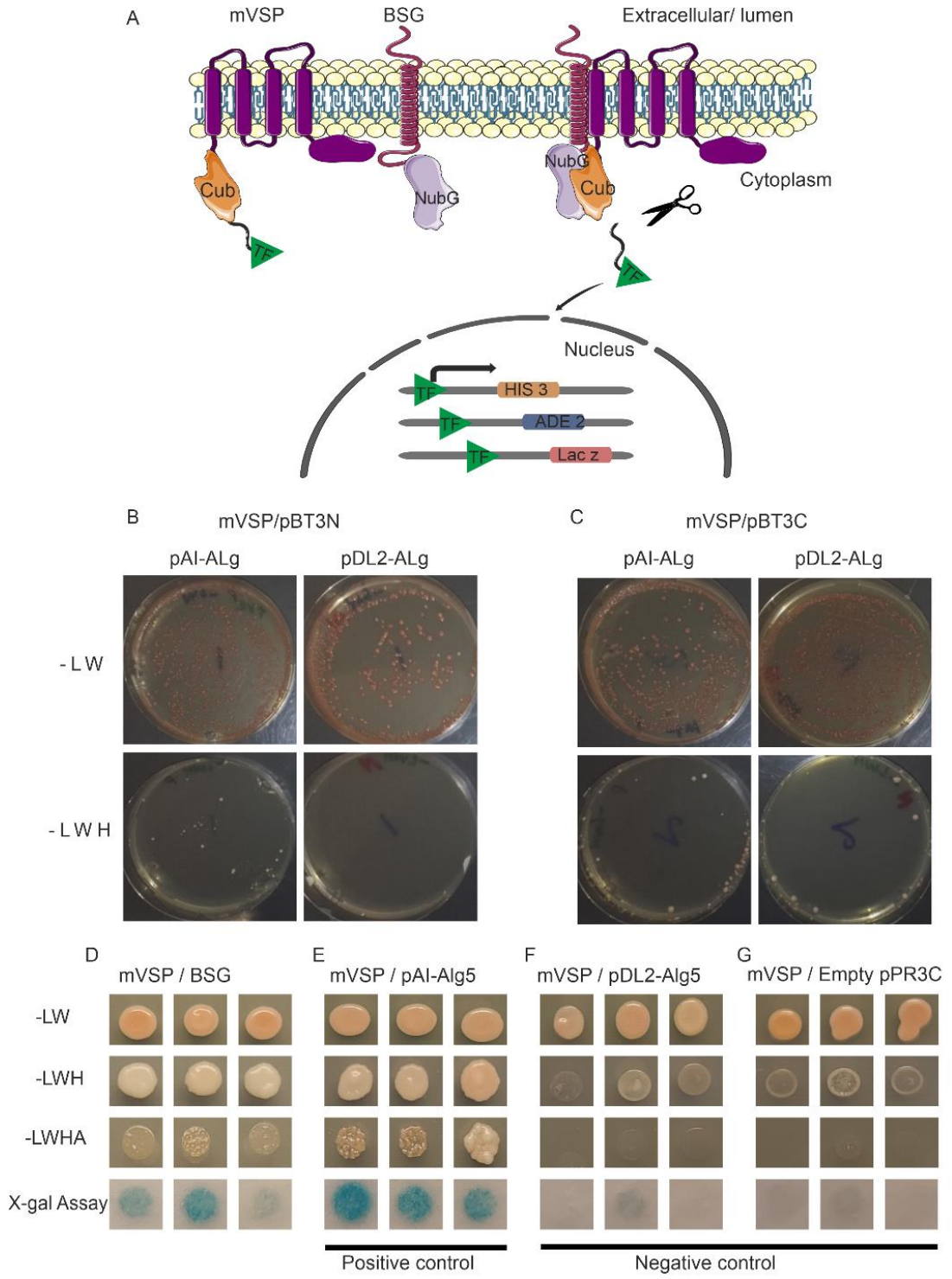

Figure 3. 1: mVSP interacts with BSG in membrane Yeast two-hybrid Assay. (A) Schematic representation of Split ubiquitin Membrane yeast two-hybrid. mVSP, fused to the C-terminal half of ubiquitin (Cub) along with an artificial transcriptional factor (TF) and a downstream reporter cassette, was used as bait, and BSG fused to the N-terminal half of ubiquitin (NubG) was used as prey. Control assay was performed to check proper expression of bait vector. mVSP fused to N-terminal half of ubiquitin (pBT3N) **(B)** and C-terminal half of ubiquitin (pBT3C) **(C)** were used as bait and expressed with positive control vector (pAI-Alg5) and Negative control vector (pDl2-Alg5) to check for any self-activation of bait. This finding further supports the correct expression of the bait. **(D)** Membrane yeast-two-hybrid direct interaction experiments showing positive interaction between mVSP and BSG. The control vectors pAI-AIg5 and pDL2-AIg5 were used as positive **(E)** and negative controls **(F)**, respectively. pPR3C prey vector was used as an

additional negative control **(G)**. Shown are plates with selective drop-out medium lacking leucine and tryptophan (-LW), indicating the transformation of both bait and prey vectors; with selective drop-out medium lacking leucine, tryptophan, histidine, and adenine (-LWHA), indicating the expression of reporter genes HIS3 and ADE2; and with b-galactosidase as a second reporter assay, indicating positive interaction.

Consequently, it was observed that the bait vector PBT3N exhibited proper expression in the control assay, as evidenced by growth on SD-trp-leu-his plates when co-expressed with the positive control prey vector pAI-Alg5, while no significant growth was observed when co-expressed with the negative control vector pDL2-Alg (Figure 3.1B). Screening with brain cDNA-encoded proteins fused to the N-terminal half of ubiquitin (Molecular Biotechnology) led to the identification of several potential interaction partners by sequencing the prey vector inserts from the respective colonies. One of the positive prey vector inserts encoded the transmembrane glycoprotein BSG, also known as CD147.

To address the potential issue of false interactors in the Y2H membrane system, the identified potential interactor, BSG, in the prey vector (pPR3N), was re-transformed alongside the bait vector (mVSP-pBT3N) into yeast strain NMY51. The transformed yeast cells were then plated on SD-LW plates. From the resulting colonies, three were selected and spotted onto SD-LW, SD-LWH, and SD-LWHA plates. Robust growth was observed on the SD-LWH plates, indicating a strong direct interaction between both the bait and prey proteins (Figure 3.1D). As a positive control, pAI-Alg5 was used (Figure 3.1E), while pDL2-Alg5 and empty pPR3N served as negative controls (Figure 3.1F and G, respectively). No colony growth was observed on SD-LWH and SD-LWHA plates for the negative controls. To further investigate the strength of the direct interaction between BSG and mVSP, an X-GAL assay was performed on SD-LW plates. As shown in the Figure 3.1D, X-gal assay resulted in blue color formation with mVSP and BSG in the bait and prey vectors, respectively, confirming strong and robust interaction between both proteins.

3.1.2. mVSP and BSG interaction validated by co-immunoprecipitation assay

To further validate the putative interaction between mVSP and BSG, co-immunoprecipitation studies were performed using flag antibody coated magnetic beads from the manufacturer (Sigma). HeLa cells were co-transfected with BSG and mVSP constructs. 48 hours post-transfection, protein extraction was performed, and the obtained HeLa cell lysate was incubated with magnetic flag beads, as depicted in Figure 3.2A. In

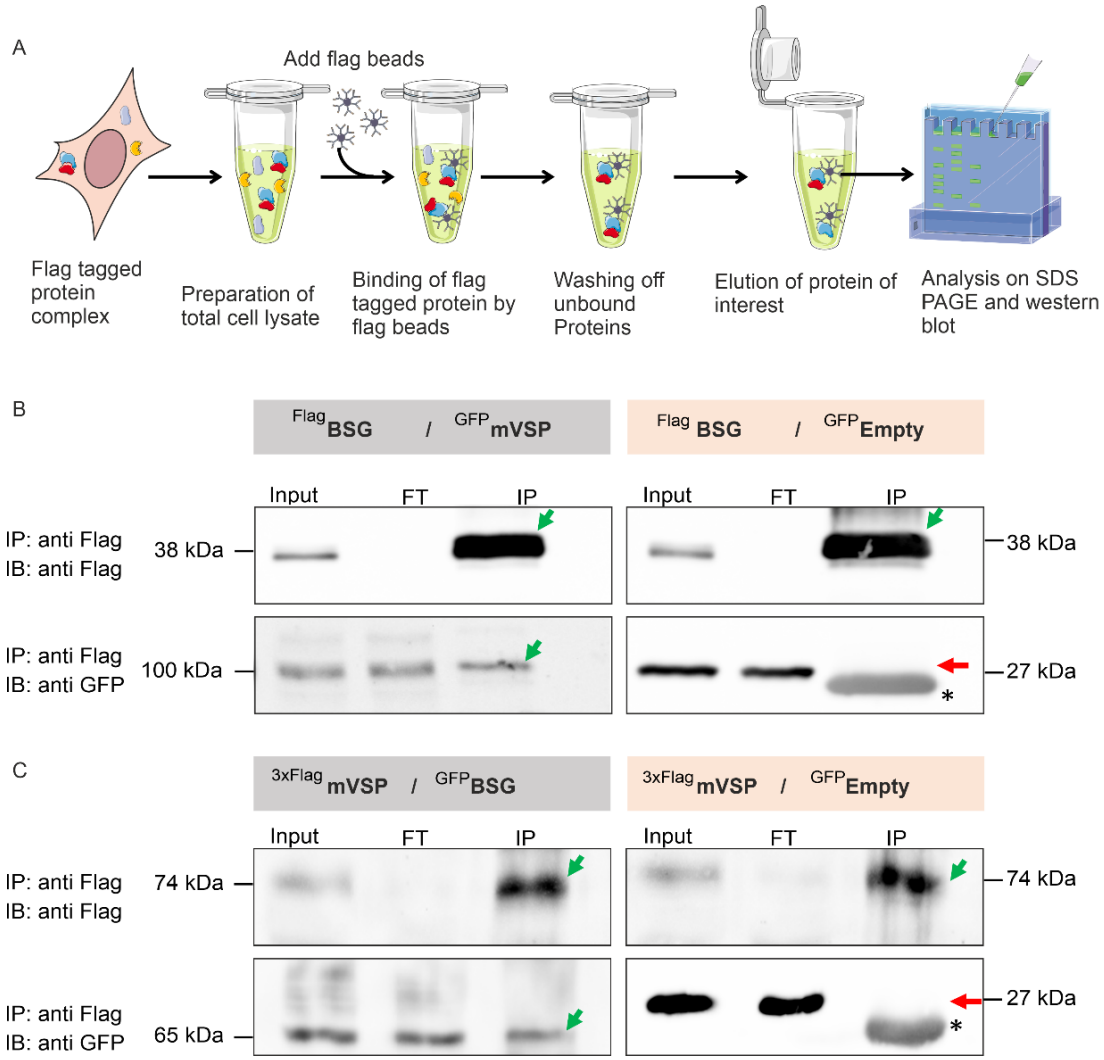

Figure 3.2: Validation of mVSP and BSG interaction using Co-immunoprecipitation Assay **(A)**Schematic diagram representing the principle of Co-immunoprecipitation assay. Flag and GFP-tagged proteins were heterologously expressed in HeLa cells, proteins were extracted and immunoprecipitated using magnetic flag beads and later analyzed by SDS-PAGE and Western Blot analysis **(B)** Co-immunoprecipitation of GFP-tagged VSP and flag-tagged BSG heterologously expressed in HeLa cells. **(C)** Co-immunoprecipitation of 3x flag-tagged VSP and GFP-tagged BSG heterologously expressed in HeLa cells. The complex containing VSP and BSG was precipitated from cell lysate using anti-FLAG antibody M2-conjugated agarose beads, and a western blot of the precipitate was probed with FLAG and GFP antibodies; the cell lysate (input) was used as a positive control. Co-immunoprecipitation performed with GFP alone was used as a negative control (right). n=3 experiments.

one set of experiments cell lysates from HeLa cells expressing (^{GFP}mVSP + BSG^{flag} constructs) and in another set of experiments (BSG^{GFP} + ^{flag}mVSP constructs) were used (Figure 3.2 left panel B and C respectively). Lysates from HeLa cells expressing GFP alone were used as a negative control (red arrow, Figure 3.2B, C). We detected GFP-tagged BSG protein in the anti-Flag immunoprecipitates of HeLa cells expressing 3xFlag-

tagged mVSP and GFP-tagged BSG proteins, as illustrated in Figure 3.2C. Conversely, GFP-tagged mVSP protein was immunoprecipitated by anti-Flag antibodies from HeLa cell lysates expressing GFP-tagged mVSP and Flag-tagged BSG proteins (Figure 3.2B). It should be noted that the two bands detected in the immunoprecipitate (Figure 3.2B, C marked with an asterisk) are not due to GFP, but to immunoglobulin from the beads, which is detected by the secondary antibody alone. Taken together, Y2H results and the reciprocal co-immunoprecipitation experiments with mVSP and BSG from transfected mammalian cells strongly indicate a bona-fide protein-protein interaction between the two membrane proteins.

3.2. mVSP localization at the cell surface requires co-expression of BSG

Multiple studies involving over-expression of mammalian VSPs in cell lines have demonstrated exclusive localization to intracellular compartments (Wu *et al*., 2001; Rosasco *et al*., 2015). BSG on the other hand is a transmembrane glycoprotein known for its multiple functions and has been the subject of extensive research (Miyauchi *et al*., 1990; Tang *et al*., 2004; Huang *et al*., 2013). Given that mVSP and BSG interact robustly in Y2H and Co-immunoprecipitation experiments, it can be inferred that these proteins are located in close proximity within living cells. To investigate the interaction between BSG and mVSP concerning trafficking, a comprehensive approach was adopted in this study. Both proteins were labelled with distinct fluorophores, and their localization was monitored using confocal microscopy.

3.2.1. Validation and Quantification of mVSP localization to PM using membrane marker

To explore the localization of mVSP and BSG and a potential impact of BSG on localization of mVSP, HeLa cells were transfected with GFP-tagged mVSP. In each case investigated, no localization of GFP-tagged mVSP to the PM could be resolved by confocal light microscopy. Instead, most of the protein remained associated with perinuclear compartments (Figure 3.3B). In contrast, RFP-tagged BSG over-expressed in HeLa cells showed predominant PM localization (Figure 3.3C). Strikingly, co-expression of GFP-tagged mVSP and RFP-tagged BSG resulted in localization of mVSP at the cell surface rather than intracellular retention (Figure 3.3D). In fact, a similar effect was previously observed for an unrelated group of membrane protein named as monocarboxylate transporters (MCTs), where co-expression of BSG resulted in

translocation of MCTs to the PM in HeLa cells (Kirk *et al*., 2000; Wilson *et al*, 2013).

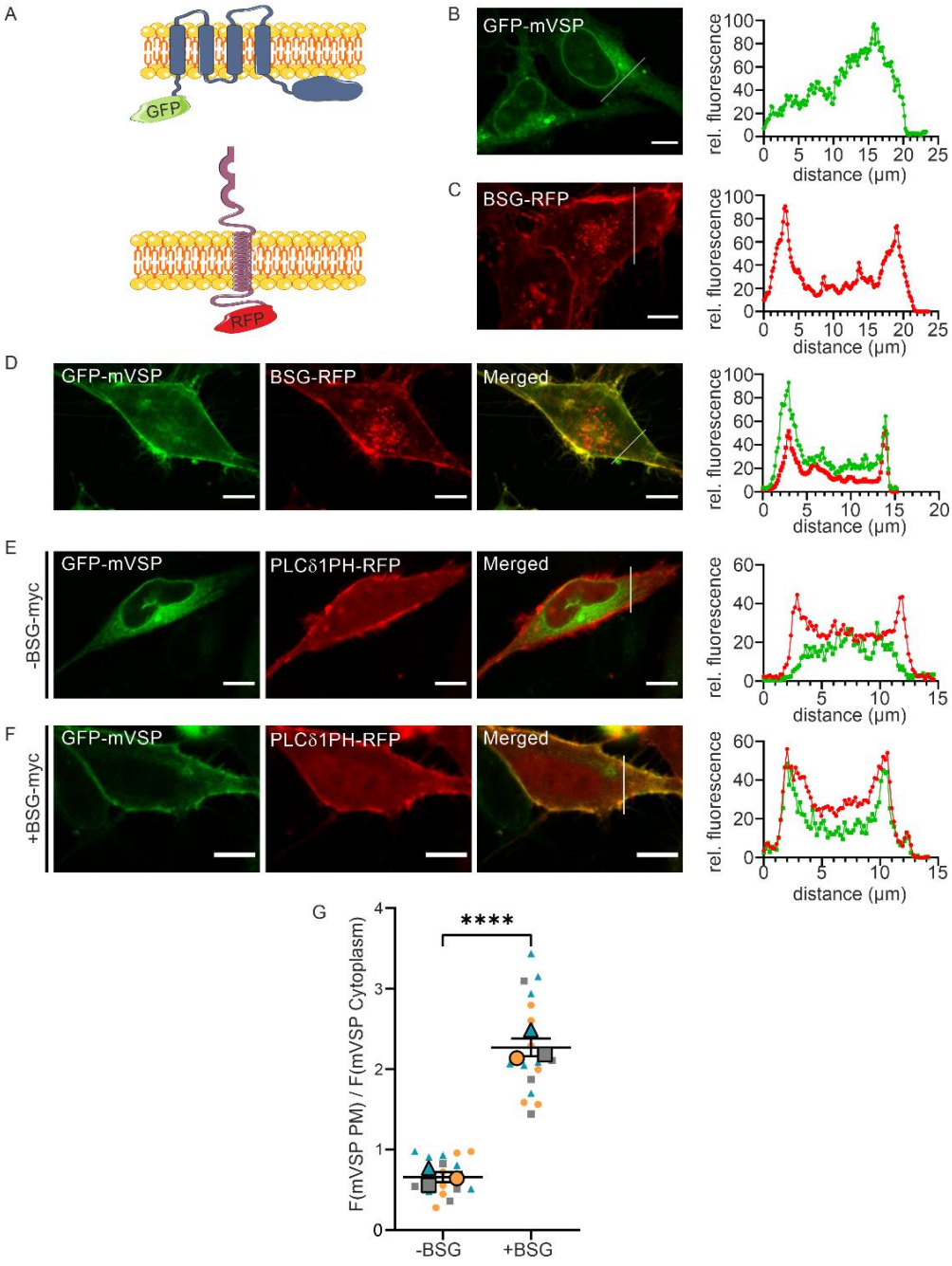

Figure 3.3: mVSP is translocated to the surface of the membrane with the help of BSG in HeLa cells. (A) Schematic representation of GFP-tagged mVSP and RFP-tagged BSG constructs. **(B)** Cells transfected with either GFP-tagged mVSP or (**C**) RFP-tagged BSG with the corresponding fluorescence intensity profiles. **(D)** Cells co-transfected with GFP-tagged mVSP and RFP-tagged BSG with corresponding fluorescence intensity profile at right**.** (**E**) Cells co-transfected with GFP-tagged mVSP and RFP-tagged PLCδ1-PH (PM marker) in the absence of exogenous BSG and its fluorescence intensity profile. (**F**) Cells co-transfected with GFP-tagged mVSP and RFP-tagged PLCδ1-PH in the presence of exogenous Myc-tagged BSG and its fluorescence intensity profile. The green and red curves in the line-scan profiles represent the fluorescence intensity from GFP and RFP respectively. **(G)** Surface localization analysis of VSP

with and without exogenous BSG (mean±s.e.m., -BSG (control), n=19 cells, three experiments; +BSG, n=18 cells, three experiments; ****P<0.0001; unpaired t-test: P= <0.0001). All images were taken 48 h after transfection. n = 3 transfections. Scale bars: 10 μm.

To further validate the trafficking of mVSP to cell surface, RFP-tagged PLCδ1-PH was used as PM marker, allowing for quantification of mVSP PM/cytosol ratio. In one set of experiments, GFP-tagged mVSP and RFP-tagged PLCδ1-PH was transfected into HeLa cells in the absence of exogenous BSG. Live cell images showed no co-localization of GFP-tagged mVSP with RFP-tagged PLCδ1-PH in absence of exogeneous BSG (Figure 3.3E). Upon co-expression with myc-tagged BSG, GFP-tagged mVSP translocated to PM and co-localized with PLCδ1-PH. This indicated that mVSP is localized at PM only upon co-expression of BSG (Figure 3.3F). This observation was further confirmed by the quantification of the mVSP PM/cytosol ratio, where GFP-tagged mVSP in the absence of exogenous BSG with 0,72 ± 0,04 had a value below one, which represents cytosolic localization but whereas GFP-tagged mVSP in the presence of BSG with 2.5 ± 0,04 had a value above one representing the PM localization (Figure 3.3G).

3.2.2. Immunocytochemistry assay confirms the effect of BSG on PM localization of mVSP

To scrutinize the translocation of mVSP to the PM in the presence of BSG, a complementary study was conducted using fixed cells. In order to assess the surface expression of mVSP, an HA (Haemagglutinin) tag was inserted at the extracellular side at position 301 between the S3 and S4 transmembrane domains (Figure 3.4C).

This modification allowed us for the detection of mVSP at the PM under non-permeabilized conditions, and thereby providing a decisive detection of PM-localized protein. HeLa cells were transfected with GFP-tagged mVSP containing the extracellular HA-tag (GFP-mVSP-Ex HA). Under non-permeabilizing conditions, immunostaining was carried out 48 hours after transfection using a mouse monoclonal anti-HA antibody specific to the epitope, followed by a secondary antibody conjugated to a fluorophore. Consistent with the observations from live cell imaging, the immunostaining of GFP-mVSP-Ex HA revealed surface staining in HeLa cells only when myc-tagged BSG (BSG-myc) was co-expressed (Figure 3.4B, right panel). In contrast, no surface staining of GFP-mVSP-Ex HA was observed in the absence of BSG-myc (Figure 3.4B, left panel), consistent with the differential localization of GFP fluorescence emitted by the protein (Figure 3.4A). These results provide further support for the translocation of mVSP to the

PM upon co-expression with BSG.

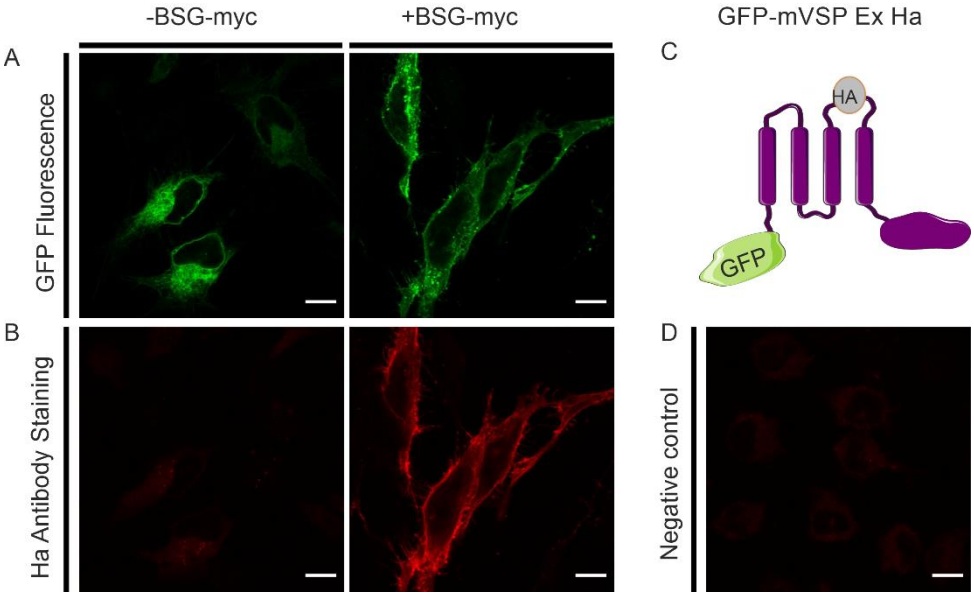

Figure 3.4: mVSP is translocated to the surface of the membrane with the help of BSG in HeLa cells. 2 (**A)** Confocal microscopy of HeLa cells transfected with GFP-mVSP-Ex HA construct in the absence (Left) and in the presence of exogenous Myc-tagged BSG (right). (**B)** Immunofluorescence (IF) confocal microscopy of HeLa cells performed under non-permeabilized conditions transfected with GFP-mVSP-Ex HA construct in the absence (Left) and in the presence of exogenous Myc-tagged BSG (right). (**C**) Schematic drawing showing the extracellular HA tag and the intracellular GFP tag on the mVSP. (**D**) Mock-transfected cells served as negative controls. Similar results were obtained in n = 3 transfections. Similar results were obtained in n = 3 transfections. The scale bars represent 10 μm

3.2.3. Exogeneous BSG also promotes surface localization of mVSP in CHO and HEK293 cells

To investigate whether the effect of BSG on the PM targeting of mVSP extends beyond HeLa cells, GFP-tagged mVSP and RFP-tagged BSG were transfected into CHO and HEK293 cells. Live cell imaging was performed 48 hours post-transfection to assess the subcellular localization of the proteins.

Similar to the observations in HeLa cells, co-expression of RFP-tagged BSG with GFP-tagged mVSP resulted in the translocation of mVSP to the PM in both CHO and HEK293 cells (Figure 3.5B and D respectively).

To quantify the membrane expression of mVSP in CHO and HEK293 cells, the mVSP PM/cytosol ratio was calculated. The ratios obtained in both CHO and HEK293 cells were comparable to the ratio observed in HeLa cells in previous experiments (Figure 3.3). Thus, the effect of BSG is not specific to a particular cellular context since it was observed consistently across different cell types (CHO, HEK293, and HeLa cells). This consistency in results strengthens the validity and generalizability of the observed phenomenon.

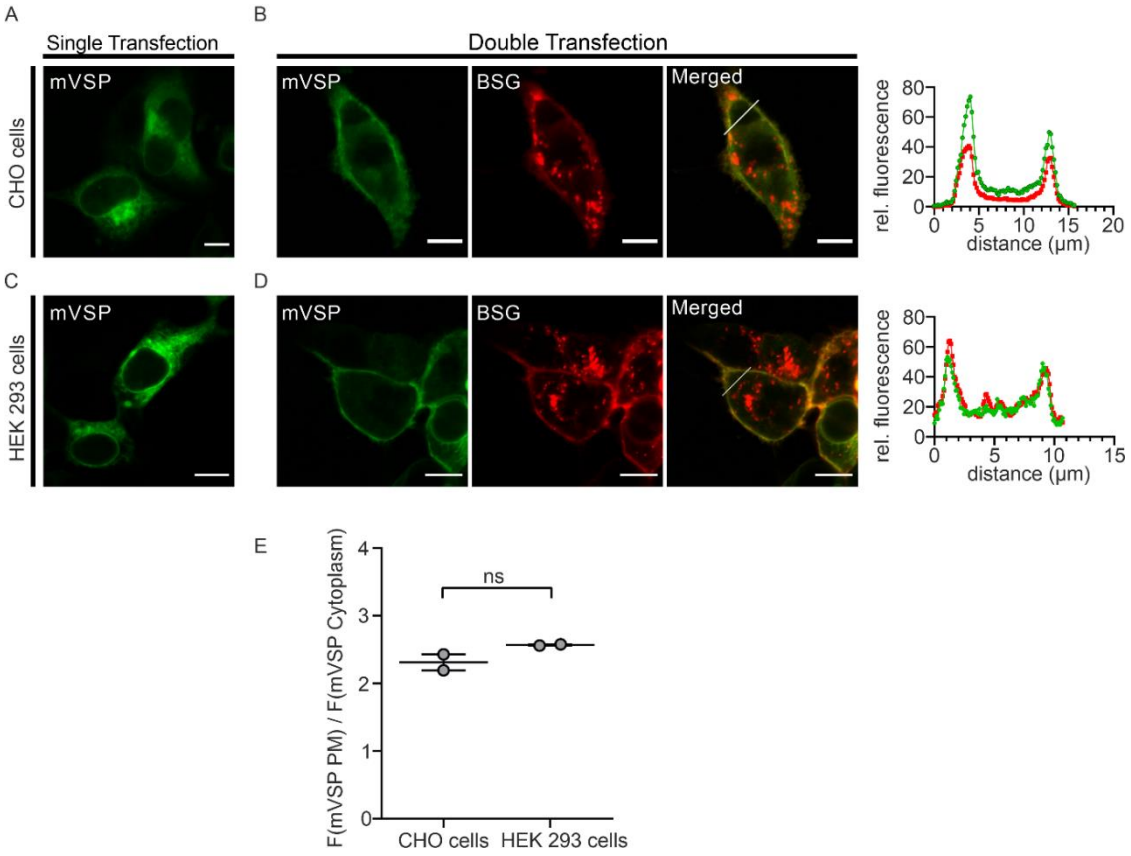

Figure 3.5: BSG promotes mVSP trafficking to the PM in other mammalian cell lines. (**A**) CHO cells and (**C**) HEK293 cells were transfected with GFP-tagged mVSP alone or co-transfected with RFP-tagged BSG (**B, D**) and imaged after 48 h. and the corresponding fluorescence intensity profiles are shown at the right. (**E**) Quantification of mVSP surface expression in the presence of exogenous BSG in CHO and HEK293 cells (mean±s.e.m., CHO, n=13 cells, two experiments; HEK293, n=11 cells, two experiments. ns., not significant; unpaired t-test: P =0.3668). Similar results were obtained in n = 2 transfections. Scale bars: 10 µm.

3.2.4. Lack of exogenous BSG results in mVSP localization to the ER

Previous studies investigating the cellular localization of mVSP have yielded conflicting results, with some suggesting its localization in the Golgi apparatus while others in the ER (Guipponi *et al.*, 2001; Wu *et al.*, 2001; Rosasco *et al.*, 2015). In Hela cells, exogenous expression of GFP-tagged mVSP has been shown to result in its intracellular retention. To gain further insight into the specific cellular compartments in which mVSP is localized, GFP-tagged mVSP was co-transfected with RFP-tagged organelle markers. The co-localization analysis revealed a significant overlap between mVSP and the ER (pDsRed2-ER) as well as the Golgi apparatus (galT-DsRed) (Figure 3.6A, second and third rows, respectively). However, no co-localization was observed between mVSP and

the PM (Lyn11) or endosomes (LysoTracker Red) (Figure 3.6A, first and fourth rows). In contrast, when GFP-tagged mVSP and RFP-tagged organelle markers were co-transfected with myc-tagged BSG, it was observed that mVSP relocalized and exhibited co-localization with Lyn11, representing the PM (Figure 3.6B, first row). Only a small fraction of mVSP remained localized in the ER, Golgi apparatus, and lysosomes (Figure 3.6B, second, third, and fourth rows, respectively). This finding demonstrates that in the absence of BSG, mVSP is retained in the ER and Golgi. However, in the presence of BSG, it undergoes translocation specifically to the PM.

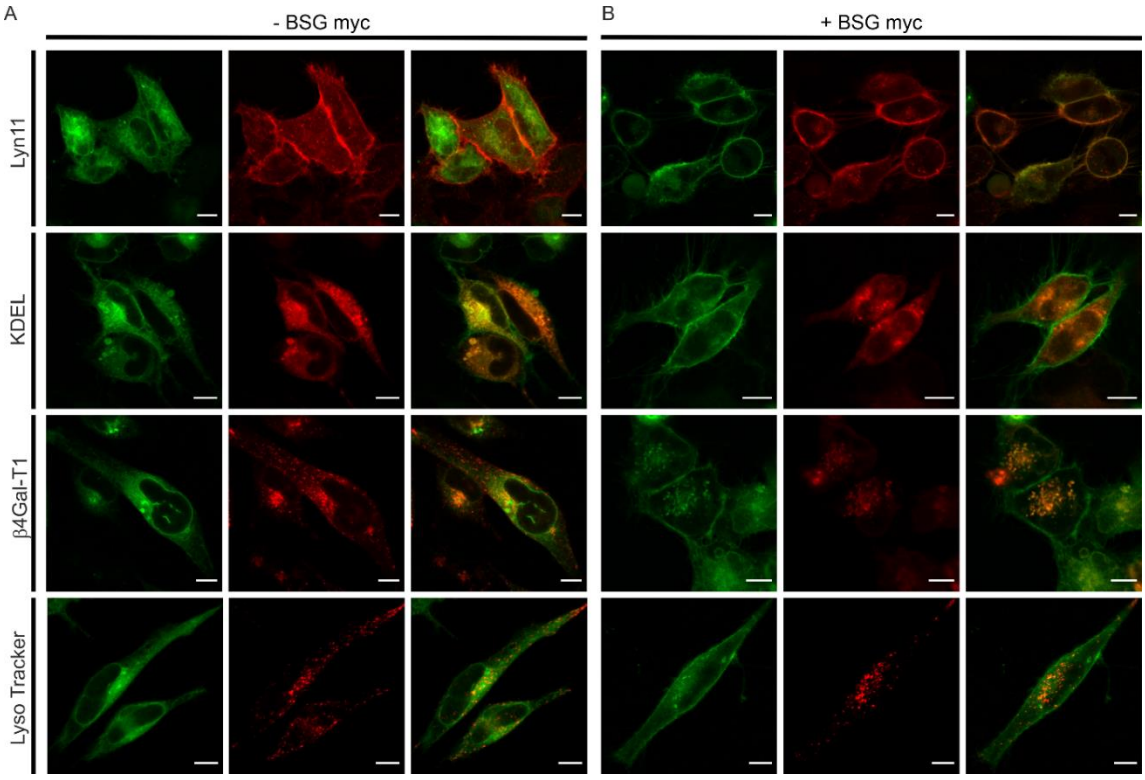

Figure 3.6: Co-localization of mVSP with the organelle markers. HeLa cells co-transfected with GFP-tagged mVSP and RFP-tagged organelle markers (PM: Lyn11; ER: calreticulin; Golgi: beta 1,4-galactosyltransferase; Lysosomes: Lyso Tracker Red) in the **(A)** absence and **(B)** presence of exogenous Myc-tagged BSG. All images were taken 48 h post-transfection. Similar results were obtained in n = 3 transfections. The scale bars represent 10 μm.

3.2.5. Translocation of mVSP to PM evident only after 48h of post transfection

To investigate whether the effect of BSG on mVSP trafficking is time-dependent, HeLa cells were transfected with GFP-tagged mVSP and RFP-tagged BSG. Live cell imaging was performed 24 and 48h post-transfection to examine the subcellular localization of the proteins. When expressed individually, mVSP was localized in ER (Figure 3.7A), while BSG exhibited PM localization (Figure 3.7B) at both time points.

Surprisingly, upon co-expression, BSG and mVSP were co-localized within the ER at 24 hours post-transfection (Figure 3.7C top). This suggests association of BSG with mVSP

already occurs within the ER compartment. Translocation of mVSP to the PM was observed only after 48 hours post-transfection suggesting that BSG-dependent forward trafficking to the PM is a comparatively slow process (Figure 3.7 bottom).

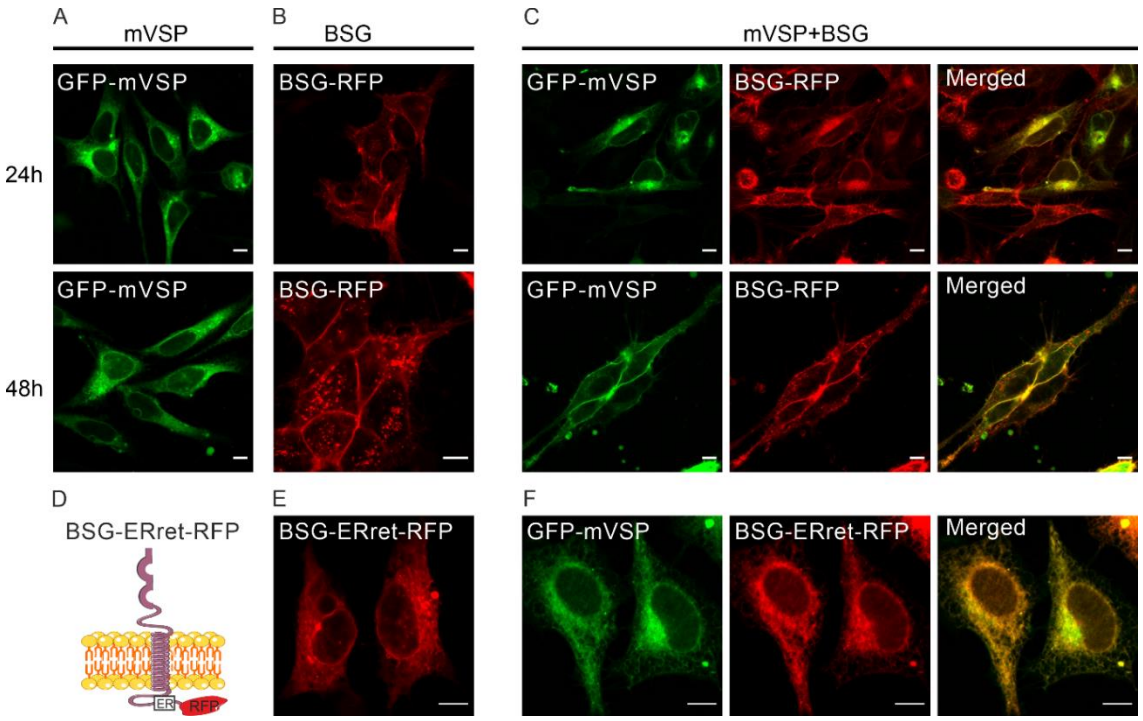

Figure 3.7: BSG facilitated trafficking of mVSP to the PM requires 48 h post-transfection. HeLa cells were transfected with either GFP-tagged mVSP **(A)** or RFP-tagged BSG **(B)** or co-transfected with both **(C)** and imaged after 24 h (first row) and 48 h (second row). **(D)** Schematic diagram of RFP-tagged mutant form of BSG that is retained in ER (BSG-ERret). HeLa cells were transfected with either RFP-tagged BSG-ERret **(E)** or co-transfected with GFP -tagged mVSP **(F).** Similar results were obtained in n = 3 transfections. The scale bars represent 10 µm.

The time dependent translocation of mVSP to the PM in the presence of BSG suggests the involvement of complex cellular processes. Further investigations are needed to elucidate the mechanisms underlying this time-dependent translocation and the interplay between mVSP and BSG during this process. However, we hypothesized that the BSG dependent forward trafficking of mVSP might result from two distinct mechanisms. First, the presence of BSG in ER might influence the sorting/trafficking machinery of the ER resulting in the escape of mVSP from the ER independent of its interaction with mVSP. This proposition gains support from the observation that other members of the BSG family have demonstrated a similar impact on the trafficking of unrelated membrane proteins like MCTs and PMCAs1 (Wilson *et al.*, 2013; Schmidt *et al.*, 2017). Alternatively, it can be hypothesized that the interaction of mVSP with the trafficking machinery could be altered by binding of mVSP to BSG. Our finding of a protein-protein

interaction between BSG and mVSP argues in favor of the latter mechanism. To distinguish between both possibilities, we devised an experiment, where BSG was equipped with a strong ER retention motif (BSG_{ERret}; Figure 3.7D), analogously to a strategy implemented previously to address neuroplastin's impact on PMCA (Schmidt *et al.*, 2017). In contrast to wildtype BSG, BSG_{ERret} was completely localized to intracellular compartments in a pattern consistent with predominant residence in the ER (Figure 3.7E). When co-expressed with BSG_{ERret}, mVSP was completely retained with the same ER-like distribution and closely co-localized with the BSG construct (Figure 3.7F). These findings indicate that the presence of BSG in the ER compartment is not sufficient to relieve ER retention of mVSP. Further, the data support the association of both proteins into a complex at the ER level.

Together, we conclude that mVSP associates with BSG (or its homologs) at the ER and that formation of this complex then escapes ER retention of mVSP, enabling forward trafficking to the PM.

3.2.6. Human BSG also affects the PM targeting of mVSP upon co-expression in HeLa cells

BSG protein in Human and Mouse share 58% of identical amino acids, whereas 80% of amino acid residues are conserved (Miyauchi *et al.*, 1991). While human BSG (hBSG) is endogenously expressed in HeLa cells, transiently transfecting mVSP alone in HeLa cells does not result in its surface expression. To further investigate whether the trafficking effect of BSG on mVSP might be restricted to the mouse variant, co-expression experiments were conducted in HeLa cells using RFP-tagged hBSG and GFP-tagged mVSP. Confocal images taken after 48 hours showed the presence of both GFP-mVSP and hBSG-RFP at the cell surface upon co-expression in HeLa cells (Figure 3.8D), similar to the pattern with over-expression of BSG-RFP (Figure 3.8E). This indicates that hBSG can substitute the mouse ortholog in trafficking mVSP to the PM. Notably, the transmembrane region and cytoplasmic tail of human and mouse BSG are highly conserved with only one amino acid difference in the transmembrane region and 70% identical homology in the cytoplasmic region. This allowed us to hypothesize that these conserved regions, i.e. transmembrane region or cytoplasmic terminus of BSG might act as the interaction region with mVSP, as also observed for interaction with MCTs (Wang *et al.*, 2021).

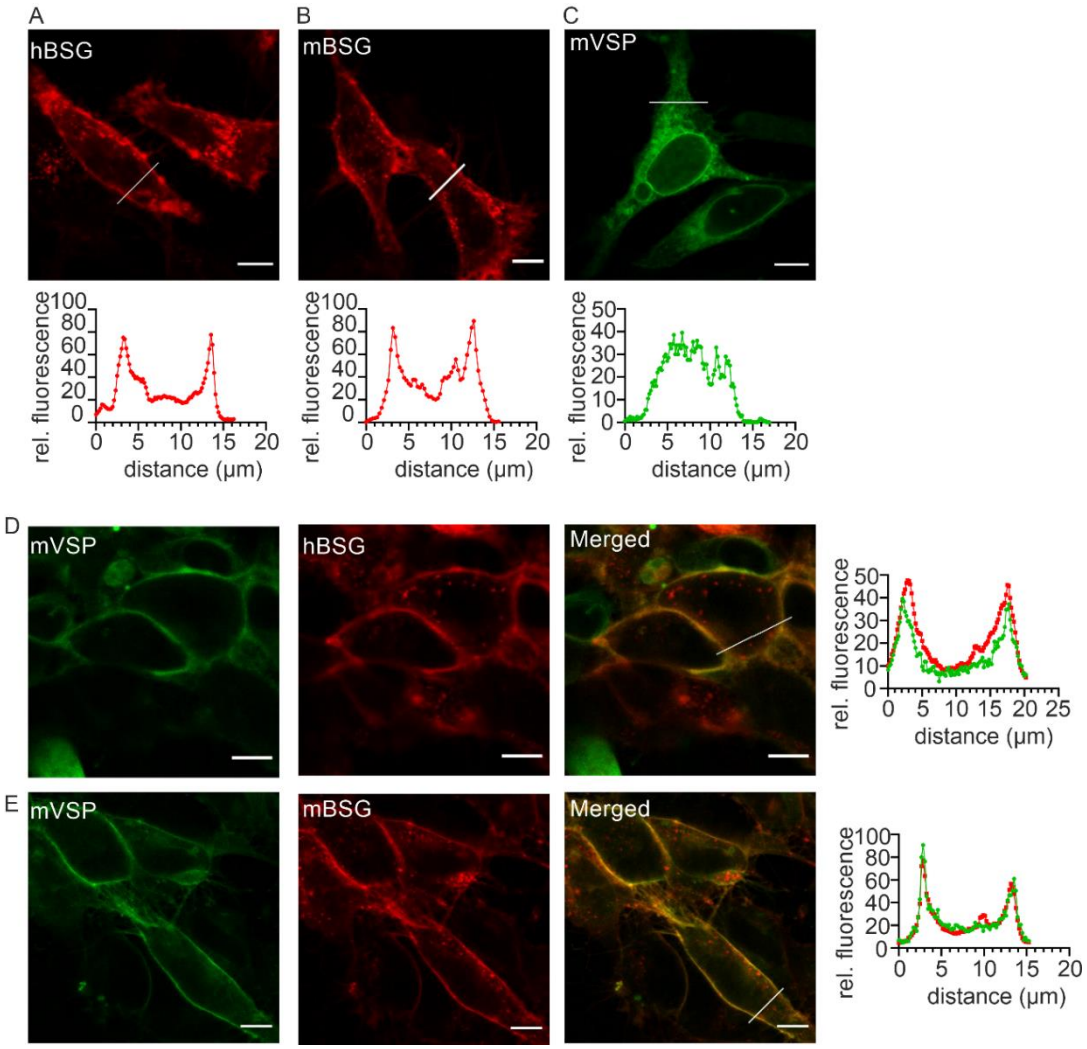

Figure 3.8: Human BSG is equally effective in translocating mVSP to the PM in HeLa cells. HeLa cells over expressed with RFP-tagged hBSG **(A)**, BSG **(B)**, GFP-tagged mVSP **(C)** and the corresponding fluorescence intensity profiles are shown at the bottom. Cells co-transfected with GFP-tagged mVSP and RFP-tagged hBSG **(D)**, RFP-tagged BSG **(E)** and the corresponding fluorescence intensity profiles are shown at the right. All images were taken 48 h post-transfection. Similar results were obtained in n = 3 transfections. The scale bars represent 10 µm.

3.2.7. BSG KO HeLa and HEK293 cells show similar response of mVSP PM targeting to exogenous BSG

Despite detectable levels of BSG within HeLa (Schmidt *et al.*, 2017) and HEK293 cells (Gallagher *et al.*, 2007), transiently transfected mVSP remained localized intracellularly. This observation led us to speculate that the dependence of mVSP for its PM localization might rely on the amount of available BSG molecules to exert its PM targeting effect on mVSP. To further investigate the role of endogenous BSG on mVSP PM targeting, we generated BSG knockout Hela and HEK293 cell lines by using Crispr cas9 gene editing strategy.

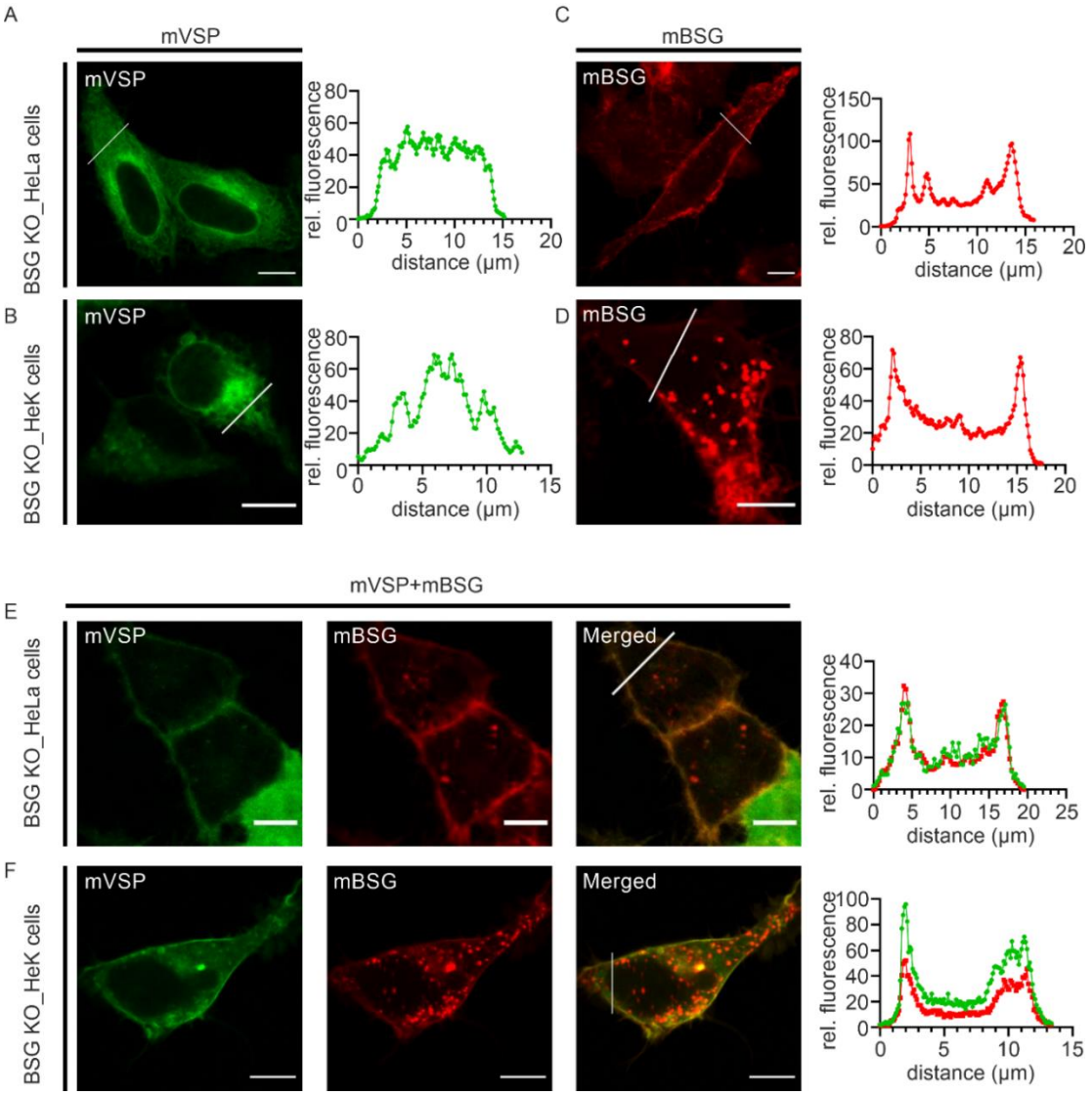

Figure 3.9: Effect of exogenous BSG in BSG knockout HeLa and HEK293 cells. Shown are the images of BSG knockout HeLa **(A)** and HEK293 cells **(B)** over-expressed with GFP-tagged mVSP with corresponding fluorescence intensity profile. RFP-tagged BSG was over expressed in BSG knockout HeLa and HEK293 **(C, D)** cells and to its right are the corresponding fluorescence intensity profile. Cells co-transfected with GFP-tagged mVSP and RFP-tagged BSG in BSG knockout HeLa cells **(E),** HEK293 cells **(F)** and to its right are corresponding fluorescence intensity profile. All images were taken 48 h post-transfection. Similar results were obtained in n = 3 transfections. The scale bars represent 10 µm.

The human BSG gene was targeted using a guide RNA scaffold sequence (sense, 5′-CACCGTTCACTACCGTAGAAGACT3’ and anti-sense 5’AAACAGGTCTTCTACG-GTAGTGAAC-3’) published by Satchwell and colleagues which was designed in a way to knock off at least three splice variants of human BSG (Satchwell et al., 2019). Upon over-expression of GFP-mVSP in BSG knockout HeLa and HEK293 cells, GFP-mVSP was localized in the ER and Golgi compartments (Figure 3.9A, B), which was similar to our previous observation in wild-type (WT) HeLa and HEK293 cells (Figure 3.4A and

3.7D). Moreover, GFP-mVSP showed its strong presence at the cell surface in BSG KO HeLa and HEK293 cells only upon over-expression of BSG-RFP (Figure 3.9E, F). A plausible explanation would be that the endogenously expressed BSG in HeLa cells may be involved in other cellular functions, and the available BSG molecules are not sufficient to facilitate mVSP trafficking to the cell surface.

3.3. Interaction of other BSG family members with mVSP

Next, I investigated whether the homologous family members of BSG, NPTN and EMB, can also facilitate the membrane localization of mVSP in HeLa cells.

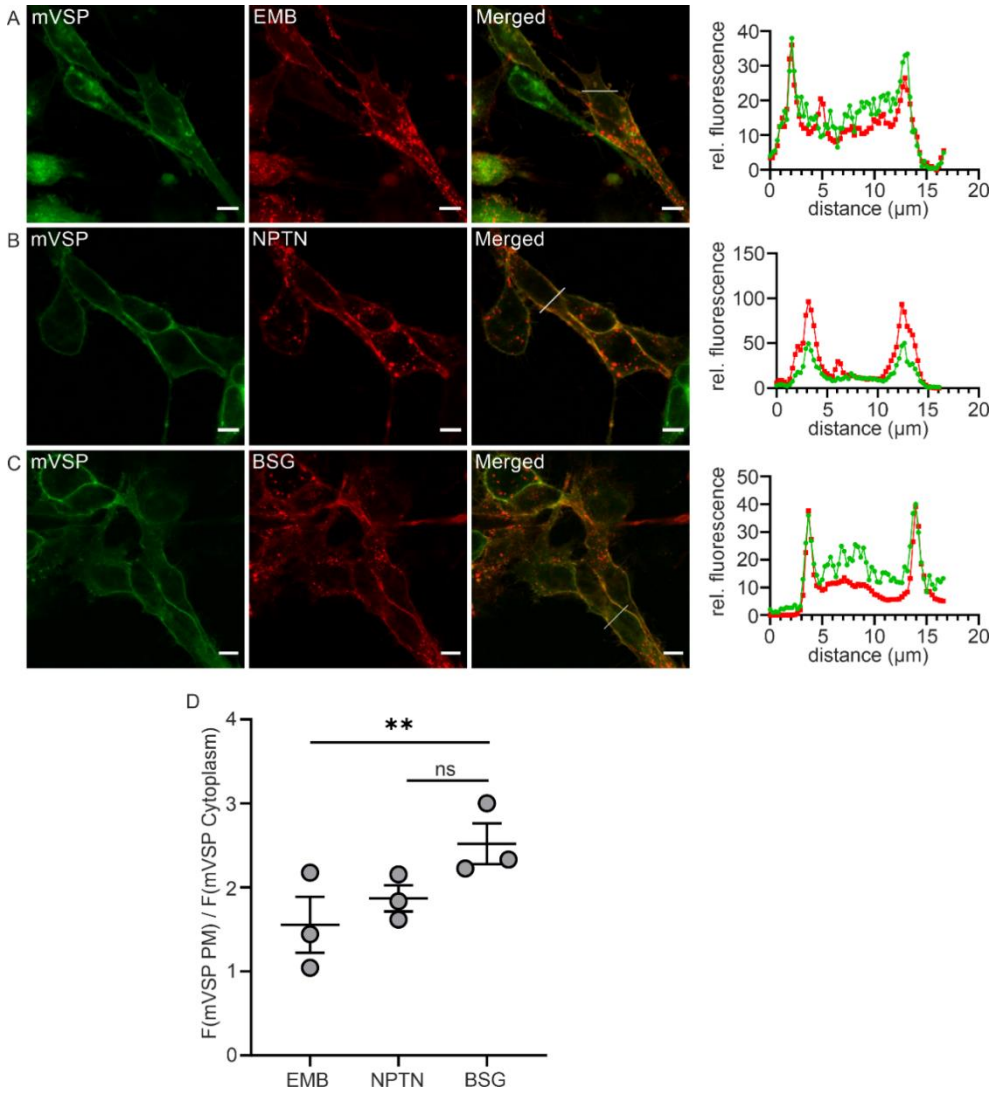

Figure 3.10: Co-localization of mVSP with BSG family members. Live-cell imaging of HeLa cells co-transfected with GFP-tagged mVSP and RFP-tagged **(A)** EMB, **(B)** NPTN, and **(C)** BSG respectively and their corresponding fluorescence intensity profiles at the right. **(D)** Quantification of VSP surface expression in the presence of exogenous EMB, NPTN or BSG. n=18 cells in three independent experiments each. **P<0.01; ns., not significant; Dunnett's test: neuroplastin, P=0.3053; embigin, P=0.0067). All images were taken 48 h post-transfection. The scale bars represent 10 µm

Previous studies have demonstrated that BSG and its homologues increase the cell surface localization of a crucial lactate transporter, MCT (Xu *et al.*, 2022; Kirk *et al*., 2000; Wilson *et al*, 2013). BSG specifically increases cell surface localization of MCT1 and MCT4, whereas NPTN preferentially affects MCT2 trafficking (Wilson *et al*, 2013), suggesting specificity in interactions. However, this specificity of interaction has not been extensively studied.

To this end, either BSG, NPTN, and EMB (RFP-tagged) were co-expressed with mVSP (GFP-tagged) in HeLa cells. As shown in Figure 3.10, all three BSG family members were able to translocate GFP -tagged mVSP to the PM (Figure 3.10). The membrane localization of mVSP was strongest with BSG, followed by NPTN and EMB (Figure 3.10D). Taken together, these results indicate that BSG or its homologs are functionally redundant in their interaction with mVSP, ensuring the localization of a mammalian VSP to the PM, irrespective of the probed cell type

3.4. Characterization of domains in BSG responsible for its effects on mVSP

Numerous studies have demonstrated that BSG exhibits distinct interaction patterns with its binding partners. Some studies propose that the extracellular region of BSG interacts with proteins like cyclophilin A, while others suggest that the transmembrane region interact with proteins such as MCTs facilitating their trafficking from intracellular compartments to the cell surface (Yurchenko *et al*.,2010; Wang *et al.,* 2021). We therefore investigated the domains or regions of BSG that are responsible for the translocation of mVSP to PM. Deletion mutagenesis was used to generate BSG ΔIgDs, which lacks the extracellular Ig domains (aa1-112+aa208-273), and BSG ΔC-term, which lacks the intracellular C-terminus (aa1-273, excluding aa239-273), both tagged with an RFP marker. Co-expression of these RFP-tagged BSG mutants with GFP-tagged mVSP revealed that deletion of either the N-terminal Ig domain (Figure 3.11B) or the C-terminal region of BSG (Figure 3.11C) did not affect the translocation of GFP-tagged mVSP to the PM (Figure 3.11B and C, first column). These results suggest that the extracellular and cytoplasmic regions of BSG are not required for the interaction with mVSP and the membrane targeting of mVSP. Hence, the transmembrane (TM) segment of BSG was sufficient for translocation of mVSP to the PM.

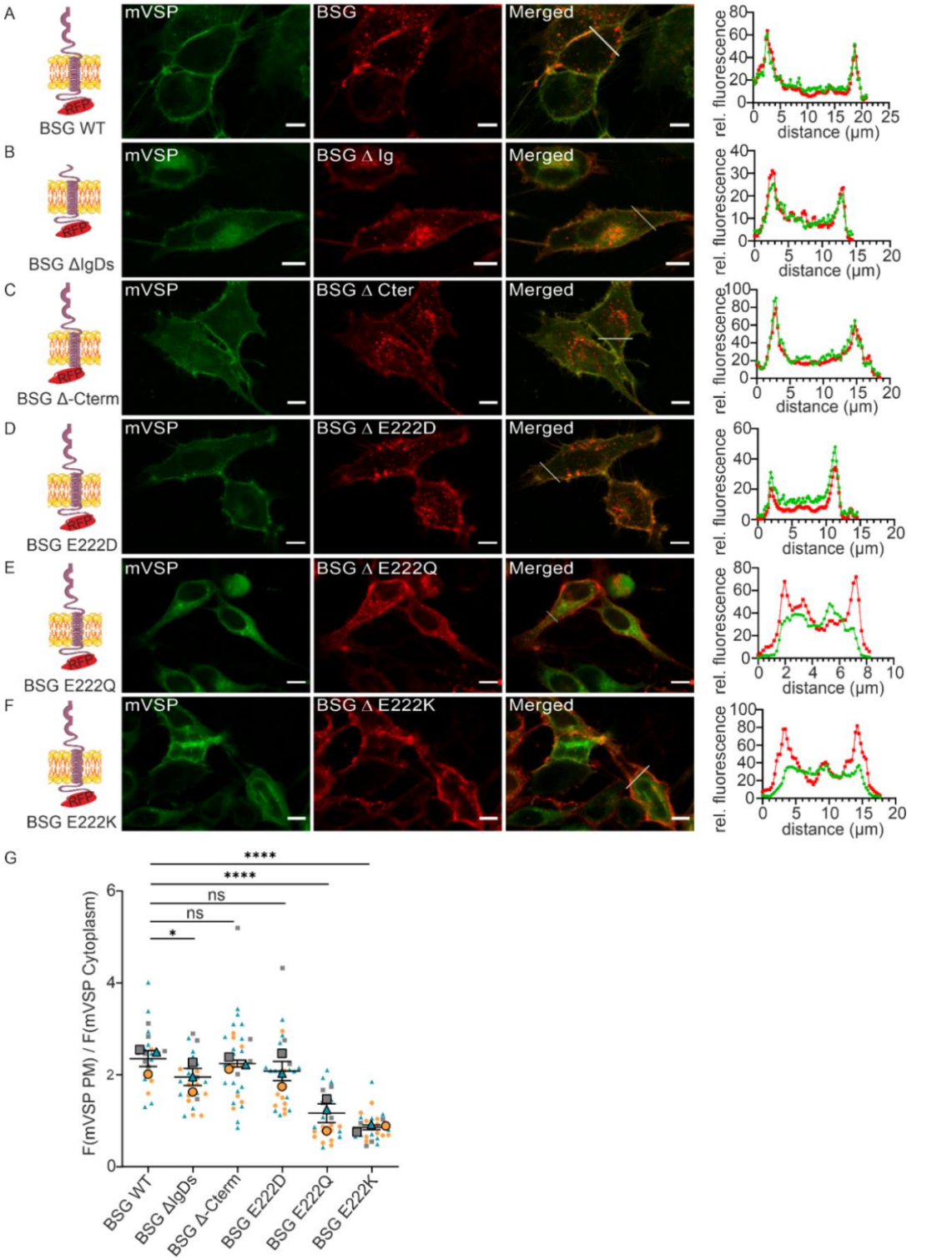

Figure 3.11: Mapping of mVSP binding site on BSG. Confocal images of HeLa cells co-transfected with GFP-tagged mVSP and RFP-tagged **(A)** BSG wt **(B)** BSG Δ Ig **(C)** BSG Δ C ter **(D)** BSG-E222D **(E)** BSG-E222Q **(F)** E222K constructs and their corresponding fluorescence intensity profiles are shown at the right. **(G)** Quantification of mVSP surface expression in the presence of exogenous BSG mutants (mean±s.e.m., BSG (control), n=21 cells; BSG Δ Ig, n=25 cells; BSG Δ C ter, n=30 cells; BSG E222D, n=28 cells; BSG E222Q, n=24 cells; BSG E222K, n=26 cells, in three independent experiments each. ****P<0.0001; *P<0.05; ns., not significant; Dunnett's test: BSG Δ Ig P=0.0155; BSG Δ C ter, P=0.8998; BSG E222D, P=0.1527; BSG E222Q, P=<0.0001; BSG E222K, P=<0.0001). All images were taken 48 h post-transfection. Similar results were obtained in n = 3 transfections. The scale bars represent 10 μm.

We further scrutinized the interaction of the TM region of BSG with mVSP. Sequence comparison reveals a high degree of conservation in the TM domains of BSG, NPTN, and EMB with a particularly notable conserved glutamate residue (E222) situated at the center of the TM. Consequently, we undertook mutational studies targeting this central glutamate and examined its impact on mVSP trafficking. When co-expressing these mutants with mVSP, we observed that a conservative mutation maintaining the charge (E222D) did not alter BSG's ability to facilitate mVSP trafficking (Figure 11D, G). In contrast, neutralization (E222Q) or charge reversal (E222K) of this central glutamate substantially disrupted BSG-dependent forward trafficking of mVSP to the PM (Figure 3.11E-G). It's worth noting that the mutations had no discernible effect on BSG's own targeting to the PM. Thus, it becomes evident that the transmembrane segment of BSG, particularly the central negatively charged residue, plays a pivotal role in its functional interaction with mVSP. Considering the evidence pointing toward a direct interaction between both proteins, these residues are highly likely to be an essential part of the protein-protein interaction interface.

3.5. Intracellular retention of mVSP is mediated by N and C termini

Transmembrane proteins destined for the PM, follow the secretory pathway (Barlowe *et al.*, 2013). Our results as well as previously published reports showed complete intracellular retention of mVSP along the secretory pathway, largely in the ER, and, to some degree, in the Golgi complex (Figure 3.6, columns 2 and 3). Several known mechanisms can mediate ER retention of a protein, such as improper folding or the presence of ER retention signals (Vashist *et al.*, 2001). We therefore aimed to identify domains or motifs responsible for its retention in the ER. To this end, we conducted a series of dissection studies on the N- and C-terminal regions of mVSP and also utilized a chimeric approach by swapping domains between mVSP and Ci-VSP, which does not experience ER retention.

3.5.1. Identification of a retention motif in the C-terminal region of mVSP

Previous studies conducted in our laboratory by Halaszovich *et al.,* have demonstrated that deletion of the cytoplasmic C-terminal catalytic domain of the human orthologue of

VSP (hVSP1γ) significantly enhances the surface localization. Inspired by these findings, we employed a similar approach by introducing a stop codon immediately following the

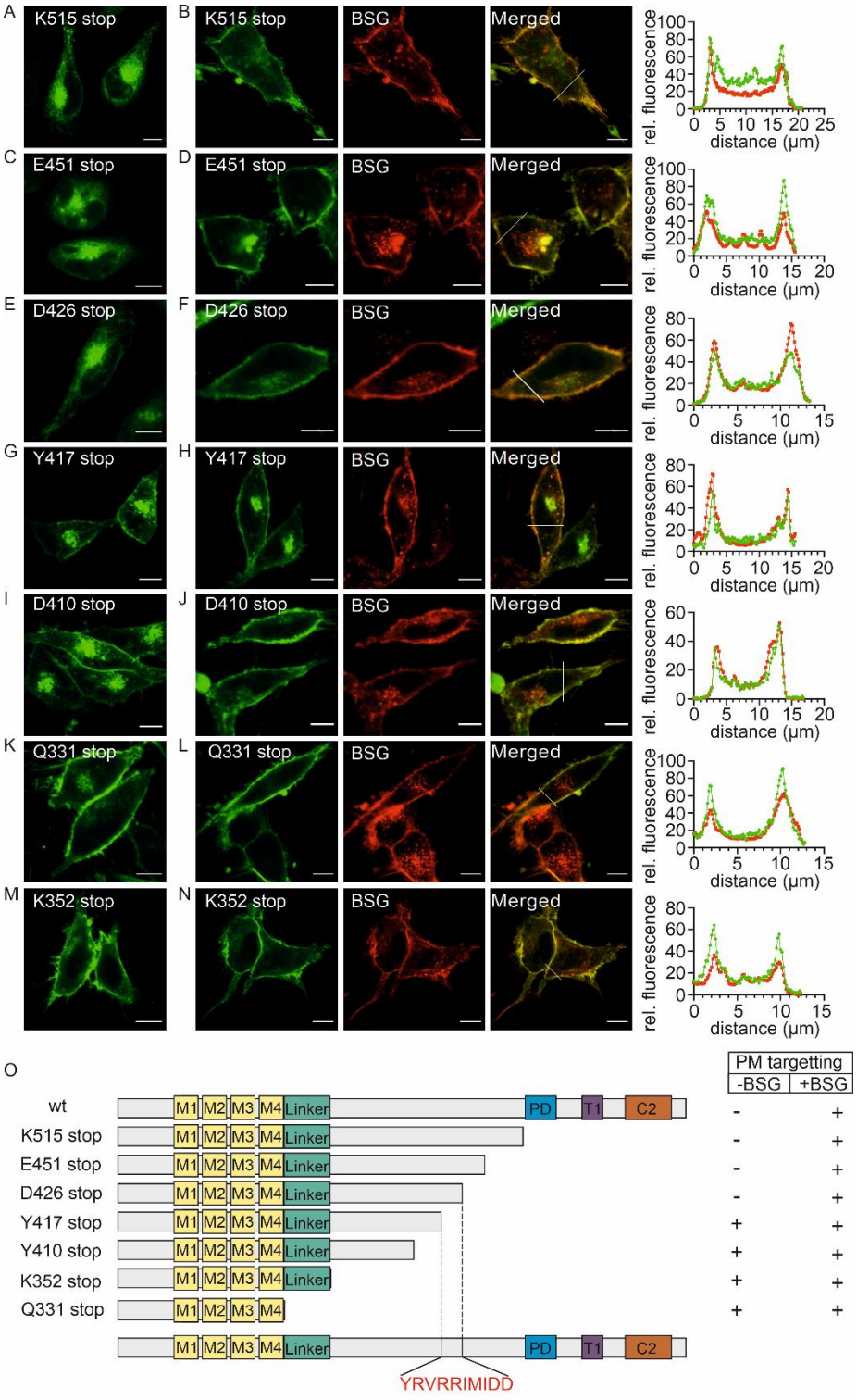

Figure 3.12: Mapping of retention motif on C-terminus of mVSP. Shown are the confocal images of Hela cells transfected with GFP-tagged mVSP C-terminal truncation mutants; mVSP K515 stop **(A)**, mVSP E451 stop**(C)**, mVSP D426 stop **(E)**, mVSP Y417 stop **(G)**, mVSP Y410 stop **(I)**, mVSP K352 stop **(K)** and mVSP Q331 stop **(M).** Cells were co-transfected with RFP-tagged BSG and GFP-tagged truncation mutants, namely mVSP K515 stop **(B)**, mVSP E451 stop **(D)**, mVSP D426 stop **(F)**, mVSP Y417 stop **(H)**, mVSP Y410 stop **(J)**, mVSP K352 stop **(L)**,

and mVSP Q331 stop **(N)**, to investigate the impact of BSG on these mutants, and their corresponding fluorescence intensity profiles are shown at the right. **(O)** Schematic diagram depicting mVSP-GFP truncation mutants (M, transmembrane region; linker, linker region; PD, Phosphatase Domain; T1, T1-loop; C2, C2-domain). The region (417-426 aa) from the mVSP C-terminus (putative retention region) is highlighted in red. Effect of BSG on mVSP mutants were scored as + (positive/PM targeting) or – (negative/no PM targeting) in the presence and absence of BSG. The scale bars represent 10 μm.

VSD in the N-terminally GFP-tagged mVSP (GFP-mVSP Q331 stop; Figure 3.12O).

Over-expression of this mutant construct in HeLa cells revealed its localization at the cell surface (Figure 3.12M). This led us to hypothesize that the region responsible for ER retention in mVSP lies within the C-terminal domain, specifically between amino acid positions 331-664. To identify the potential ER retention motif(s), we subsequently generated partial C-terminal truncation mutants by introducing stop codons: mVSP K515 stop, mVSP E451 stop, mVSP D426 stop, mVSP Y417 stop, mVSP Y410 stop, and mVSP K352 stop (Figure 3.12O). Over-expression of these truncation mutants in HeLa cells revealed that the mVSP K352 stop, mVSP Y410 stop, and mVSP Y417 stop mutants localized to the PM (Figure 3.12G, I, K), whereas the mVSP K515 stop, mVSP E451 stop, and mVSP D426 stop mutants were retained in the ER (Figure 3.12A, C, E). When these mutants were coexpressed with C-terminally RFP-tagged BSG, they were robustly localized to the PM, indicating that their ER retention was not due to a general folding defect induced by truncation, but by the retention mechanism that can be bypassed by BSG interaction.

These observations indicated that an ER retention region in mVSP may be located immediately proximal to D426, specifically the sequence YRVRRIMIDD.

3.5.2. Further microdissection of the retention region ^{417}YRVRRIMIDD^{426} in C-terminal region of mVSP

To further investigate the specific amino acids within the region ^{417}YRVRRIMIDD^{426} that are responsible for the ER retention of mVSP, we carried out amino acid substitutions in this segment. The substitutions involved incorporating amino acids from other VSPs which are known to be localized at the PM. Consistent with a recent study performed in our laboratory by Renigunta *et al*., it has been shown that hVSP1g predominantly targets to the PM (unpublished results). Based on this information, we examined amino acid similarities within the ^{417}YRVRRIMIDD^{426} region of mVSP corresponding to hVSP1. Notably, we identified diverging amino acids in hVSP1g, specifically at positions Y417 and R420, which were hypothesized to play a pivotal role in the PM targeting of mVSP.

We introduced amino acid substitutions in mVSP based on the corresponding residues in hVSP1g. Specifically, we substituted tyrosine (Y417) in mVSP with asparagine (N279) from hVSP1 and arginine (R420) in mVSP with serine (S282) from hVSP1, and implemented a double substitution of both Y417N and R420S in mVSP. (Figure 3.14M). Additionally, we introduced amino acid substitutions based on Ci-VSP, that likewise does not experience ER retention: mVSP (412-426 Ci-VSP). When these mutants were transfected into HeLa cells, they all exhibited ER localization, similar to the full-length mVSP protein (Figure 3.13A, C, E, and K). Upon co-expression with RFP-tagged BSG, the mutants mVSP Y417N, mVSP R420S, and mVSP Y417N/R420S were targeted to the PM (Figure 3.13B, D, and F), confirming structural integrity and hence persistent retention in the ER despite the point mutations. In contrast, the mutant mVSP (412-426 Ci-VSP) (containing the sequence motif from Ci-VSP) remained in the ER when over-expressed with BSG in HeLa cells (Figure 3.13L), indicating that this mutant may be affected structurally and cannot be used for analyzing the role of this sequence stretch.

Inspection of the ^{417}YRVRRIMIDD^{426} region of mVSP revealed the presence of an arginine-based potential retention/retrieval signal RXRR. RXRR signals have been identified in the gamma-aminobutyric acid type B (GABA(B)) receptors (Gassmann *et al.*, 2005). The C-terminal region of GABA B1 receptors contains an RSRR motif that prevents the protein from exiting the ER and restricts its surface expression. We thus investigated the RVRR residues in the C-terminal region of mVSP. Since the arginine residues at positions 418 and 421 were conserved between hVSP1g and mVSP, we initially substituted R420 individually with alanine, and over-expressed it in HeLa cells. The mVSP R420A mutant trafficked to the PM only when coexpressed with BSG (Figure 3.13G, H), indicating persistence of ER retention.

We therefore mutated all three basic positions to alanine (mVSP RRR418, 420, 421AAA). Imaging revealed that the triple arginine substitution localized to intracellular compartments irrespective of BSG co-expression (Figure 3.14I, J), precluding the use of this mutant on analyzing a potential ER retention signal.

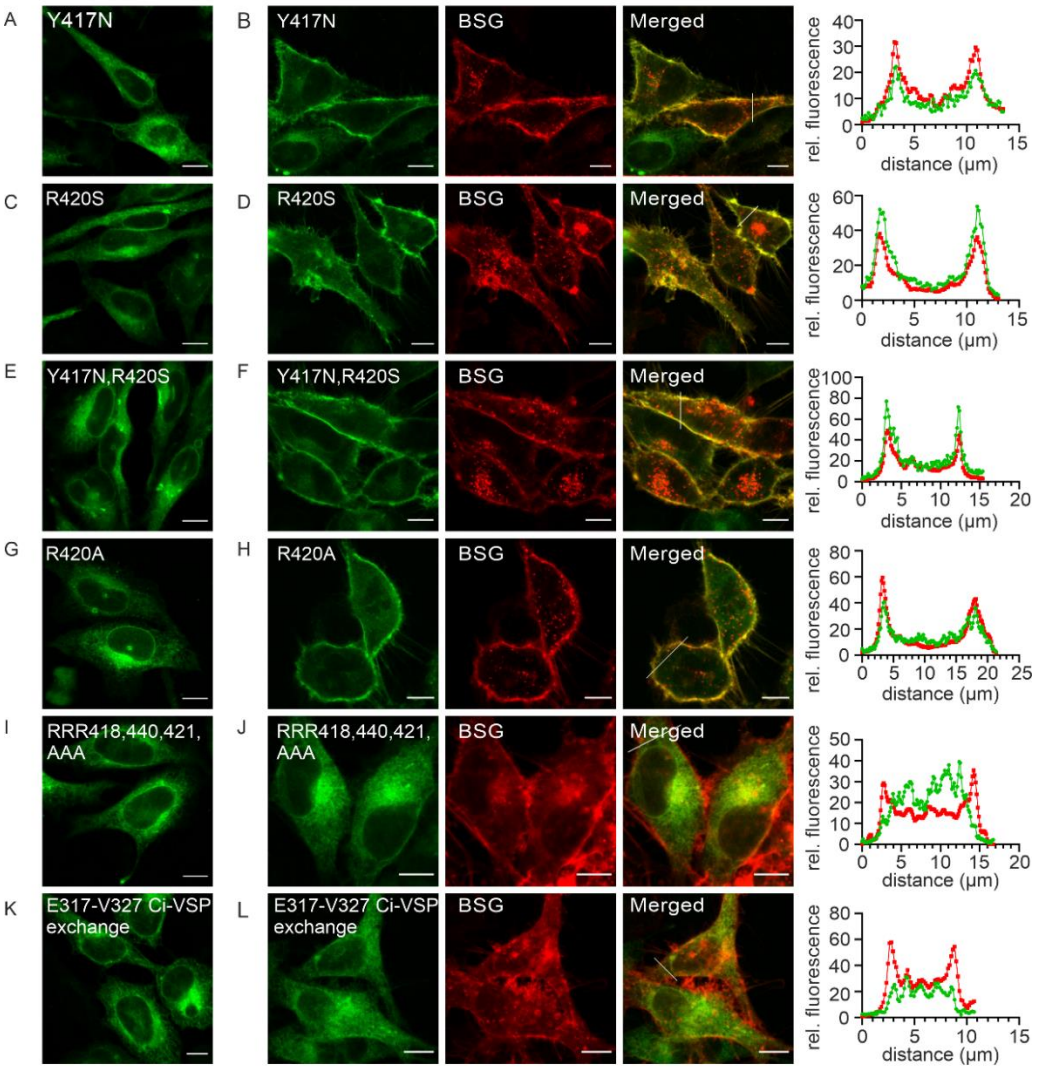

M

		PM targetting	
		-BSG	+BSG
Ci-VSP	317 E T K F D N H V Y R V M I D D 331		
hVSP1γ	274 P K H F H N R V S R I M I D D 288		
mVSP	412 P K H F H Y R V R R I M I D D 426		
Y417N	P K H F H N R V R R I M I D D	-	+
R420S	P K H F H Y R V S R I M I D D	-	+
Y417N,R420S	P K H F H N R V S R I M I D D	-	+
R420A	P K H F H Y R V A R I M I D D	-	+
RRR418,420,421AAA	P K H F H Y A V A A I M I D D	-	-
E317-V327 Ci-VSP exchange	E T K F D N H V Y R V M I D D	-	-

Figure 3.13: Analysis of the putative retention region in C-terminus of mVSP. Shown are the confocal images of Hela cells transfected with GFP-tagged mVSP C-terminal mutants; mVSP Y417N **(A)**, mVSP R420S **(C)**, mVSP Y417N, R420S **(E)**, mVSP R420A **(G)**, mVSP RRR418,420,421AAA **(I)** and mVSP (412-426 Ci-VSP) **(K).** HeLa cells were co-transfected using RFP-tagged BSG and GFP-tagged mVSP Y417N **(B)**, mVSP R420S **(D)**, mVSP Y417N, R420S **(F)**, mVSP R420A **(H)**, mVSP **(J)** and mVSP (412-426 Ci-VSP) **(L)** and their corresponding fluorescence intensity profiles are shown at the right. **(M)** The top rows of the schematic diagram depict the amino acid alignments of the putative region at the C-terminus of Ci-VSP, hVSP, and mVSP, while the bottom rows show mVSP mutants with amino acid substitutions highlighted in red. The effect of BSG on the mVSP mutants was assessed and indicated as either + (positive/PM targeting) or - (negative/no PM targeting) in the presence or absence of BSG. Similar results were obtained in n = 3 transfections. The scale bars represent 10 µm.

3.5.3. Dissection of the N-terminal regions of mVSP

The PM targeting of C-terminal truncations of mVSP suggested a region that plays a significant role in mediating ER retention. However, since disturbance of the potential retention motif alone was insufficient to release the ER retention (Figure 3.13), we considered that additional retention signals may act additively or cooperatively with the C-terminal signal.

This conclusion prompted us to investigate the N-terminal region of mVSP for potential retention signals. To explore the presence of any retention signal in the N-terminal region of mVSP, we performed truncation studies by generating five N-terminal truncation mutants: mVSP M60 start, mVSP M110 start, mVSP 160 start, mVSP M188 start, and mVSP M204 start. When over-expressed in HeLa cells, none of these mutants exhibited trafficking to the PM (Figure 3.14A, C, E, G, I, respectively). Interestingly, when these mutants were co-expressed with RFP-tagged BSG, only mVSP M60 start and mVSP M110 start were targeted to the membrane (Figure 3.15 B, D), whereas mVSP 160 start, mVSP M188 start, and mVSP M204 start remained localized intracellularly (Figure 3.14F, H, J). These observations suggest that the dissection of the N-terminal segment of mVSP may have led to protein misfolding, preventing its transport to the PM through BSG interaction.

The study conducted by Rosasco *et al.*, in 2015 suggested the existence of a naturally existing splice variant of VSP in mouse brain, known as mVSPΔExon9, which lacks exon 9 at the N-terminal region. According to that study, over-expression of mVSPΔExon9 in HEK293 cells showed its localization to the Golgi apparatus in contrast to full-length mVSP which is resided in ER. Thus, this splice variant might provide an indication of a possible ER retention signal in the region of exon 9. As shown in Figure 3.14K, GFP-tagged mVSPΔExon9 in HeLa cells was still localized in ER, similar to mVSP full length protein. Co-expression with BSG shows a clear localization of the mVSPΔExon9 variant at the PM (Figure 3.14L) suggesting that this region may not be critical for ER retention.

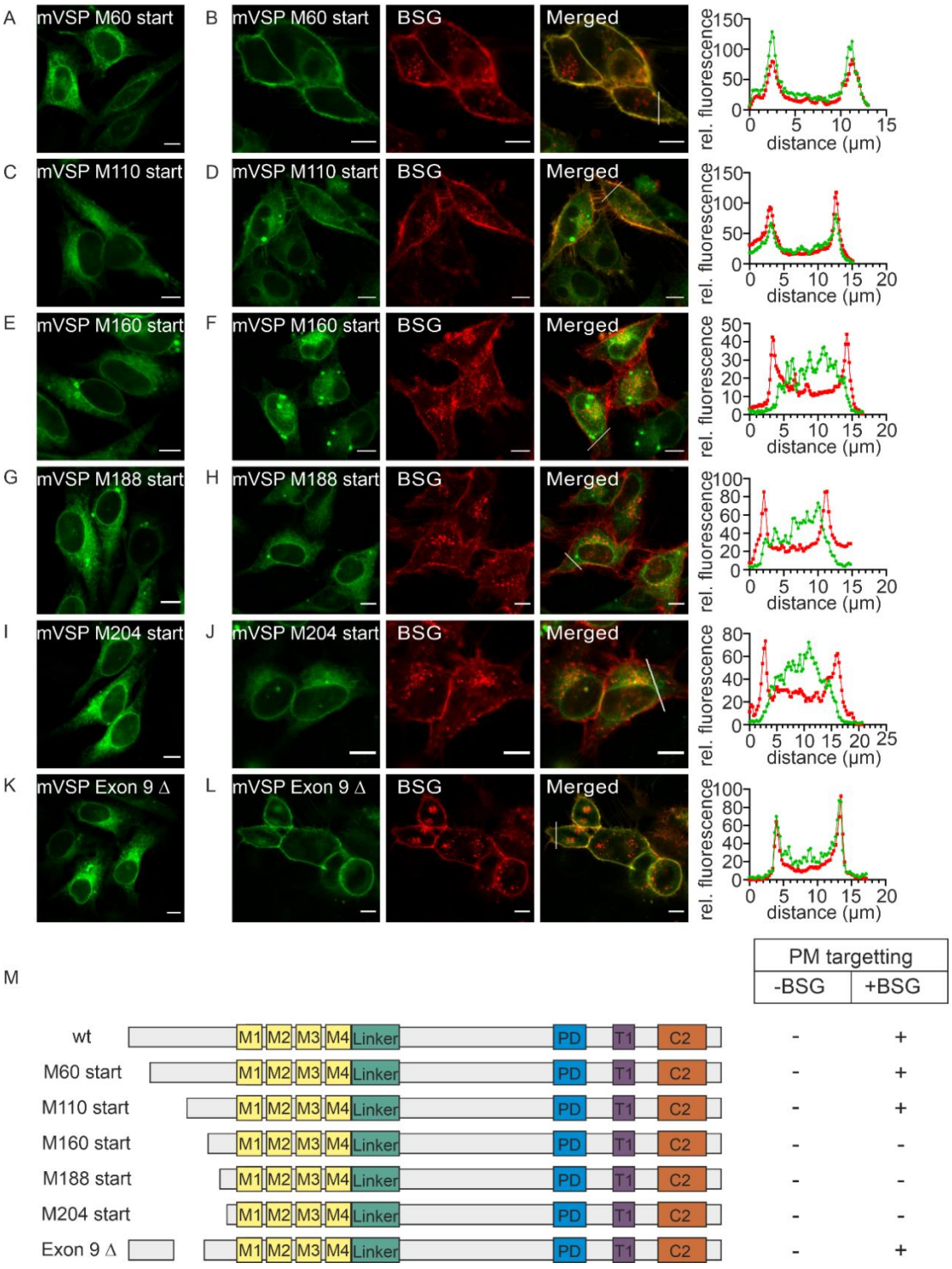

Figure 3.14: Mapping potential retention signals at the N-terminus of mVSP. To check for a retention signal at the N-terminus of mVSP, HeLa cells were transfected with GFP-tagged mVSP N-terminal mutants; mVSP M60 start **(A)**, mVSP M110 start **(C)**, mVSP 160 start **(E)**, mVSP M188 start **(G)**, mVSP M204 start **(I)**, mVSP exon 9 deletion **(K)**. Cells were co-transfected using RFP-tagged BSG and GFP-tagged mVSP M60 start **(B)**, mVSP M110 start**(D)**, mVSP 160 start **(F)**, mVSP M188 start **(H)**, mVSP M204 start **(J)**, mVSP exon 9 deletion **(L)**. and their corresponding fluorescence intensity profiles are shown at the right**. (M)** Schematic diagram depicting GFP-tagged mVSP- N-terminal truncation mutants (M, transmembrane region; linker, linker region; PD, Phosphatase Domain; T1, T1-loop; C2, C2-domain) and their PM targeting ability in the presence and absence of was scored as + (positive/PM targeting) or – (negative/no PM targeting). The scale bars represent 10 µm.

3.5.4. Identification of retention motifs in the intracellular regions of mVSP

From the above dissection studies, we did not gain much insight into the identification of a single independent retention motif that is responsible for the ER retention of mVSP.

To further investigate the factors influencing retention of mVSP in the ER, we generated molecular chimeras by exchanging domains between Ci-VSP and mVSP. Specifically, we created six different chimeras, as illustrated in Figure 3.16. Chimera-1, with the C-terminus of mVSP replaced by the homologous domain of Ci-VSP (Figure 3.15M), was retained in the ER in a manner similar to wild-type mVSP (Figure 3.15A). However, co-expression of chimera-1 with BSG resulted in robust translocation to the PM that closely resembling the translocation effect observed with wild-type mVSP (Figure 3.15B). This observation strongly suggests the ability of BSG to effectively bind to chimera-1 and, more importantly, to bind in the absence of the C-terminal region of mVSP, resulting in its translocation to the PM.

We tested the second chimera (Chimera 2), in which only the N-terminal region of mVSP was exchanged with that of Ci-VSP (as depicted in Figure 3.16M). In contrast to chimera-1, chimera-2 effectively translocated to the PM without the need for co-expression of BSG (Figure 3.15C). Additionally, when chimera 2 was co-expressed with BSG, it further confirmed our findings as it resulted in robust translocation to the PM, indicating that the N-terminus of mVSP is not crucial for BSG binding or for the observed translocation effects (Figure 3.15D).

We generated the third chimera, Chimera 3, by exchanging the transmembrane domain of Ci-VSP with that of mVSP (as depicted in Figure 3.15M). Remarkably, when chimera 3 was transiently transfected into HeLa cells, it was trafficked to the cell surface independent of BSG (Figure 3.15E). The results obtained from our study strongly suggest that the transmembrane segment of mVSP does not play a role in ER retention. Notably, when BSG and chimera 3 were co-expressed, we observed a substantial expression of chimera 3 at the PM (Figure 3.15F). This finding highlights the significant contribution of the transmembrane domain of mVSP in facilitating proper localization and trafficking of the protein to the PM. Furthermore, the presence of BSG further enhanced the translocation effect, emphasizing its role in promoting the translocation of chimera 3 to the PM.

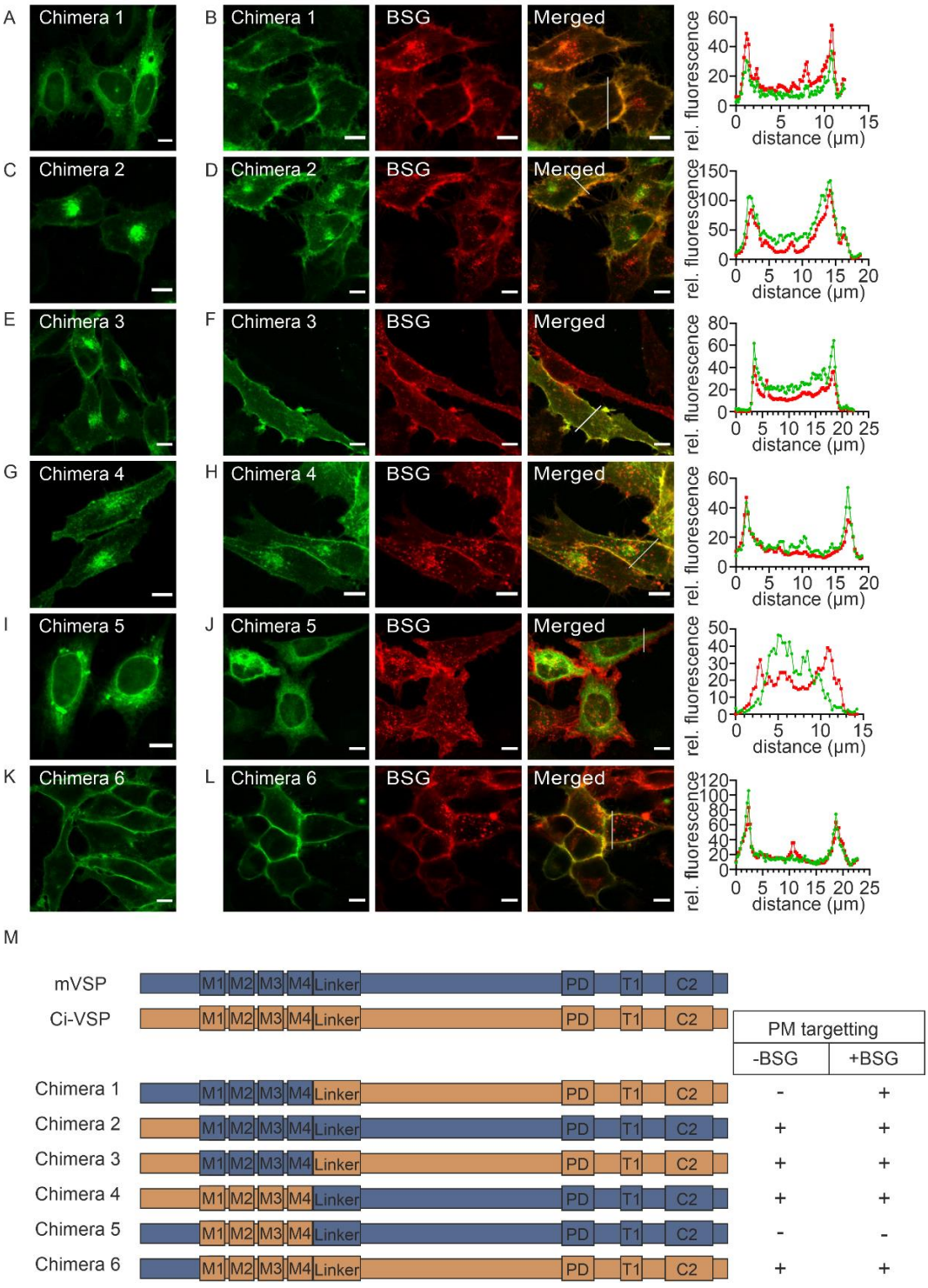

Figure 3.15: The retention mechanism of mVSP was investigated using a chimeric approach. Shown are the confocal images transfected with GFP-tagged mVSP/Ci-VSP chimeras; chimera 1 **(A)**, chimera 2 **(C)**, chimera 3 **(E)**, chimera 4 **(G)**, chimera 5 **(I)**, chimera 6 **(K).** Cells were co-transfected with RFP-tagged BSG and chimera 1 **(B)**, chimera 2 **(D)**, chimera 3 **(F)**, chimera 4 **(H)**, chimera 5 **(J)**, chimera 6 **(L)** and their corresponding fluorescence intensity profiles are shown at the right. **(M)** Schematic diagram representing of mVSP (blue) and Ci- VSP (Orange) at the top row and mVSP/Ci-VSP chimeras at the bottom rows (M, transmembrane region; linker, linker region; PD, Phosphatase Domain; T1, T1-loop; C2, C2-domain). PM targeting ability in presence and absence of BSG was rated as + (positive/PM targeting) or – (negative/no PM targeting). All images were taken 48 h after transfection. Similar results were obtained in n = 3 transfections. The scale bars represent 10 µm.

The fourth chimera, chimera 4, was created by fusing the cytoplasmic phosphatase domain of mVSP with the VSD of Ci-VSP (as depicted in Figure 3.15M). Similar to Chimera 2 and 3, Chimera 4 exhibited translocation to the PM without the assistance of BSG, when transiently transfected into HeLa cells (Figure 3.15G). This observation suggests that there might be no retention motif in the phosphatase domain of mVSP that hinders its membrane targeting. Furthermore, the co-expression of Chimera 4 with BSG also led to the targeting of Chimera 4 to the PM, which was also observed in the absence of BSG (Figure 3.15H).

In further investigation of the transmembrane segments of mVSP, we created Chimera 5 by exchanging the transmembrane domain of mVSP with that of Ci-VSP (as depicted in Figure 3.15M). Interestingly, when expressed in HeLa cells, Chimera 5 displayed a similar pattern of retention in the ER as observed with wild-type mVSP (Figure 3.15I). This finding, in conjunction with the previous assumption based on Chimera 3, suggests that both the N- and C-termini of mVSP may contribute equally to the retention of the intact protein in the ER.

Furthermore, when Chimera 5 was co-expressed with BSG, it remained retained in the ER, indicating that the transmembrane region of mVSP plays a crucial role in the binding of BSG and the subsequent membrane targeting of mVSP (Figure 3.15J). These results highlight the significance of the transmembrane domain in mediating the interaction between mVSP and BSG, leading to the proper subcellular localization of mVSP.

Having established that the C-terminus of mVSP does not contribute to retention, we turned our attention to the N-terminus of mVSP. To investigate this, we generated chimera 6 in which only the N-terminal region of Ci-VSP was exchanged with that of mVSP (as shown in Figure 3.15M). Surprisingly, chimera 6 showed a robust translocation to the PM that was independent of BSG (Figure 3.15K). In addition, the co-expression of BSG with Chimera 6 also resulted in a translocation to the PM (Figure 3.15L).

In agreement with our previous observation in Figure 3.13M, where the C-terminal truncation of mVSP (mVSP Q331 stop) had no effect on membrane targeting, we observed a similar phenomenon with Chimera 6. Collectively, these results demonstrate that both the N- and C-termini of mVSP are critical for mVSP retention in the ER.

3.6. Uncovering voltage-dependent phosphatase activity of PM-localized mVSP

While the voltage-sensitive catalytic activity of non-mammalian VSPs has been extensively studied, the catalytic activity of VSPs in mammals is still unknown. This knowledge gap could be attributed to their inability to access PM. To address this issue, researchers have employed diverse chimeric approaches that involve combining the VSD and phosphatase domains of mammalian VSPs with those of non-mammalian VSPs. A pivotal study conducted in 2012 by Halaszovich *et al*., demonstrated that the fusion of the catalytic domain of human VSP1 with the VSD of non-mammalian VSPs resulted in enzymatic activity, that closely resembled the behaviour observed in non-mammalian VSPs (Halaszovich *et al*., 2012). Moreover, a study conducted in 2015 by Rosasco *et al*., demonstrated that the VSD of mVSP, when fused to the pore domain of a voltage-gated K+ channel, imparted voltage-dependence to the channel pore. Additionally, this study revealed that fusion of the phosphatase domain of mVSP to the voltage-sensing domain of a non-mammalian species, specifically Dr-VSP, resulted in voltage-dependent phosphatase activity against $PI(4,5)P_2$. For the first time, we evaluated the voltage-dependent phosphatase activity of mVSP in vivo by enabling its membrane localization through BSG. We investigated the lipid phosphatase activity of mVSP through a live-cell assay, which involved the use of fluorescence biosensors (PLCδ1-PH-GFP and TubbyCT) designed to monitor the substrates of VSP (Halaszovich *et al*., 2012), and the measurements were performed using TIRF microscopy. Additionally, we controlled the cell membrane potential by varying the extracellular K+ concentration, ensuring a comprehensive examination of mVSP activity. To support the latter method, we employed the Flp-In™ 293 cell line that exhibits stable expression of the ROMK2 K^+ channel (Renigunta *et al*., 2011). This channel imparts significant constitutive K^+ permeability, allowing the adjustment of membrane potentials to closely match with the K^+ reversal potential. Specifically, the estimated potentials are -115 mV at 2 mM and 0 mV at 150 mM extracellular K^+, respectively. Depolarization of the membrane potential by application of 150 mM K^+ resulted in a reversible dissociation of the probe from the membrane (Figure 3.16) in cells co-expressing mVSP, BSG**,** and either the $PI(4,5)P_2$ sensor PLCδ1-PH-GFP (Figure 3.16 A) or tubbyCT (Figure 3.16D), indicating $PI(4,5)P_2$ depletion, which was traced using TIRF microscopy. PLCδ1-PH-GFP or tubbyCT-GFP translocation was completely absent when catalytically dead mVSP C458S was co-

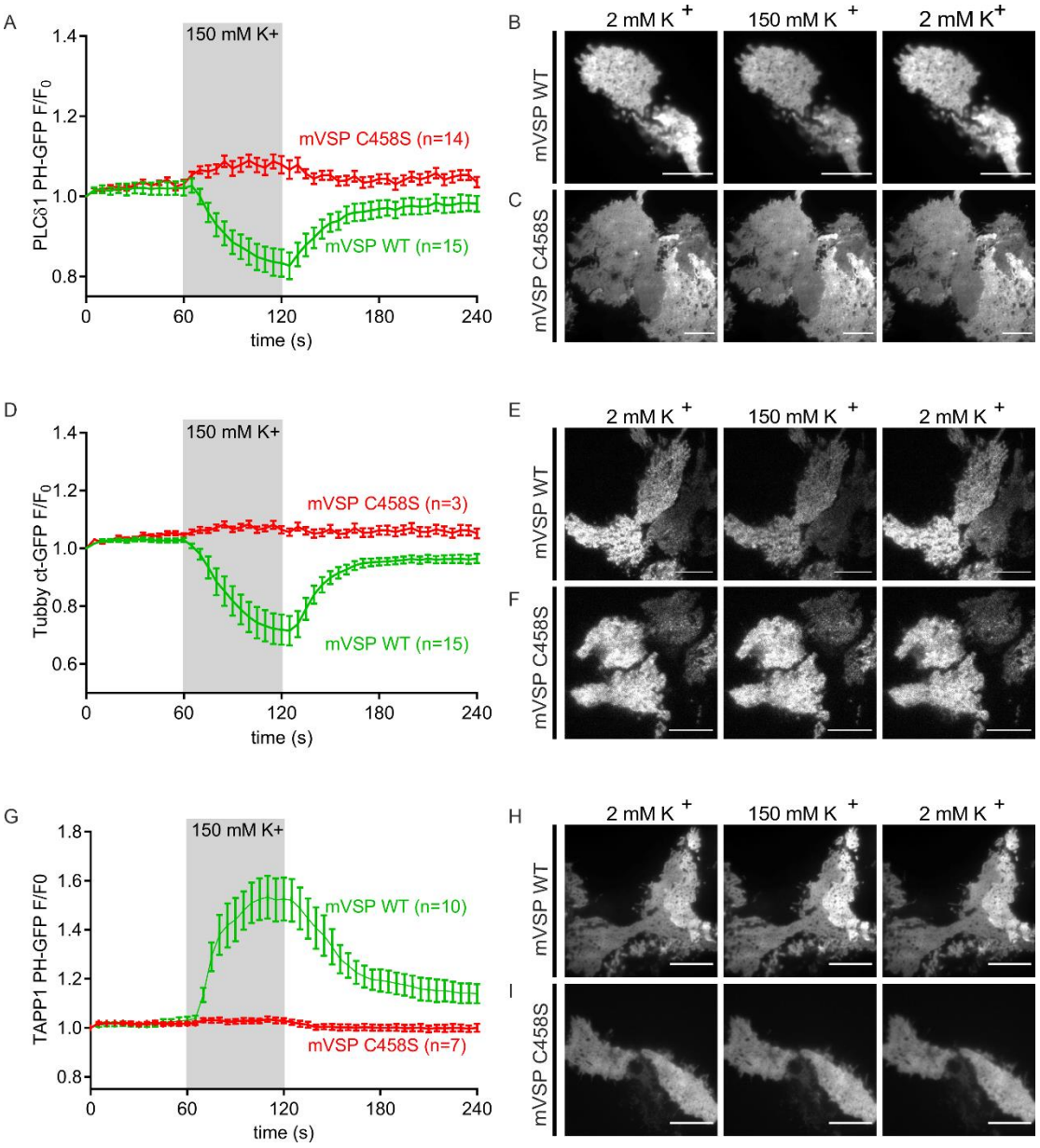

Figure 3.16: Phosphatase activity and substrate specificity of mVSP. TIRF signals in response to the depolarization (150 mM K^+, gray shading) from cells expressing RFP-mVSP (green), mVSP dead (red) with the PI(4,5)P_2 sensor PLCδ1-PH-GFP (**A**),TubbyCT-GFP **(D)** or the PI(3,4)P_2 sensor TAPP1 PH-GFP **(G)**. Dissociation and association of the probes from and to the membrane are indicated by decreasing and increasing fluorescence signals, respectively. For the mVSP mutant (C458S), no voltage-dependent sensor translocation was observed. On average, PLCδ1-PH-GFP and tubbyCT-GFP showed a decrease in membrane association (n = 15 respectively) upon activation of mVSP by depolarization. Whereas TAPP1 PH showed a strong increase in membrane association (n = 10), indicating the generation of PI(3,4)P_2**.** TIRF images of a ROMK2- Flp-In 293 cell line coexpressing PLCδ1-PH-GFP with (**B**) mRFP-mVSP and myc BSG (**C**) mVSP-C458S (dead mutant) and myc BSG acquired before (left), during (middle) and after (right) application of 150 mM K^+. TIRF images of a ROMK2- Flp-In 293 cell line coexpressing TubbyCT-GFP with **(E)** mRFP-mVSP and myc BSG **(F)** mVSP-C458S (dead mutant) and Myc BSG acquired before (left), during (middle) and after (right) application of 150 mM K^+. TIRF images of a ROMK2- Flp-In 293 cell line coexpressing TAPP1 PH-GFP with **(H)** mRFP-mVSP and myc BSG **(I)** mVSP-C458S (dead mutant) and Myc BSG acquired before (left), during (middle) and after (right) application of 150 mM K^+. Similar results were obtained in n = 3 transfections. The scale bars represent 10 µm.

transfected with BSG (Figure 3.16A, D, red trace), indicating that the sensor translocation was caused by mVSP-induced PI(4,5)P_2 depletion. Thus, mVSP has phosphoinositide phosphatase activity in vivo, and, in particular it dephosphorylates PI(4,5)P_2. Fluorescent probe tests also demonstrated that mVSP can use PI(3,4,5)P_3 as an alternative substrate, by removing the phosphate group at position 5. Depolarization by high K+ increased the membrane concentration of PI(3,4)P_2, as shown by the increased membrane binding of the specific PI(3,4)P_2 probe PH-TAPP1-GFP (Figure 3.18G, green trace). Similar to the translocation observed with PLCδ1-PH-GFP, the translocation of PH-TAPP1-GFP was completely absent when the catalytically inactive mVSP C458S was employed (Figure 3.16G, red trace). In essence, mVSP functions as a voltage-activated PI 5-phosphatase, mirroring crucial characteristics that were previously identified in non-mammalian VSPs.

4. Discussion

Over the past decade, voltage-sensing phosphatases have garnered significant attention due to their distinctive ability to dephosphorylate phosphoinositides in response to changes in membrane potential. The ability of VSPs to modulate PI concentration levels within the PM has entitled them as valuable tools for studying the complexities of PI-mediated cell biology (Rjasanow *et al*., 2011; Mavrantoni *et al*., 2015).

Non-mammalian VSPs have been studied extensively at the molecular level, revealing enzymatic specificity and deep insights into the mechanism of activation by membrane voltage. In contrast, the understanding of mammalian VSPs has remained limited due to their inability to demonstrate their phosphatase activity against PIs. A crucial distinction lies in their subcellular localization when expressed in heterologous systems. Notably, VSPs from *Ciona intestinalis* (Ci-VSP) and *Danio rerio* (dr-VSP) have been extensively characterized, predominantly due to their robust presence at the PM (Kawanabe *et al.*, 2020; Halaszovich *et al.*, 2009). On the contrary, most mouse and human isoforms exclusively localize to intracellular compartments upon over-expression in heterologous cells (Halaszovich *et al.*, 2012; Walker *et al.*, 2001; Tapperel *et al.*, 2003; Rosasco *et al*., 2015). This phenomenon has hindered the exploration of their enzymatic properties and voltage-dependent behaviour. Only through a chimeric approach, involving the fusion of the catalytic domain of mammalian VSP to the VSD of non-mammalian VSPs, the catalytic domain of mammalian VSP demonstrated phosphatase activity against PIs, resembling that of their non-mammalian counterparts (Halaszovich *et al.*, 2012; Rosasco *et al*., 2015). However, the membrane targeting and voltage-dependent phosphatase activity of the complete protein of mammalian VSPs has remained unknown.

In my PhD thesis, we are addressing some of the unanswered questions using mouse VSP as a representative model for mammalian VSPs. A pivotal finding of our investigation is that single-transmembrane proteins, such as BSG, NPTN, or EMB, can recruit mVSP from the ER to the PM. This finding was consistent across various mammalian cell lines studied, and BSG was particularly effective at this recruitment.

BSG has been discovered several times independently in different species, as it has been called by different names such as cluster of differentiation (CD147) (Muramatsu *et al*., 2003), Hepatoma-associated antigen HAb18G (Li *et al*., 2009), extracellular matrix metalloproteinase inducer (EMMPRIN) (Biswas *et al*., 1995), blood group OK antigen (Spring *et al*., 1997). It is a highly glycosylated protein and is expressed in multiple

epithelial, neuronal, lymphoid and myeloid cell types (Fossum *et al*., 1991; Kasinrerk *et al*., 1992; Kanekura *et al*., 1991; Nakai *et al*., 2006). BSG has diverse functions in nutrient transport, wound healing, inflammation, developmental processes, spermatogenesis and many more. (Agrawal *et al*., 2011; Gabison, *et al*., 2009; Muramatsu *et al*., 2003; Bi *et al*., 2013)

BSG along with a subset of cell surface glycoproteins including, NPTN (Beesley *et al*., 2014) and EMB (Ozawa *et al*., 1998; Tachikui *et al*., 1999) belong to immunoglobulin superfamily (IgSF). These proteins have garnered extensive research attention and are grouped together due to their striking structural similarity (Beesley *et al*., 2014). They consist of a single transmembrane domain with one or more Ig domains at the amino terminus, depending on the splice variant, and a short cytoplasmic tail at the carboxyl terminus (Juliano *et al*., 2002). Although the structure of these proteins is identical, they share a high number of conserved amino acid residues in the transmembrane region and cytoplasmic tail (Miyauchi *et al*., 1991). The most promising identity of the transmembrane domain is the glutamate residue which is conserved in all three proteins and plays a significant role in molecular interaction with other proteins (Manoharan *et al*., 2006).

Through this work, we are beginning to understand the complex mechanism underlying the subcellular localization of mammalian VSPs and may pave the way for a more comprehensive understanding of their physiological roles and potential applications in cell biology.

4.1. Mechanism behind BSG-mediated cellular trafficking of mVSP

The mechanism underlying BSG-dependent forward trafficking is a fascinating problem in cell biology. Extensive literature highlights involvement of BSG in various physiological processes and pathophysiological contexts. Remarkably, BSG has been implicated as ancillary protein, facilitating PM localization of two unrelated group of proteins, the plasma membrane Ca^{2+} ATPases (PMCA) and MCTs (Kirk *et al*., 2000; Schmidt *et al.,* 2017). Despite this noteworthy observation, the underlying mechanisms that orchestrate PM localization remain elusive in all the cases. Evidence suggests that in the case of PMCA, there is likely co-trafficking of a PMCA-BSG complex from the ER to the PM, as supported by proteomic analysis of native complexes (Schmidt *et al*., 2017). Likewise, the proposition has been made that the assembly of the BSG-MCT complex in the ER is necessary for the trafficking of MCT to the PM (Kirk *et al*., 2000).

Neither the retention signal that determines ER localization of mammalian VSPs in the absence of BSG, nor the mechanism, by which BSG mediates forward trafficking is currently known. However, the extensive subcellular co-localization of both proteins and the stable physical association of both proteins shown by Y2H and co-IP analysis suggest that secretory co-transport occurs as a heteromeric complex assembled from both proteins in the ER. This conclusion was further supported by the observation, that BSG construct with ER-restricted localization was unable to facilitate forward trafficking of mVSP but closely co-localized with mVSP in an ER like subcellular pattern (Figure 3.7 D-F).

We consider three potential mechanisms of action underlying PM trafficking of VSP. Firstly, the association between mVSP and BSG could function to mask an ER retention signal present in mVSP allowing mVSP to exit the ER. Secondly, the interaction might lead to the exposure of ER export signals present in the cytosolic region of mVSP, thereby facilitating its transit from the ER to the PM. Lastly, the binding of BSG could exert an allosteric effect, enhancing the stability and/or proper folding of mVSP within the heteromeric complex, potentially aiding in its functional maturation. Further investigation is warranted to elucidate the precise mechanism underlying this intriguing relationship.

4.2. BSG family members are equally involved in forward trafficking of mVSP

Previous research has established that BSG serves as an auxiliary protein for MCT1 and MCT4, while EMB and NPTN play roles in promoting the membrane expression of MCT2 (Wilson *et al*., 2013; Ovens MJ *et al*., 2010). The interactions among BSG homologs and MCTs are mediated by the transmembrane region shared among BSG family members (Wang *et al.,* 2021; Xu *et al.,* 2022; Schmidt *et al*., 2017). Notably, the transmembrane segments of BSG, NPTN, and EMB exhibit substantial homology, with BSG sharing 61% homology with NPTN and 57% with EMB. The structural basis for the formation of heteromers of BSG family members and their cargo proteins is similar for all three cargo protein classes (Wang *et al.,* 2021; Xu *et al.*, 2022; Gong *et al*., 2018).

To delve deeper, our investigation extended to the examination of whether the principles of action discovered for BSG could be extrapolated to other family members. Employing live cell imaging in HeLa cells, our findings unveiled that the forward trafficking effect on mVSP is not exclusive to BSG alone but extends to NPTN and EMB as well. This discovery suggests the existence of conserved elements within the transmembrane segment that facilitate similar modes of action across these family members. Together,

the striking resemblance in the biochemical binding mechanism and the consequential regulation of forward trafficking to the PM across three diverse classes of membrane proteins suggest the presence of a universal operating principle. Hence, the protein family comprising BSG, NPTN, and EMB may act as a central hub in the complex network of trafficking proteins intended for PM delivery. An exciting avenue for future exploration lies in investigating whether additional membrane proteins localized to the PM also depend on BSG or its homologs for efficient trafficking. The question of how these proteins interact with the sorting and trafficking machinery remains unanswered and warrants meticulous investigation.

4.3. Region of interaction between mVSP and BSG

Our investigation aimed at identifying the precise regions within BSG required for its interaction with mVSP, and consequently for the observed effect on forward trafficking. Notably, the binding of NPTN to PMCA (Gong *et al*., 2018) and BSG or EMB to MCTs (Wang *et al*., 2021; Xu *et al*., 2022), through TM-TM interaction has been directly observed in experimental structures obtained by cryo-EM.

To identify the interaction interface with mVSP, we first employed truncation experiments and generated BSG mutants lacking the IG2 domain or the C-terminus. By subjecting these mutants to live cell imaging in HeLa cells, we found that the translocation of mVSP persisted even after removal of the IG2 domain or the cytoplasmic tail. Consistently, the interaction with BSG was independent of the intracellular domains of mVSP, indicating binding of BSG to the transmembrane VSD domain of mVSP (Figure 3.16).

We next harnessed site-directed mutagenesis to investigate the role of the conserved charged glutamic acid residue. This moiety is known from existing literature to be pivotal in the interaction with a XK-related protein (Xkr8) (Sakuragi *et al*., 2021). Replacing glutamic acid with aspartic acid (E222D) minimally disturbed the forward trafficking effect of BSG on mVSP. However, when glutamic acid (E222Q) was substituted with glutamine or lysine (E222K), a significant impact on the forward trafficking of mVSP to the PM was observed. This implies that the conserved glutamic acid residue likely holds importance for the forward trafficking of mVSP.

This phenomenon aligns with previous findings. Just as binding of BSG to PMCA and MCTs via transmembrane interactions has been directly observed through crystallography and cryo-EM (Schmidt *et al*., 2017; Wang *et al*., 2021), it was also noted

that the substitution of glutamic acid to arginine (E222R) was not sufficient to disrupt the interaction in the case of MCTs (Manoharan *et al.*, 2006). A later study indicated that multiple amino acids within the transmembrane region of MCTs are responsible for their interaction with BSG (Wang *et al.*, 2021). This collective evidence underscores the complicated nature of protein interactions within the transmembrane context, highlighting the need for a broad investigation to unravel the underlying molecular mechanisms.

4.4. The N- and C-termini of mVSP are collectively responsible for ER retention

In order to address the reasons behind the retention of mVSP within the ER, we embarked on an elaborative investigation. This involved generating various truncation and substitution mutants to pinpoint the specific mVSP regions responsible for ER retention. The C-terminal truncation mutants mVSP K352 stop, mVSP Y410 stop, and mVSP Y417 stop showed PM localization, suggesting that the ER retention signal is likely to be located proximal to D426. The subsequent amino acid substitutions within the ^{417}YRVRRIMIDD^{426} region, based on similar motifs in hVSP and Ci-VSP, further supported the existence of an arginine-based potential retention/retrieval signal RXRR. However, the triple arginine substitution (mVSP RRR418,420,421AAA) did not result in PM localization. Notably, regardless of BSG co-expression, these mutants localized to intracellular compartments, suggesting that this region within mVSP may be critical and could lead to structural reformation of mVSP affecting its PM translocation.

Then we looked for the potential ER retention signals in the N-terminal region that might be responsible for ER retention. Truncation studies revealed no potential ER retention signals similar to the observations made with the C-terminal region. The study also explored a naturally occurring splice variant, mVSPΔExon9 (lacking exon 9), which was reported to be localized to Golgi (Rosasco *et al.*, 2015). Interestingly, in our experiments, mVSPΔExon9 showed ER localization (Figure 3.15), indicating that exon 9 region may not be critical for ER retention.

To address potential folding defects arising from truncation studies, we engaged in chimeric studies that combined portions of mVSP and Ci-VSP. This approach shed light on the intricate interplay between different regions of the protein. Notably, the transmembrane domain of mVSP emerged as pivotal for BSG interaction and proper subcellular localization. Moreover, both the N and C-termini of mVSP were identified as equal contributors to ER retention, suggesting a delicate balance between these regions

in governing localization of mVSP. Collectively, these findings demonstrated from our dissection and chimeric studies contribute to a deeper understanding of the complex mechanisms governing subcellular localization of mVSP. Beyond the scope of our study, these revelations hold broader implications for our understanding of protein trafficking and localization processes within cells.

4.5. Catalytic activity of mVSP

The catalytic activity and voltage-sensing capabilities of mammalian VSPs have remained elusive. Limited direct evidence for the enzymatic activity of mammalian VSPs has emerged from studies involving chimeric proteins. In these instances, the catalytic domain of human VSP1 was artificially combined with the VSD of Ci-VSP, or the catalytic domain of mVSP was fused with the VSD of VSP from Danio rerio (Halaszovich *et al.*, 2012; Rosasco *et al*., 2015). Notably, in both cases, the resulting chimeric proteins were directed to the PM and exhibited voltage-dependent phosphatase activity against phosphoinositides.

Here in my thesis, we achieved a significant milestone by successfully measuring the voltage-dependent phosphatase activity of the complete mVSP protein by targeting it to the PM using BSG in HEK293 cells. Our findings demonstrated that, upon depolarization, mVSP shows characteristics of a 5-phosphatase by converting $PI(4,5)P_2$ to PI(4)P and $PI(3,4,5)P_3$ to $PI(3,4)P_2$. For nonmammalian VSPs, additional 3-phosphatase activity was reported (*Keum et al.*, 2016; Grimm *et al.*, 2016; Kurokawa *et al*., 2012). Additional detailed studies will be required to test whether mVSP also features such 3-Ptase activity.

4.6. Biological role of mVSP in mouse sperm

The presence of voltage-sensitive phosphatases in the testis has long been recognized, but their biological significance in reproduction has remained largely unexplored. Only recently, Kawai *et al*., 2019 shed light on this enigma by demonstrating the presence of VSP in the murine sperm tail, where its activity was detected. In-depth investigations into the cellular mechanisms involved indicated that the polarized distribution of VSP leads to an asymmetric concentration of $PI(4,5)P_2$ in the sperm PM. Through experiments with VSP-null mice, Kawai *et al*. demonstrated that an excess of PIP_2 in the sperm tail enhances SLO3 activity, resulting in increased calcium influx and abnormal circular motion of mouse sperm during capacitation.

How does this model align with the functional properties revealed by BSG-dependent

forward trafficking? Firstly, the enzymatic specificity of mVSP is in line with the depletion of PI(4,5)P_2 in the sperm tail. As we have demonstrated that mVSP also depletes PI(3,4,5)P_3 and generates PI(3,4)P_2, these phosphoinositides might also contribute to VSPs function in sperm. However, it is noteworthy that the knockout of mVSP did not impact PI(3,4,5)P_3 levels in sperm, and PI(3,4)P_2 was not detected at all (Kawai *et al*., 2019). These findings can be reconciled with the observed enzymatic activity of mVSP against PI(3,4,5)P_3 if PI(3,4,5)P_3 is primarily located in the sperm head, in contrast to the predominant location of VSP in the tail.

However, Kawai *et al*., found no obvious differences in PI(4,5)P_2 content before and after capacitation, suggesting that mVSP influence on sperm motility occurs primarily after capacitation. This suggests ongoing, constitutive catalytic activity of mVSP. According to current findings, mVSP activation necessitates significant depolarization. Kawai *et al*. reported strongly depolarized membrane potentials (-12 mV) in mouse sperm, closely resembling the approximately 0 mV required in our experiments to activate mVSP. It's established that the membrane potential of mammalian sperm hyperpolarizes during capacitation (to around -65 mV). Given these results, the reversible activation by depolarization with limited activity at typical resting potentials suggests that capacitation might lead to the deactivation of mVSP. This raises the question of whether mVSP activity, and subsequently PI(4,5)P_2 levels, are dynamically regulated in sperm. A thorough investigation into the enzymatic activity of VSP and PI(4,5)P_2 levels across various stages of sperm life, from resting epididymal spermatozoa to capacitation and hyperactivation, could provide more insights in the distinct role of mammalian VSP in sperm function.

4.7. Outlook

In this study, we have advanced our understanding of various facets related to PM trafficking and the function of mVSP. Despite significant progress, there are still unanswered questions that require further investigation.

The live cell imaging data from our study demonstrate that, in an over-expression system, mVSP predominantly localizes to the ER. Through the implementation of a chimeric approach, we have effectively identified that both the N and C-terminal sequence stretches of mVSP may exert a significant influence on its retention. Therefore, a detailed examination is warranted to understand the exact retention mechanism of mVSP in the absence of BSG.

Future investigations should explore a detailed molecular mechanism in understanding BSG-mediated forward trafficking of mVSP. Structural studies, utilizing high-resolution techniques like cryo-EM or X-ray crystallography, are crucial for unveiling the precise binding interfaces between BSG and mVSP transmembrane domains. Furthermore, extended future studies should be carried out to examine the role of BSG-mediated PM trafficking of other mammalian or non-mammalian VSPs.

In this study, we propose that the BSG protein family serves as a central hub for the trafficking of mVSP destined for PM delivery. BSG and its homologs have previously known to have a similar effect on the PM trafficking of other group of proteins, but the underlying mechanism that enables PM localization remains unknown so far in any of the cases. A detailed investigation should be carried out to know the precise trafficking mechanism of BSG protein family.

Our study demonstrates that the enzymatic activity of mVSP is controlled by membrane depolarization, remaining inactive at resting membrane potential but becoming activated under strong depolarization conditions of 0 mV. The precise voltage dependence of mVSP has not been elucidated to date. Generating a permanent mVSP cell line with stable mVSP expression and employing a step-wise depolarization approach using patch clamp technique to alter the membrane potential could provide information on the precise voltage dependent catalytic activity of mVSP. Additionally, our research demonstrated that mVSP functions as a phosphatidylinositol 5-phosphatase, exhibiting activity against $PI(4,5)P_2$ and $PI(3,4,5)P_3$, coupled with voltage-dependent activation. Further investigations are needed to determine the enzymatic specificity of mVSP against various PIPs.

While the knockout mouse model suggests a role for mVSP in sperm motility, further investigation is hampered by the lack of suitable antibodies. Overcoming this limitation would pave the way for in vivo studies to confirm this association. In addition, elucidating the native distribution of mVSP in BSG knockout mice, again dependent on antibody availability, could provide valuable insights.

This study calls for an investigation into the presence and functional relevance of BSG-mVSP interaction in various cell types and tissues where both the proteins are expressed. This broader perspective aims to deepen our understanding of the physiological implications of this interaction.

5. References

Agrawal S.M., Yong V.W. The many faces of EMMPRIN–roles in neuroinflammation. *Biochim. Biophys. Acta.* 2011;1812:213–219. doi: 10.1016/j.bbadis.2010.07.018.

Alberts B, Johnson A, Lewis J, *et al*. Molecular Biology of the Cell. 4th edition. New York: Garland Science; 2002. The Lipid Bilayer. Available from: https://www.ncbi.nlm.nih.gov/books/NBK26871/

Alberts, B., Johnson, A., Lewis, J., Morgan, D., Raff, M., Roberts, K., Walter, P. 2015. *Molecular Biology of the Cell.* 6th edn. New York: Garland Science.

Astle MV, Seaton G, Davies EM, Fedele CG, Rahman P, Arsala L, Mitchell CA. Regulation of phosphoinositide signaling by the inositol polyphosphate 5-phosphatases. IUBMB Life. 2006; 58:451–456. [PubMed: 16916781

Balla T. Phosphoinositides: tiny lipids with giant impact on cell regulation. Physiol Rev. 2013 Jul;93(3):1019-137. doi: 10.1152/physrev.00028.2012. PMID: 23899561; PMCID: PMC3962547.

Barlowe CK, Miller EA. Secretory protein biogenesis and traffic in the early secretory pathway. Genetics. 2013 Feb;193(2):383-410. doi: 10.1534/genetics.112.142810. PMID: 23396477; PMCID: PMC3567731.

Beesley P.W., Herrera-Molina R., Smalla K.H., Seidenbecher C. (2014) The Neuroplastin adhesion molecules: key regulators of neuronal plasticity and synaptic function. *J. Neurochem.* 131, 268–283

Bi J, Li Y, Sun F, Saalbach A, Klein C, Miller DJ, Hess R, Nowak RA. BSG null mutant male mice are sterile and exhibit impaired interactions between germ cells and Sertoli cells. Dev Biol. 2013 Aug 15;380(2):145-56. doi: 10.1016/j.ydbio.2013.05.023. Epub 2013 May 28. PMID: 23727514; PMCID: PMC3778672.

Biswas C, Zhang Y, DeCastro R, Guo H, Nakamura T, Kataoka H, Nabeshima K. The human tumor cell-derived collagenase stimulatory factor (renamed EMMPRIN) is a member of the immunoglobulin superfamily. Cancer Res. 1995 Jan 15;55(2):434-9. PMID: 7812975.

Blondeau F, Laporte J, Bodin S, Superti-Furga G, Payrastre B, Mandel JL. Myotubularin, a phosphatase deficient in myotubular myopathy, acts on phosphatidylinositol 3-kinase and phosphatidylinositol 3-phosphate pathway. Hum Mol Genet. 2000; 9:2223–2229. [PubMed: 11001925]

Casares D, Escribá PV, Rosselló CA. Membrane Lipid Composition: Effect on Membrane and Organelle Structure, Function and Compartmentalization and Therapeutic Avenues. Int J Mol Sci. 2019 May 1;20(9):2167. doi: 10.3390/ijms20092167. PMID: 31052427; PMCID: PMC6540057.

Chen H, Rossier C, Morris MA, Scott HS, Gos A, Bairoch A, Antonarakis SE. A testis-specific gene, TPTE, encodes a putative transmembrane tyrosine phosphatase and maps to the pericentromeric region of human chromosomes 21 and 13, and to chromosomes 15, 22, and Y. *Hum Genet* 105: 399–409, 1999. doi:10.1007/s004390051122.

Chi Y, Zhou B, Wang WQ, Chung SK, Kwon YU, Ahn YH, Chang YT, Tsujishita Y, Hurley JH, Zhang ZY. Comparative mechanistic and substrate specificity study of inositol polyphosphate 5-phosphatase Schizosaccharomyces pombe Synaptojanin and SHIP2. J Biol Chem. 2004; 279:44987–44995. [PubMed: 15316017]

Damen JE, Liu L, Rosten P, Humphries RK, Jefferson AB, Majerus PW, Krystal G. The 145-kDa protein induced to associate with Shc by multiple cytokines is an inositol tetraphosphate and phosphatidylinositol 3,4,5-triphosphate 5-phosphatase. Proc Natl Acad Sci U S A. 1996; 93:1689–1693. [PubMed: 8643691]

Di Paolo G, De Camilli P. Phosphoinositides in cell regulation and membrane dynamics. Nature. 2006 Oct 12;443(7112):651-7. doi: 10.1038/nature05185. PMID: 17035995

Dickson EJ, Hille B. Understanding phosphoinositides: rare, dynamic, and essential membrane phospholipids. *Biochem J*. 2019;476(1):1-23. Published 2019 Jan 7. doi:10.1042/BCJ20180022

Ernst R, Ballweg S, Levental I. Cellular mechanisms of physicochemical membrane homeostasis. Curr Opin Cell Biol. 2018 Aug; 53:44-51. doi: 10.1016/j.ceb.2018.04.013. Epub 2018 May 19. Erratum in: Curr Opin Cell Biol. 2020 Apr; 63:212. PMID: 29787971; PMCID: PMC6131038.

Falkenburger BH, Jensen JB, Dickson EJ, Suh BC, Hille B. Phosphoinositides: lipid regulators of membrane proteins. J Physiol. 2010 Sep 1;588(Pt 17):3179-85. doi: 10.1113/jphysiol.2010.192153. Epub 2010 Jun 2. PMID: 20519312; PMCID: PMC2976013.

Fetchko M, Stagljar I. Application of the split-ubiquitin membrane yeast two-hybrid system to investigate membrane protein interactions. Methods. 2004 Apr;32(4):349-62. doi: 10.1016/j.ymeth.2003.10.010. PMID: 15003597.

Fossum S., Mallett S., Barclay A.N. The MRC OX-47 antigen is a member of the immunoglobulin superfamily with an unusual transmembrane sequence. *Eur. J. Immunol.* 1991;21:671–679. doi: 10.1002/eji.1830210320.

Gabison E.E., Huet E., Baudouin C., Menashi S. Direct epithelial–stromal interaction in corneal wound healing: role of EMMPRIN/CD147 in MMPs induction and beyond. *Prog. Retin. Eye Res.* 2009;28:19–33.

Gallagher SM, Castorino JJ, Wang D, Philp NJ. Monocarboxylate transporter 4 regulates maturation and trafficking of CD147 to the plasma membrane in the metastatic breast cancer cell line MDA-MB-231. Cancer Res. 2007 May 1;67(9):4182-9. doi: 10.1158/0008-5472.CAN-06-3184. PMID: 17483329.

Gassmann M, Haller C, Stoll Y, Abdel Aziz S, Biermann B, Mosbacher J, Kaupmann K, Bettler B. The RXR-type endoplasmic reticulum-retention/retrieval signal of GABAB1 requires distant spacing from the membrane to function. Mol Pharmacol. 2005 Jul;68(1):137-44. doi: 10.1124/mol.104.010256. Epub 2005 Apr 1. PMID: 15805225.

Gong D, Chi X, Ren K, Huang G, Zhou G, Yan N, Lei J, Zhou Q. Structure of the human plasma membrane Ca^{2+}-ATPase 1 in complex with its obligatory subunit neuroplastin. Nat Commun. 2018 Sep 6;9(1):3623. doi: 10.1038/s41467-018-06075-7. PMID: 30190470; PMCID: PMC6127144.

Grimm SS, Isacoff EY. Allosteric substrate switching in a voltage-sensing lipid phosphatase. Nat Chem Biol. 2016 Apr;12(4):261-7. doi: 10.1038/nchembio.2022. Epub 2016 Feb 15. PMID: 26878552; PMCID: PMC4798927.

Guipponi., M., Tapparel, C., Jousson, O. *et al.* The murine orthologue of the Golgi-localized TPTE protein provides clues to the evolutionary history of the human TPTE gene family. *Hum Genet* 109, 569–575 (2001). https://doi.org/10.1007/s004390100607

Guo S, Stolz LE, Lemrow SM, York JD. SAC1-like domains of yeast SAC1, INP52, and INP53 and of human synaptojanin encode polyphosphoinositide phosphatases. J Biol Chem. 1999; 274:12990–12995. [PubMed: 10224048]

Halaszovich CR, Leitner MG, Mavrantoni A, Le A, Frezza L, Feuer A, Schreiber DN, Villalba-Galea CA, Oliver D. A human phospholipid phosphatase activated by a transmembrane control module. J Lipid Res. 2012 Nov;53(11):2266-74. doi: 10.1194/jlr.M026021. Epub 2012 Aug 15. PMID: 22896666; PMCID: PMC3465996.

Halaszovich CR, Schreiber DN, Oliver D. Ci-VSP is a depolarization-activated phosphatidylinositol-4,5-bisphosphate and phosphatidylinositol-3,4,5-trisphosphate 5'-phosphatase. J Biol Chem. 2009 Jan 23;284(4):2106-13. doi: 10.1074/jbc.M803543200. Epub 2008 Dec 1. PMID: 19047057.

Halestrap AP. The monocarboxylate transporter family--Structure and functional characterization. IUBMB Life. 2012 Jan;64(1):1-9. doi: 10.1002/iub.573. Epub 2011 Nov 30. PMID: 22131303.

Hershko A. The ubiquitin system for protein degradation and some of its roles in the control of the cell-division cycle (Nobel lecture). Angew Chem Int Ed Engl. 2005 Sep 19;44(37):5932-43. doi: 10.1002/anie.200501724. PMID: 16142823.

Hobiger, K., T. Utesch, M.A. Mroginski, and T. Friedrich. 2012. Coupling of Ci-VSP modules requires a combination of structure and electrostatics within the linker. *Biophys. J.* 102:1313–22. doi:10.1016/j.bpj.2012.02.027.

Hossain MI, Iwasaki H, Okochi Y, Chahine M, Higashijima S, Nagayama K, Okamura Y. Enzyme domain affects the movement of the voltage sensor in ascidian and zebrafish voltage-sensing phosphatases. J Biol Chem 283: 18248 –18259, 2008. doi:10. 1074/jbc.M706184200.

Hsu F, Mao Y. The structure of phosphoinositide phosphatases: Insights into substrate specificity and catalysis. Biochim Biophys Acta. 2015 Jun;1851(6):698-710. doi: 10.1016/j.bbalip.2014.09.015. Epub 2014 Sep 28. PMID: 25264170; PMCID: PMC4377127.

Huang W., Luo W.-J., Zhu P., Tang J., Yu X.-L., Cui H.-Y., Wang B., Zhang Y., Jiang J.-L., Chen Z.-N. Modulation of CD147-induced matrix metalloproteinase activity: role of CD147 *N*-glycosylation. *Biochem. J.* 2013;449:437–448. doi: 10.1042/BJ20120343.

Igakura T, Kadomatsu K, Kaname T, Muramatsu H, Fan QW, Miyauchi T, Toyama Y, Kuno N, Yuasa S, Takahashi M, Senda T, Taguchi O, Yamamura K, Arimura K, Muramatsu T. A null mutation in BSG, an immunoglobulin superfamily member, indicates its important roles in peri-implantation development and spermatogenesis. Dev Biol. 1998 Feb 15;194(2):152-65. doi: 10.1006/dbio.1997.8819. PMID: 9501026.

Iwasaki H, Murata Y, Kim Y, Hossain MI, Worby CA, Dixon JE, Mccormack T, Sasaki T, Okamura Y. A voltage-sensing phosphatase, Ci-VSP, which shares sequence identity with PTEN, dephosphorylates phosphatidylinositol 4,5-bisphosphate. Proc Natl Acad Sci U S A. 2008; 105:7970–7975. [PubMed: 18524949]

Jiang Y, Lee A, Chen J, Ruta V, Cadene M, Chait BT, MacKinnon R. X-ray structure of a voltage-dependent K channel. Nature 423: 33– 41, 2003. doi:10.1038/ nature01580.

Juliano RL. Signal transduction by cell adhesion receptors and the cytoskeleton: functions of integrins, cadherins, selectins, and immunoglobulin-superfamily members. *Annual Review of Pharmacology and Toxicology*. 2002;42:283–323.

Kadamur G, Ross EM. Mammalian phospholipase C. Annu Rev Physiol. 2013;75:127-54. doi: 10.1146/annurev-physiol-030212-183750. Epub 2012 Nov 5. PMID: 23140367.

Kalappa BI, Soh H, Duignan KM, Furuya T, Edwards S, Tzingounis AV, Tzounopoulos T. Potent KCNQ2/3-specific channel activator suppresses in vivo epileptic activity and prevents the development of tinnitus. J Neurosci. 2015 Jun 10;35(23):8829-42. doi: 10.1523/JNEUROSCI.5176-14.2015. PMID: 26063916; PMCID: PMC4461688.

Kanekura T., Miyauchi T., Tashiro M., Muramatsu T. BSG, a new member of the immunoglobulin superfamily: genes in different mammalian species, glycosylation changes in the molecule from adult organs and possible variation in the N-terminal sequences. *Cell Struct. Funct.* 1991;16:23–30. doi: 10.1247/csf.16.23.

Kasinrerk W., Fiebiger E., Stefanova I., Baumruker T., Knapp W., Stockinger H. Human leukocyte activation antigen M6, a member of the Ig superfamily, is the species homologue of rat OX-47, mouse BSG, and chicken HT7 molecule. *J. Immunol.* 1992;149:847–854.

Kawai T, Miyata H, Nakanishi H, Sakata S, Morioka S, Sasaki J, Watanabe M, Sakimura K, Fujimoto T, Sasaki T, Ikawa M, Okamura Y. Polarized PtdIns(4,5)P_2 distribution mediated by a voltage-sensing phosphatase (VSP) regulates sperm motility. Proc Natl Acad Sci U S A. 2019 Dec 17;116(51):26020-26028. doi: 10.1073/pnas.1916867116. Epub 2019 Nov 27. PMID: 31776261; PMCID: PMC6925991.

Kawanabe A, Mizutani N, Polat OK, Yonezawa T, Kawai T, Mori MX, Okamura Y. Engineering an enhanced voltage-sensing phosphatase. J Gen Physiol. 2020 May 4;152(5):e201912491. doi: 10.1085/jgp.201912491. PMID: 32167537; PMCID: PMC7201886.

Keum D, Kruse M, Kim DI, Hille B, Suh BC. Phosphoinositide 5- and 3-phosphatase activities of a voltage-sensing phosphatase in living cells show identical voltage dependence. Proc Natl Acad Sci U S A. 2016 Jun 28;113(26):E3686-95. doi: 10.1073/pnas.1606472113. Epub 2016 May 24. Erratum in: Proc Natl Acad Sci U S A. 2016 Aug 9;113(32):E4755. PMID: 27222577; PMCID: PMC4932978.

Kimber, W.A., L. Trinkle-Mulcahy, P.C.F. Cheung, M. Deak, L.J. Marsden, A. Kieloch, S. Watt, R.T. Javier, A. Gray, C.P. Downes, J.M. Lucocq, and D.R. Alessi. 2002. Evidence that the tandem-pleckstrin-homology-domain-containing protein TAPP1 interacts with Ptd(3,4)P2 and the multi-PDZ-domain-containing protein MUPP1 in vivo. *Biochem. J.* 361:525–536. doi:10.1042/0264-6021:3610525.

Kirk P, Wilson MC, Heddle C, Brown MH, Barclay AN, Halestrap AP. CD147 is tightly associated with lactate transporters MCT1 and MCT4 and facilitates their cell surface expression.

EMBO J. 2000 Aug 1;19(15):3896-904. doi: 10.1093/emboj/19.15.3896. PMID: 10921872; PMCID: PMC306613.

Kumánovics A, Levin G, Blount P. Family ties of gated pores: evolution of the sensor module. FASEB J. 2002 Oct;16(12):1623-9. doi: 10.1096/fj.02-0238hyp. PMID: 12374785.

Kuno N, Kadomatsu K, Fan QW, Hagihara M, Senda T, Mizutani S, Muramatsu T. Female sterility in mice lacking the BSG gene, which encodes a transmembrane glycoprotein belonging to the immunoglobulin superfamily. FEBS Lett. 1998 Mar 27;425(2):191-4. doi: 10.1016/s0014-5793(98)00213-0. PMID: 9559645.

Kurokawa T, Takasuga S, Sakata S, Yamaguchi S, Horie S, Homma KJ, Sasaki T, Okamura Y. 3' Phosphatase activity toward phosphatidylinositol 3,4-bisphosphate [PI(3,4)P2] by voltage-sensing phosphatase (VSP). Proc Natl Acad Sci U S A. 2012 Jun 19;109(25):10089-94. doi: 10.1073/pnas.1203799109. Epub 2012 May 29. PMID: 22645351; PMCID: PMC3382541.

Li H, Marshall AJ. 2015. Phosphatidylinositol (3,4) bisphosphate-specific phosphatases and effector proteins: A distinct branch of PI3K signaling.Cell Signal.;27(9):1789-98

Li M, Ho PW-L, Pang SY-Y, Tse ZH-M, Kung MH-W, Sham P-C, *et al*. (2014) PMCA4 (ATP2B4) Mutation in Familial Spastic Paraplegia. PLoS ONE 9(8): e104790.

Li Y, Xu J, Chen L, Zhong WD, Zhang Z, Mi L, Zhang Y, Liao CG, Bian HJ, Jiang JL, Yang XM, Li XY, Fan CM, Zhu P, Fu L, Chen ZN. HAb18G (CD147), a cancer-associated biomarker and its role in cancer detection. Histopathology. 2009 May;54(6):677-87. doi: 10.1111/j.1365-2559.2009.03280.x. Erratum in: Histopathology. 2009 Jun;54(7):918. Chen, Li [corrected to Chen, Ling]. PMID: 19438743.

Li YP, Mikrani R, Hu YF, Faran Ashraf Baig MM, Abbas M, Akhtar F, Xu M. Research progress of phosphatidylinositol 4-kinase and its inhibitors in inflammatory diseases. Eur J Pharmacol. 2021 Sep 15;907:174300. doi: 10.1016/j.ejphar.2021.174300. Epub 2021 Jul 1. PMID: 34217706.

Li, Q., S. Wanderling, M. Paduch, D. Medovoy, A. Singharoy, R. McGreevy, C. a Villalba-Galea, R.E. Hulse, B. Roux, K. Schulten, A. Kossiakoff, and E. Perozo. 2014. Structural mechanism of voltage-dependent gating in an isolated voltage-sensing domain. *Nat. Struct. Mol. Biol.* 21:244–52. doi:10.1038/nsmb.2768.

Liao C.-G., Kong L.-M., Song F., Xing J.-L., Wang L.-X., Sun Z.-J., Tang H., Yao H., Zhang Y., Wang L., *et al*. Characterization of BSG isoforms and the inhibitory function of BSG-3 in human hepatocellular carcinoma proliferation and invasion. *Mol. Cell. Biol.* 2011;31:2591–2604. doi: 10.1128/MCB.05160-11.

Liu, L., S.C. Kohout, Q. Xu, S. Müller, C.R. Kimberlin, E.Y. Isacoff, and D.L. Minor. 2012. A glutamate switch controls voltage-sensitive phosphatase function. *Nat. Struct. Mol. Biol.* 19:633–41. doi:10.1038/nsmb.2289.

Lu Z, Klem AM, Ramu Y. Coupling between voltage sensors and activation gate in voltage-gated K channels. J Gen Physiol 120: 663– 676, 2002. doi:10.1085/jgp. 20028696.

Majerus PW, York JD. Phosphoinositide phosphatases and disease. J Lipid Res. 2009 Apr;50 Suppl(Suppl):S249-54. doi: 10.1194/jlr.R800072-JLR200. Epub 2008 Nov 11. PMID: 19001665; PMCID: PMC2674710.

Mannowetz N, Wandernoth P, Wennemuth G. BSG interacts with both MCT1 and MCT2 in murine spermatozoa. J Cell Physiol. 2012 May;227(5):2154-62. doi: 10.1002/jcp.22949. PMID: 21792931.

Manoharan C, Wilson MC, Sessions RB, Halestrap AP. The role of charged residues in the transmembrane helices of monocarboxylate transporter 1 and its ancillary protein BSG in determining PM expression and catalytic activity. Mol Membr Biol. 2006 Nov-Dec;23(6):486-98. doi: 10.1080/09687860600841967. PMID: 17127621; PMCID: PMC2409183.

Matsuda, M., K. Takeshita, T. Kurokawa, S. Sakata, M. Suzuki, E. Yamashita, Y. Okamura, and A. Nakagawa. 2011. Crystal structure of the cytoplasmic phosphatase and tensin homolog (PTEN)-like region of Ciona intestinalis voltage-sensing phosphatase provides insight into substrate specificity and redox regulation of the phosphoinositide phosphatase activity. *J. Biol. Chem.* 286:23368–77. doi:10.1074/jbc.M110.214361.

Matsuda, M., K. Takeshita, T. Kurokawa, S. Sakata, M. Suzuki, E. Yamashita, Y. Okamura, and A. Nakagawa. 2011. Crystal structure of the cytoplasmic phosphatase and tensin homolog (PTEN)-like region of Ciona intestinalis voltage-sensing phosphatase provides insight into substrate specificity and redox regulation of the phosphoinositide phosphatase activity. *J. Biol. Chem.* 286:23368–77. doi:10.1074/jbc.M110.214361.

Matzaris M, Jackson SP, Laxminarayan KM, Speed CJ, Mitchell CA. Identification and characterization of the phosphatidylinositol-(4, 5)-bisphosphate 5-phosphatase in human platelets. J Biol Chem. 1994; 269:3397–3402. [PubMed: 8106379]

Mayinger P. Phosphoinositides and vesicular membrane traffic. Biochim Biophys Acta. 2012 Aug;1821(8):1104-13. doi: 10.1016/j.bbalip.2012.01.002. Epub 2012 Jan 14. PMID: 22281700; PMCID: PMC3340507

Mcpherson PS, Garcia EP, Slepnev VI, David C, Zhang X, Grabs D, Sossin WS, Bauerfeind R, Nemoto Y, De Camilli P. A presynaptic inositol-5-phosphatase. Nature. 1996; 379:353–357. [PubMed: 8552192]

Minagawa T, Ijuin T, Mochizuki Y, Takenawa T. Identification and characterization of a sac domain-containing phosphoinositide 5-phosphatase. J Biol Chem. 2001; 276:22011–22015. [PubMed: 11274189]

Mishra RR, Chaudhary JK, Bajaj GD, Rath PC. A novel human TPIP splice-variant (TPIP-C2) mRNA, expressed in human and mouse tissues, strongly inhibits cell growth in HeLa cells. *PLoS One* 6: e28433, 2011. doi:10.1371/journal.pone.0028433.

Mitchell CA, Connolly TM, Majerus PW. Identification and isolation of a 75-kDa inositol polyphosphate-5-phosphatase from human platelets. J Biol Chem. 1989; 264:8873–8877. [PubMed: 2542294]

Miyauchi T, Masuzawa Y, Muramatsu T. The BSG group of the immunoglobulin superfamily: complete conservation of a segment in and around transmembrane domains of human and mouse BSG and chicken HT7 antigen. J Biochem. 1991 Nov;110(5):770-4. doi: 10.1093/oxfordjournals.jbchem.a123657. PMID: 1783610.

Miyauchi T., Jimma F., Igakura T., Yu S., Ozawa M., Muramatsu T. Structure of the mouse BSG gene, a unique member of the immunoglobulin superfamily. *J. Biochem.* 1995;118:717–724.

Miyauchi T., Kanekura T., Yamaoka A., Ozawa M., Miyazawa S., Muramatsu T. (1990) BSG, a new, broadly distributed member of the immunoglobulin superfamily, has strong homology with both the immunoglobulin V domain and the β-chain of major histocompatibility complex class II antigen. *J. Biochem.* 107, 316–323

Muramatsu T, Miyauchi T. BSG (CD147): a multifunctional transmembrane protein involved in reproduction, neural function, inflammation and tumor invasion. Histol Histopathol. 2003 Jul;18(3):981-7. doi: 10.14670/HH-18.981. PMID: 12792908.

Muramatsu T. BSG (CD147), a multifunctional transmembrane glycoprotein with various binding partners. J Biochem. 2016 May;159(5):481-90. doi: 10.1093/jb/mvv127. Epub 2015 Dec 18. PMID: 26684586; PMCID: PMC4846773.

Murata, Y., Iwasaki, H., Sasaki, M. et al. Phosphoinositide phosphatase activity coupled to an intrinsic voltage sensor. Nature 435, 1239–1243 (2005). https://doi.org/10.1038/nature03650

Nakada-Tsukui K, Watanabe N, Maehama T, Nozaki T. Phosphatidylinositol Kinases and Phosphatases in *Entamoeba histolytica*. Front Cell Infect Microbiol. 2019 Jun 6;9:150. doi: 10.3389/fcimb.2019.00150. PMID: 31245297; PMCID: PMC6563779.

Nakai M., Chen L., Nowak R.A. Tissue distribution of BSG and monocarboxylate transporter 1 in the adult male mouse: a study using wild-type and BSG gene knockout mice. *Anat. Rec. A.* 2006;288:527–535. doi: 10.1002/ar.a.20320.

Norris FA, Atkins RC, Majerus PW. The cDNA cloning and characterization of inositol polyphosphate 4-phosphatase type II. Evidence for conserved alternative splicing in the 4-phosphatase family. J Biol Chem. 1997; 272:23859–23864. [PubMed: 9295334]

Norris FA, Auethavekiat V, Majerus PW. The isolation and characterization of cDNA encoding human and rat brain inositol polyphosphate 4-phosphatase. J Biol Chem. 1995; 270:16128–16133. [PubMed: 7608176]

Norris FA, Majerus PW. Hydrolysis of phosphatidylinositol 3,4-bisphosphate by inositol polyphosphate 4-phosphatase isolated by affinity elution chromatography. J Biol Chem. 1994; 269:8716–8720. [PubMed: 8132601]

Okamura Y, Kawanabe A, Kawai T. Voltage-Sensing Phosphatases: Biophysics, Physiology, and Molecular Engineering. Physiol Rev. 2018 Oct 1;98(4):2097-2131. doi: 10.1152/physrev.00056.2017. PMID: 30067160.

Ovens MJ, Manoharan C, Wilson MC, Murray CM, Halestrap AP. The inhibition of monocarboxylate transporter 2 (MCT2) by AR-C155858 is modulated by the associated ancillary protein. Biochem J. 2010 Oct 15;431(2):217-25. doi: 10.1042/BJ20100890. PMID: 20695846; PMCID: PMC2947196.

Ozawa M., Huang R.P., Furukawa T., Muramatsu T. (1988) A teratocarcinoma glycoprotein carrying a developmentally regulated carbohydrate marker is a member of the immunoglobulin gene superfamily. *J. Biol. Chem.* 263, 3059–3062

Pesesse X, Moreau C, Drayer AL, Woscholski R, Parker P, Erneux C. The SH2 domain containing inositol 5-phosphatase SHIP2 displays phosphatidylinositol 3,4,5-trisphosphate and inositol 1,3,4,5-tetrakisphosphate 5-phosphatase activity. FEBS Lett. 1998; 437:301–303. [PubMed: 9824312]

Posor, Y., Jang, W. & Haucke, V. Phosphoinositides as membrane organizers. *Nat Rev Mol Cell Biol* 23, 797–816 (2022). https://doi.org/10.1038/s41580-022-00490-x

Ran FA, Hsu PD, Wright J, Agarwala V, Scott DA, Zhang F. Genome engineering using the CRISPR-Cas9 system. Nat Protoc. 2013 Nov;8(11):2281-2308. doi: 10.1038/nprot.2013.143. Epub 2013 Oct 24. PMID: 24157548; PMCID: PMC3969860.

Ratzan WJ, Evsikov AV, Okamura Y, Jaffe LA. Voltage sensitive phosphoinositide phosphatases of Xenopus: their tissue distribution and voltage dependence. J Cell Physiol 226: 2740 –2746, 2011. doi:10.1002/jcp.22854.

Renigunta A, Renigunta V, Saritas T, Decher N, Mutig K, Waldegger S. Tamm-Horsfall glycoprotein interacts with renal outer medullary potassium channel ROMK2 and regulates its function. J Biol Chem. 2011 Jan 21;286(3):2224-35. doi: 10.1074/jbc.M110.149880. Epub 2010 Nov 16. PMID: 21081491; PMCID: PMC3023518.

Rjasanow A, Leitner MG, Thallmair V, Halaszovich CR, Oliver D. Ion channel regulation by phosphoinositides analyzed with VSPs-PI(4,5)P2 affinity, phosphoinositide selectivity, and PI(4,5)P2 pool accessibility. Front Pharmacol. 2015 Jun 19; 6:127. doi: 10.3389/fphar.2015.00127. PMID: 26150791; PMCID: PMC4472987.

Rohrschneider LR, Fuller JF, Wolf I, Liu Y, Lucas DM. Structure, function, and biology of SHIP proteins. Genes Dev. 2000; 14:505–520. [PubMed: 10716940]

Rosasco MG, Gordon SE, Bajjalieh SM. Characterization of the functional domains of a mammalian voltage-sensitive phosphatase. *Biophys J* 109: 2480–2491, 2015. doi: 10.1016/j.bpj.2015.11.004.

Sakuragi T, Kanai R, Tsutsumi A, Narita H, Onishi E, Nishino K, Miyazaki T, Baba T, Kosako H, Nakagawa A, Kikkawa M, Toyoshima C, Nagata S. The tertiary structure of the human Xkr8-BSG complex that scrambles phospholipids at PMs. Nat Struct Mol Biol. 2021 Oct;28(10):825-834. doi: 10.1038/s41594-021-00665-8. Epub 2021 Oct 8. PMID: 34625749; PMCID: PMC8500837.

Santagata, S. *et al.* (2001) 'G-protein Signaling Through Tubby Proteins', *Science*, 292(5524), pp. 2041–2050. doi: 10.1126/science.1061233.

Sasaki T, Takasuga S, Sasaki J, Kofuji S, Eguchi S, Yamazaki M, Suzuki A. Mammalian phosphoinositide kinases and phosphatases. Prog Lipid Res. 2009 Nov;48(6):307-43. doi: 10.1016/j.plipres.2009.06.001. Epub 2009 Jul 4. PMID: 19580826.

Satchwell TJ, Wright KE, Haydn-Smith KL, Sánchez-Román Terán F, Moura PL, Hawksworth J, Frayne J, Toye AM, Baum J. Genetic manipulation of cell line derived reticulocytes enables dissection of host malaria invasion requirements. Nat Commun. 2019 Aug 23;10(1):3806. doi: 10.1038/s41467-019-11790-w. PMID: 31444345; PMCID: PMC6707200.

Schindelin J, Arganda-Carreras I, Frise E, Kaynig V, Longair M, Pietzsch T, Preibisch S, Rueden C, Saalfeld S, Schmid B, Tinevez JY, White DJ, Hartenstein V, Eliceiri K, Tomancak P,

Cardona A. Fiji: an open-source platform for biological-image analysis. Nat Methods. 2012 Jun 28;9(7):676-82. doi: 10.1038/nmeth.2019. PMID: 22743772; PMCID: PMC3855844.

Schmidt, J., Bonzheim, I., Steinhilber, J. *et al.* EMMPRIN (CD147) is induced by C/EBP*β* and is differentially expressed in ALK+ and ALK− anaplastic large-cell lymphoma. *Lab Invest* **97**, 1095–1102 (2017). https://doi.org/10.1038/labinvest.2017.54

Schmidt N, Kollewe A, Constantin CE, Henrich S, Ritzau-Jost A, Bildl W, Saalbach A, Hallermann S, Kulik A, Fakler B, Schulte U. Neuroplastin and BSG Are Essential Auxiliary Subunits of PM Ca^{2+}-ATPases and Key Regulators of Ca^{2+} Clearance. Neuron. 2017 Nov 15;96(4):827-838.e9. doi: 10.1016/j.neuron.2017.09.038. Epub 2017 Oct 19. PMID: 29056295.

Simons K, Sampaio JL. Membrane organization and lipid rafts. Cold Spring Harb Perspect Biol. 2011 Oct 1;3(10):a004697. doi: 10.1101/cshperspect. a004697. PMID: 21628426; PMCID: PMC3179338.

Spring F.A., Holmes C.H., Simpson K.L., Mawby W.J., Mattes M.J., Okubo Y., Parsons S.F. (1997) The Oka blood group antigen is a marker for the M6 leukocyte activation antigen, the human homolog of OX-47 antigen, BSG and neurothelin, an immunoglobulin superfamily molecule that is widely expressed in human cells and tissues. *Eur. J. Immunol.* 27, 891–897.

Tachikui H., Kurosawa N., Kadomatsu K. and Muramatsu T. (1999). Genomic organization and promoter activity of embigin, a member of the immunoglobulin superfamily. Gene 240, 325-332.

Tang W, Hemler ME. Caveolin-1 regulates matrix metalloproteinases-1 induction and CD147/EMMPRIN cell surface clustering. J Biol Chem. 2004 Mar 19;279(12):11112-8. doi: 10.1074/jbc.M312947200. Epub 2004 Jan 5. PMID: 14707126.

Tang W., Chang S.B., Hemler M.E. Links between CD147 function, glycosylation, and caveolin-1. *Mol. Biol. Cell.* 2004;15:4043–4050. doi: 10.1091/mbc.E04-05-0402.

Tapparel C, Reymond A, Girardet C, Guillou L, Lyle R, Lamon C, Hutter P, Antonarakis SE. The TPTE gene family: cellular expression, subcellular localization and alternative splicing. *Gene* 323: 189–199, 2003. doi:10.1016/j.gene.2003.09.038.

Vashist S, Kim W, Belden WJ, Spear ED, Barlowe C, Ng DT. Distinct retrieval and retention mechanisms are required for the quality control of endoplasmic reticulum protein folding. J Cell Biol. 2001 Oct 29;155(3):355-68. doi: 10.1083/jcb.200106123. Epub 2001 Oct 22. PMID: 11673477; PMCID: PMC2150856.

Villalba-Galea, C. a, F. Miceli, M. Taglialatela, and F. Bezanilla. 2009. Coupling between the voltage-sensing and phosphatase domains of Ci-VSP. *J. Gen. Physiol.* 134:5–14. doi:10.1085/jgp.200910215

Walker SM, Downes CP, Leslie NR. TPIP: a novel phosphoinositide 3-phosphatase. Biochem J. 2001 Dec 1;360(Pt 2):277-83. doi: 10.1042/0264-6021:3600277. PMID: 11716755; PMCID: PMC1222227.

Wang N, Jiang X, Zhang S, Zhu A, Yuan Y, Xu H, Lei J, Yan C. Structural basis of human monocarboxylate transporter 1 inhibition by anti-cancer drug candidates. Cell. 2021 Jan

21;184(2):370-383.e13. doi: 10.1016/j.cell.2020.11.043. Epub 2020 Dec 16. PMID: 33333023.

Ware MD, Rosten P, Damen JE, Liu L, Humphries RK, Krystal G. Cloning and characterization of human SHIP, the 145-kD inositol 5-phosphatase that associates with SHC after cytokine stimulation. Blood. 1996; 88:2833–2840. [PubMed: 8874179]

Wills RC, Goulden BD, Hammond GRV. Genetically encoded lipid biosensors. *Mol Biol Cell*. 2018;29(13):1526-1532. doi:10.1091/mbc.E17-12-0738

Wilson MC, Kraus M, Marzban H, Sarna JR, Wang Y, Hawkes R, Halestrap AP, Beesley PW. The neuroplastin adhesion molecules are accessory proteins that chaperone the monocarboxylate transporter MCT2 to the neuronal cell surface. PLoS One. 2013 Nov 18;8(11):e78654. doi: 10.1371/journal.pone.0078654. PMID: 24260123; PMCID: PMC3832594.

Wilson MC, Meredith D, Fox JE, Manoharan C, Davies AJ, Halestrap AP. BSG (CD147) is the target for organomercurial inhibition of monocarboxylate transporter isoforms 1 and 4: the ancillary protein for the insensitive MCT2 is EMBIGIN (gp70). J Biol Chem. 2005 Jul 22;280(29):27213-21. doi: 10.1074/jbc.M411950200. Epub 2005 May 24. PMID: 15917240.

Wu Y, Dowbenko D, Pisabarro MT, Dillard-Telm L, Koeppen H, Lasky LA. PTEN 2, a Golgi-associated testis-specific homologue of the PTEN tumor suppressor lipid phosphatase. J Biol Chem. 2001 Jun 15;276(24):21745-53. doi: 10.1074/jbc.M101480200. Epub 2001 Mar 2. PMID: 11279206.

Xu B, Zhang M, Zhang B, Chi W, Ma X, Zhang W, Dong M, Sheng L, Zhang Y, Jiao W, Shan Y, Chang W, Wang P, Wen S, Pei D, Chen L, Zhang X, Yan H, Ye S. Embigin facilitates monocarboxylate transporter 1 localization to the plasma membrane and transition to a decoupling state. Cell Rep. 2022 Sep 13;40(11):111343. doi: 10.1016/j.celrep.2022.111343. PMID: 36103816.

Yamaguchi S, Kurokawa T, Taira I, Aoki N, Sakata S, Okamura Y, Homma KJ. Potential role of voltage-sensing phosphatases in regulation of cell structure through the production of PI(3,4)P2. J Cell Physiol 229: 422– 433, 2014. doi:10. 1002/jcp.24463.

Yurchenko V, Constant S, Eisenmesser E, Bukrinsky M. Cyclophilin-CD147 interactions: a new target for anti-inflammatory therapeutics. Clin Exp Immunol. 2010 Jun;160(3):305-17. doi: 10.1111/j.1365-2249.2010.04115.x. Epub 2010 Mar 16. PMID: 20345978; PMCID: PMC2883100.

FIGURES

TABLES

ACKNOWLEDGMENTS

First and foremost, I extend my heartfelt gratitude to my professor, Dr. Dominik Oliver, for entrusting me with the opportunity to work on this outstanding project. Your guidance and mentorship have been instrumental in shaping my perspective and honing my skills.

I would like to express my appreciation to my supervisor, Dr. Vijayaram Kumar Renigunta, I owe an immeasurable debt of gratitude. Your support, not just as a mentor but as an elder brother, has been a constant source of motivation during the challenging times. Your guidance has illuminated my path and your presence in every step of this journey has been inspiring.

A special mention goes to Dr. Aparna for sharing her expertise and providing invaluable guidance. I am also thankful to Dr. Ramakanth for his unwavering motivation throughout my PhD journey.

I am indebted to my colleagues Olga Ebers, Galina Zilke and Nesli Özen, whose willingness to help amidst their busy schedules has left an indelible mark. Julia Jeschke and Jonathan Schlegel’s support and positivity in assisting me with experiments have been invaluable. My sincere thanks also go to Marc Giesler, Hanna Bahr, Klara Maschke, and Rajeshwari Bisen for their support.

I'd like to express my heartfelt gratitude to my friends, Srikanth, Sirisha, Arun, Anika, Tako, Sumit and Tejaswini for being the pillars of strength in my life. I thank you for the beautiful moments we've shared, filled with laughter and joy, throughout this incredible journey.

Lastly, my family holds an irreplaceable place in my heart. To my mother, father, and my siblings, Sohail and Farnaz, your belief in me has been the foundation of my perseverance. Additionally, I extend my heartfelt gratitude to my aunt and uncle, who not only supported me but also provided invaluable guidance and a clear vision throughout my academic journey.

CURRICULUM VITAE

Name: Imran Gousebasha Shaikh
E-Mail: imran6402@gmail.com
Address: Ernst Lemmer Straße 17, 35041, Marburg
Tel: +49 1794231287
Date and place of birth: 27.02.1992, Pamur, India

EDUCATION

July 2018 - present	**PhD in Physiology,** Institute for Physiology and Pathophysiology, Philipps University, Marburg. **PhD thesis**: Role of Voltage sensing Phosphatase in Spermatogenesis
Oct. 2014 - May 2017	**Master Degree in Agrobiotechnology,** Justus Liebig University, Giessen. **Master's thesis:** "Interaction partners of Inositol Polyphosphate - 4 phosphatase"
Sept. 2009 - June 2013	**Bachelor Degree in Biotechnology,** Vinayaka Missions University, Chennai, India. **Bachelor's thesis:** "Prevalence of pre-hypertension & hypertension in a rural population from Kancheepuram district of Tamil Nadu, India & their association with risk factors of chronic kidney diseases (CKD- A study based on anthropometric, serum & genetic markers

EMPLOYMENT HISTORY

July 2018- July 2022	**Scientific Research Assistant** Institute for Physiology and Pathophysiology, Marburg **Project:** Role of Voltage sensing Phosphatase in Spermatogenesis
July 2017- June 2018	**Scientific Research Assistant** Kinder Nephrologie, UKGM, Marburg. **Project:** Characterizing the interaction partners of ROMK potassium channel

CONFERENCES

Poster presentation: German Physiological Society, ULM, March Sept, 2019. "Identification of Interaction partners of the Phosphoinositide phosphatase INPP4B". **I. Shaikh**, O. Ebers, D. Oliver, V. Renigunta.
Poster presentation: Gesellschaft für Pädiatrische Nephrologie, May,2022. "Adenylate Kinase 2 along with ATP binding cassette member regulates ROMK2 function A. Renigunta, N. Renfordt, V. Renigunta, **I. S. Gousebasha,** M. Kömhoff, S. Weber.

LIST OF ACADEMIC TEACHERS

My academic teachers were the following ladies and gentlemen in:

Marburg

Vijayaram Kumar Renigunta, Dominik Oliver, Aparna Renigunta.

India

Velmurugan, Rekha Govindan, Popatlal Chavan, Natu, Shamala

EHRENWÖRTLICHE ERKLÄRUNG

Ich erkläre ehrenwörtlich, dass ich die dem Fachbereich Medizin Marburg zur Promotionsprüfung eingereichte Arbeit mit dem Titel, **Control of cellular trafficking of mammalian voltage sensitive phosphatase (VSP) through protein-protein interactions** im Institut für Physiologie und Pathophysiologie unter Leitung von Herrn Prof. Dr. Dominik Oliver mit Unterstützung durch Herrn Dr. Vijayaram Kumar Renigunta und Herrn Prof. Dr. Dominik Oliver und ohne sonstige Hilfe selbst durchgeführt und bei der Abfassung der Arbeit keine anderen als die in der Dissertation aufgeführten Hilfsmittel benutzt habe. Ich habe bisher an keinem in- oder ausländischen Medizinischen Fachbereich ein Gesuch um Zulassung zur Promotion eingereicht, noch die vorliegende oder eine andere Arbeit als Dissertation vorgelegt.
Ich versichere, dass ich sämtliche wörtlichen oder sinngemäßen Übernahmen und Zitatekenntlich gemacht habe. Mit dem Einsatz von Software zur Erkennung von Plagiatenbin ich einverstanden.

Marburg,

Imran Gousebasha Shaikh

Die Hinweise zur Erkennung von Plagiaten habe ich zur Kenntnis genommen.

Marburg,

Prof. Dr. Dominik Oliver